DC Distribution Systems

Modeling, Stability, Control & Protection

van der Blij, N.H.

DOI
10.4233/uuid:cd8011ea-8f77-4127-9e51-b2574c4cc3e2

Publication date
2020

Document Version
Final published version

Citation (APA)
van der Blij, N. H. (2020). *DC Distribution Systems: Modeling, Stability, Control & Protection*. [Dissertation (TU Delft), Delft University of Technology]. https://doi.org/10.4233/uuid:cd8011ea-8f77-4127-9e51-b2574c4cc3e2

Important note
To cite this publication, please use the final published version (if applicable).
Please check the document version above.

DC Distribution Systems

Modeling, Stability, Control & Protection

Nils H. van der Blij

DC Distribution Systems

Modeling, Stability, Control & Protection

Proefschrift

ter verkrijging van de graad van doctor aan de Technische Universiteit Delft,
op gezag van de Rector Magnificus Prof. Dr. Ir. T.H.J.J. van der Hagen,
voorzitter van het College voor Promoties,
in het openbaar te verdedigen op

donderdag 3 september 2020 om 12:30 uur

door

Nils Hans van der BLIJ

Elektrotechnisch Ingenieur, Technische Universiteit Delft, Nederland,
geboren te Leiden, Nederland

Dit proefschrift is goedgekeurd door de promotoren.

Samenstelling promotiecommissie bestaat uit:

Rector Magnificus	voorzitter
Prof. Dr. P. Bauer	Technische Universiteit Delft, promotor
Dr. M.T.J. Spaan	Technische Universiteit Delft, promotor
Dr. L.M Ramirez-Elizondo	Technische Universiteit Delft, copromotor

Onafhankelijke leden:

Prof. Ir. P.T.M. Vaessen	Technische Universiteit Delft
Prof. Dr. M. Liserre	Universiteit van Kiel
Prof. Dr. P. Palensky	Technische Universiteit Delft
Prof. Dr. E.A. Lomonova	Technische Universiteit Eindhoven

This project has received funding in the framework of the joint programming initiative ERA-Net Smart Grids Plus, with support from the European Union's Horizon 2020 research and innovation programme.

Printed by: Ridderprint (www.ridderprint.nl)

ISBN: 978-94-6384-152-8

An electronic version of this dissertation is available at http://repository.tudelft.nl

Summary

Historically speaking, alternating current (ac) has been the standard for commercial electrical energy distribution. This is mainly because, in ac systems, electrical energy was easily transformed to different voltages levels, increasing the efficiency of transmitting power over long distances. However, technological advances in, for example, power electronics, and societal concerns such as global warming indicate that a re-evaluation of the current distribution systems is timely.

Direct current (dc) distribution systems are foreseen to have advantages over their ac counterparts in terms of efficiency, distribution lines, power conversion and control. Moreover, most renewable energy sources and modern loads produce or utilize dc, or have a dc link in their conversion steps. However, the stability, control, protection and standardization of these systems, and the market inertia of ac systems are major challenges for the broad adoption of dc distribution systems.

Steady-State, Dynamic and Transient Modeling

Adequate models of dc distribution grids are required for the analysis, design and optimization of these systems. In this thesis new and improved methods are proposed for steady-state and dynamic modeling. Two novel steady-state methods are presented, which are shown to be better than the methods in existing literature with respect to convergence, computational effort and accuracy. Furthermore, a dynamic state-space model is proposed that can be efficiently applied to any system topology, and can be used for the stability analysis of these systems. Moreover, an improved symmetrical component decomposition method is presented, which enables simplified (fault) analysis. Transient models for dc distribution systems are briefly discussed, but the development of transient models is outside of the scope of this thesis.

Algebraic and Plug-and-Play Stability

As a result of the decreasing conventional generation, the inertia of electrical grids is significantly decreased. Furthermore, more and more tightly regulated load converters that have a destabilizing effect on the system's voltage (and frequency) are proliferated throughout the grid. Consequently, the stability of systems with substantial renewable

generation is more challenging. In this thesis a method to algebraically derive the stability of any dc distribution system is presented. Moreover, utilizing a Brayton-Moser representation of these systems, two simple requirements are derived for plug-and-play stability (i.e., stability requirements that can be applied to any system, even systems that are subjected to uncertainty or change).

Decentralized Control Strategy and Algorithm

Decentralized control is essential to deal with the trend to decentralize generation and segment the distribution grid, and to manage the potential absence of a communication infrastructure. In this thesis a decentralized control scheme is proposed that ensures global stability and voltage propriety for dc distribution grids. The control scheme divides the acceptable voltage range into demand response, emission, absorption and supply response regions, and specifies the behavior of converters in these regions. Furthermore, it is shown that inadequate energy utilization can occur, when voltage dependent demand response is utilized. Therefore, the Grid Sense Multiple Access (GSMA) is proposed, which improves the system and energy utilization by employing an exponential backoff routine.

Decentralized Protection Framework and Scheme

Because of the absence of a natural zero crossing, low inertia, meshed topologies and bi-directional power flow, the protection of low voltage dc grids is more challenging than conventional ac grids. In this thesis a decentralized protection framework is presented, which partitions the grid into zones and tiers according to their short-circuit potential and provided level of protection respectively. Furthermore, a decentralized protection scheme is proposed, which consists of a modified solid-state circuit breaker topology and a specified time-current characteristic. It is experimentally shown that this protection scheme ensures security and selectivity for radial and meshed low voltage dc grids.

Samenvatting

Historisch gezien is wisselstroom de standaard voor de commerciële distributie van elektrische energie. Dit komt voornamelijk omdat wisselspanning makkelijk werd getransformeerd naar verschillende spanningsniveaus, wat de efficiëntie van vermogensdistributie over lange afstanden verhoogd. Technologische vooruitgang in bijvoorbeeld vermogenselektronica, en maatschappelijke problemen zoals de opwarming van de aarde, geven echter aan dat een herevaluatie van huidige en toekomstige distributiesystemen misschien op zijn plaats is.

Gelijkstroomdistributiesystemen hebben, naar verwachting, een aantal voordelen ten opzichte van wisselstroomsystemen op het gebied van distributie, efficiëntie, omzetting en besturing. Daar komt nog bij dat de meeste duurzame energiebronnen en moderne belastingen gebruik maken van gelijkstroom in hun omzettingstappen. De marktinertie van wisselstroomsystemen en de stabiliteit, besturing, bescherming, standaardisatie van gelijkstroomsystemen vormen echter uitdagingen voor de brede toepassing van gelijkstroomdistributiesystemen.

Statische, Dynamische en Transiënte Modellen

Adequate modellen zijn vereist voor de analyse, het ontwerp en de optimalisatie van gelijkstroomdistributiesystemen. In dit proefschrift worden nieuwe en verbeterde methoden gepresenteerd voor het bepalen van de statische en dynamische toestanden van deze systemen. De twee gepresenteerde statische methoden blijken beter te zijn dan de methoden uit de bestaande literatuur met betrekking tot de convergentie, benodigde rekenkracht en nauwkeurigheid. Verder wordt er een dynamisch state-space model gepresenteerd welke efficiënt kan worden toegepast op elke systeemtopologie, en gebruikt kan worden voor stabiliteitsanalyse. Bovendien wordt een verbeterde symmetrische componenten decompositiemethode voorgesteld, wat de analyse (van kortsluitingen) simplificieert. Transiënte modellen voor gelijkstroomsystemen worden besproken, maar de ontwikkeling van transiënte modellen valt buiten de strekking van dit proefschrift.

Algebraïsche en Plug-and-Play Stabiliteit

De afname van conventionele elektriciteitsopwekking leidt tot een aanzienlijke vermindering van de inertie in elektriciteitsnetten. Bovendien neemt de hoeveelheid strak gereguleerde belastingen die een negatief effect hebben op de stabiliteit van de spanning en frequentie alleen maar toe. Zodoende, wordt de stabiliteit van distributiesystemen met veel duurzame energieopwekking steeds uitdagender. In dit proefschrift wordt een methode gepresenteerd om de stabiliteit van gelijkstroomdistributiesystemen algebraïsch af te leiden. Verder worden, met behulp van een Brayton-Moser vertegenwoordiging van deze systemen, twee eenvoudige vereisten afgeleid voor de plug-and-play stabiliteit van gelijkstroomsystemen (i.e., stabiliteitsvereisten die toegpast kunnen worden op elk systeem, ook systemen die onderhevig zijn aan onzekerheid of veranderingen).

Decentrale Besturingsstrategie en Besturingsalgorithme

Decentrale besturing is essentieel om met de decentralisatie van elektriciteitsproductie, de segmentatie van distributienetten, en de potentiële afwezigheid van een communicatie-infrastructuur om te gaan. In dit proefschrift wordt een decentrale besturingsstrategie voorgesteld die zorgt voor globale stabiliteit en juistheid van de spanningen. De besturingsstrategie verdeelt het acceptabele spanningsbereik in belastingsturing, emissie, absorptie en productiesturing gebieden, en specificeert het gedrag van omzetters in deze gebieden. Verder wordt aangetoond dat de energiebenutting ontoerijkend kan zijn wanneer spanningsafhankelijke belasting- of productiesturing wordt gebruikt. Daarom wordt het Grid Sense Multiple Access (GSMA) algorithme gepresenteerd, die de benutting van het systeem en de energie verbetert door een exponentiële backoff routine te gebruiken.

Decentraal Beschermingsraamwerk en Beveiligingsschema

Vanwege de afwezigheid van een natuurlijke nuldoorgang, lage inertie, gemaasde topologieën en bidirectionele stroom, is de bescherming van gelijkstroomnetten een grotere uitdaging dan voor conventionele wisselstroomnetten. In dit proefschrift wordt een decentraal beveiligingsraamwerk besproken dat het netwerk verdeelt in zones en regios op basis van hun kortsluitingspotentieel en de geboden veiligheid. Verder wordt een decentraal beveiligingsschema gepresenteerd, bestaande uit een ontwerp voor een stroomonderbrekerontwerp op basis van halfgeleiders en tijdstroomkarakteristiek. Experimenteel wordt aangetoond dat dit beveiligingsschema zorgt voor veiligheid en selectiviteit voor zowel radiale en gemaasde laagspanningsnetten.

Contents

Chapter 1

Introduction

1.1 Motivation

Future distribution grids face major challenges [1]. Firstly, electrical energy demand is growing worldwide. It is estimated that the utilization of distribution systems in developed countries will reach their maximum capacity in the near future, while for developing countries there is still an increasing need for infrastructure. Secondly, the introduction of distributed renewable energy generation presents new challenges on the stability, reliability and management of these grids. Distribution grids will need to allow bidirectional power flow as distributed generation introduces highly dynamic power flows. Moreover, to ensure reliability, distribution grids should be able to cope with the variable character of renewable energy sources. Since both challenges have to be faced in the near future there is an opportunity to reassess the architecture and nature of distribution systems. Furthermore, technological advances such as renewable energy generation and societal concerns such as global warming also indicate that a re-evaluation of the current distribution system is timely [2].

Historically speaking, ac power has been the standard for commercial electrical energy systems. This was mainly because ac electrical energy was easily transformed to different voltage levels, increasing the efficiency of transmitting power over long distances [3, 4]. However, advances in power electronics have made it equally simple to convert dc electrical energy to different voltage levels. As a result, a re-evaluation of dc could be made for many distribution, industrial and domestic applications.

Nowadays dc systems are foreseen to have advantages over their ac counterparts in terms of distribution, efficiency, power conversion and control [5, 6]. Lines that operate on dc have higher capacity, lower losses, and can carry power over longer distances. Furthermore, most distributed renewable energy resources and loads have an inherent dc nature (e.g., photovoltaic panels and laptops), or have a dc link in their ac/ac conversion steps (e.g., wind turbines). Therefore, it makes sense to increase the overall efficiency by employing dc on the distribution network, reducing the number of conversion steps between supply and demand. Moreover, because the switching frequencies of power electronic converters are typically much higher than

the fundamental 50/60 Hz frequency of ac grids, the size of passive components in the conversion steps can significantly be reduced. Lastly, dc grids do not require the synchronization of frequency and phase, or reactive power governance. Consequently, the control and interconnection of dc grids are significantly simpler than their ac counterparts.

As a consequence of the advantages of dc systems their adoption is growing significantly. For example, the utilization of these systems for applications such as high voltage transmission, data centers, telecommunications, commercial and residential buildings, and street lighting is ever increasing [7–17]. Furthermore, a variety of novel applications, such as microgrids and device level distribution, have been identified [6, 18].

Although the advantages of dc distribution systems are significant, there are also several challenges for the broad adoption of dc grids. Therefore, this thesis aims to aid broad adoption of dc distribution grids by addressing the main technical challenges. Non-technical challenges, such as the standardization of dc grids and the market inertia of ac systems, are outside the scope of this thesis. Due to practical limitations, the focus of this thesis is mainly low voltage grids with a voltage rating below 1500 V and a power rating below 100 kW (e.g., microgrids), but most of the theories and results of this thesis can also be applied to larger scale grids.

1.2 Thesis Objective and Research Questions

In this section it will be explained why the stability, control and protection of dc distribution systems are identified as key technical challenges for their broad adoption. Furthermore, to tackle these challenges appropriate modeling techniques are required. Therefore, the primary objective of this thesis is

"To improve the modeling, stability, control and protection of dc distribution systems".

The main research is partitioned into several research questions with their individual objectives. The research questions correspond to the different chapters in this thesis and are given by

Chapter 2. *How can the modeling of dc distribution systems be improved?*

To assess the behavior, stability, control and protection of dc distribution systems accurate and computationally efficient models are required. Although accurate, most dc distribution system models are derived from their ac counterparts, leading to computationally suboptimal solutions. Therefore, this chapter aims to introduce novel and improved methods to model the behavior of dc distribution systems. Transient models, which take propagation delay into account, are discussed, but the development of novel transient methods outside the scope of this thesis.

Chapter 3. *How can the stability of dc systems be analyzed and ensured?*

With conventional generation, the kinetic energy of the rotor's moment of inertia is linked to the frequency of the distribution grid. Consequently, conventional generation provides inertia to the grid's frequency. However, with the increasing share of renewable energy sources, the inertia of future distribution grids is significantly decreased [19]. Moreover, tightly regulated load converters behave as constant power loads. Constant power loads exhibit negative incremental input impedance, which has a destabilizing effect on distribution systems [20]. Therefore, stability is a significant challenge for future ac and dc distribution grids.

Literature presents several methods for analyzing the stability of dc distribution systems. However, these methods do not allow for generalized conclusions about the sensitivity to specific system parameters, or the derivation of stability guidelines that can be applied to any system. Therefore, methods to analyze the stability of any dc distribution system, regardless of its topology, and the derivation of plug-and-play stability guidelines are the main focus of this chapter.

Chapter 4. *How should the decentralized control of dc systems be organized?*

Traditionally, electrical power grids have had a centralized and radial structure. However, large scale renewable power generation is likely to occur in regions of high resource availability, rather than regions of high consumption. Furthermore, because of the decentralization of generation, the power flow in distribution grids is no longer unidirectional [21–23]. Additionally, the notion of segmenting the grid into, for example, microgrids is increasing [24, 25]. Moreover, because of the reducing inertia, faster response of the control will be required. Therefore, the control strategies for electrical power grids need to be adapted to ensure the balance of supply and demand on shorter time scales, for varying system topologies and varying power flow.

Because of the distributed nature of future electrical power grids it is often not desirable to use communication. Furthermore, for systems with a communication infrastructure, it is imperative that the system sustains operation when there is a communication malfunction. Therefore, decentralized control is essential for future electrical power grids [26, 27]. The goal of this chapter is to establish decentralized control that ensures global stability and energy utilization in dc distribution grids.

Chapter 5. *How should the decentralized protection of dc systems be organized?*

The protection of low voltage dc grids is more challenging than the protection of conventional low voltage ac systems. Fundamentally, it is more difficult to interrupt inductive currents and extinguish arcs, since the voltages and currents in dc grids do not have a natural zero crossing [28, 29]. Furthermore, these grids are often meshed and/or subjected to bi-directional power flows, complicating the detection and selectivity compared to conventional radial networks [30]. Moreover, to prevent high fault currents and blackouts, low voltage dc grids usually require fast fault interruption (in the order of microseconds) [31, 32].

Bi-directional power flow, and fast fault interruption complicates selective fault clearance. Literature presents several methods to establish selectivity via communication or by utilizing knowledge about the grid's topology and parameters. However, in

order to reduce reliance on a communication infrastructure and improve scalability, this chapter endeavors to achieve selective plug-and-play protection of dc systems, without utilizing communication.

Appendix A *How can the research in this thesis be experimentally verified?*

To verify the developed models, theoretical derivations and simulation results, a laboratory scale dc microgrid was developed. In this chapter the designs of the developed power electronic converters, line emulation circuits and solid-state circuit breakers are described.

Appendix B *How can the built power electronic converters be modeled and tuned?*

The scientific contribution of the modeling and tuning of power electronic converters in the laboratory setup is marginal. However, it is described in this chapter to make it easier to reproduce the results that are presented in this thesis.

1.3 Contributions

The main contributions of this thesis to the field of low voltage dc distribution systems, and the sections in which they can be found, are summarized below

Section 2.3 Two steady-state modeling methods that are better than existing methods in terms of computational effort, convergence and accuracy

Section 2.4 A state-space modeling method that can be applied to any system, includes the mutual coupling between parallel conductors and can also be employed for stability analysis

Section 2.5 An improved symmetrical component decomposition method, which allows for the inclusion of the neutral conductor and ground fault analysis

Section 3.3 An algebraic method for the derivation of the stability of any dc system from the system's state-space matrices

Section 3.4 The requirements for plug-and-play stability of dc systems, derived from a Brayton-Moser representation of the system

Section 4.2 A decentralized control strategy that ensures plug-and-play stability and voltage propriety

Section 4.3 The GSMA algorithm, which improves the energy utilisation of systems with voltage dependent demand or supply response

Section 5.2 A decentralized protection framework, which provides insight into the dangers and requirements of interacting with different parts dc grids

Section 5.3 A decentralized plug-and-play protection scheme that ensures security and selectivity for radial and meshed low voltage dc grids

1.4 Thesis Outline

The outline of the remainder of this thesis, of which the details were discussed in Section 1.2 and Section 1.3, and the interrelation between the chapters are schematically shown in Figure 1.1.

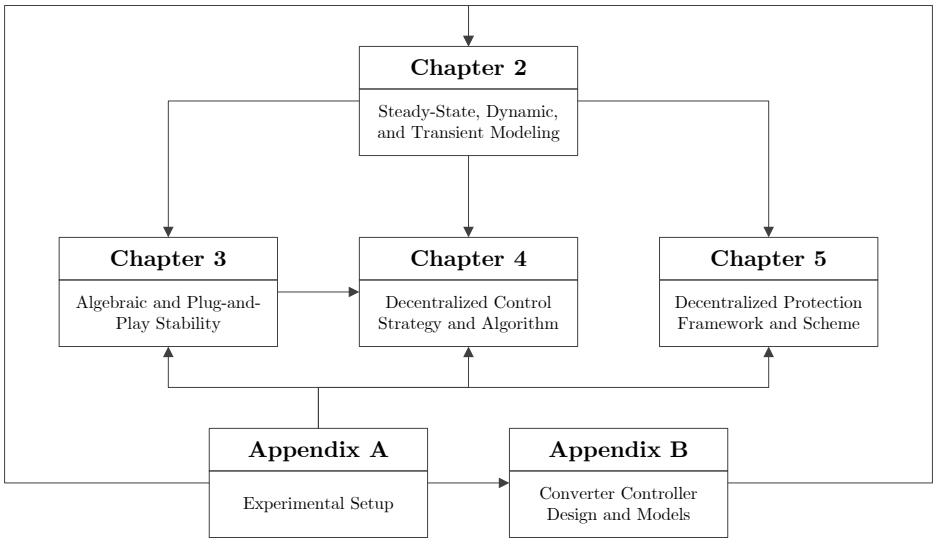

Figure 1.1: Outline of this thesis and the interrelation between the chapters

Chapter 2

Steady-State, Dynamic, and Transient Modeling

Appropriate models of dc distribution grids are required for the analysis, design and optimization of these systems. Therefore, literature on existing modeling methods is reviewed and several novel methods are developed to aid the research into, for example, stability, control and protection of dc distribution systems. In this chapter two novel steady-state modeling methods are derived that significantly reduce computational effort, while retaining or improving on accuracy and convergence, compared to existing methods. Furthermore, a state-space dynamic model is presented that, unlike methods presented in literature, includes mutual couplings between the lines' multiple conductors, can be applied to any system and facilitates stability analysis. Additionally, an improved symmetrical component decomposition method is proposed that allows for the ground fault analysis of bipolar dc distribution systems. Future research into the transient modeling of these systems is still imperative for the design and analysis of protection devices and schemes for these systems.

This chapter is based on

- N. H. van der Blij, L. M. Ramirez-Elizondo, M. T. J. Spaan and P. Bauer, "A State-Space Approach to Modelling DC Distribution Systems", IEEE Transactions on Power Systems, vol. 33, no. 1, Jan. 2018.
- N. H. van der Blij, L. M. Ramirez-Elizondo, M. T. J. Spaan and P. Bauer, "Symmetrical Component Decomposition of DC Distribution Systems", IEEE Transactions on Power Systems, vol. 33, no. 3, May 2018.
- N. H. van der Blij, D. Chaifouroosh, T. B. Soeiro, L. M. Ramirez-Elizondo, M. T. J. Spaan, Claudio A. Cañizares and P. Bauer, "Novel Power Flow Methods for DC Grids", 29th International Symposium on Industrial Electronics (ISIE), 2020.

2.1 Introduction

The aim of any model is to simulate, visualize and analyze the behavior of the system it is modeling. To model dc distribution grids it is important to identify the relevant system aspects that the user wants to model. Therefore, it is imperative to first define the end-goal in order to choose the appropriate modeling method. For example, dc distribution grid models can be used for the analysis, design and optimization of markets, stability, control and protection.

In this thesis, the models of dc distribution grids are divided into three categories. Firstly, when frequency dependent effects and propagation delays need to be taken into account a transient model is required. These models are accurate from time steps in the order of picoseconds, but are often too computationally intensive for simulations longer than several microseconds [33]. Secondly, when propagation delays can be neglected but the dynamic behavior of capacitances, inductances and discrete elements in the grid are of importance a dynamic model is recommended. These models are generally accurate in timescales from a few microseconds, but still require a lot of computational effort for simulations longer than several seconds. Lastly, for simulations spanning longer than several seconds, a steady-state model often suffices. The different types of models and the respective timescales they are generally applied to are graphically depicted in Figure 2.1.

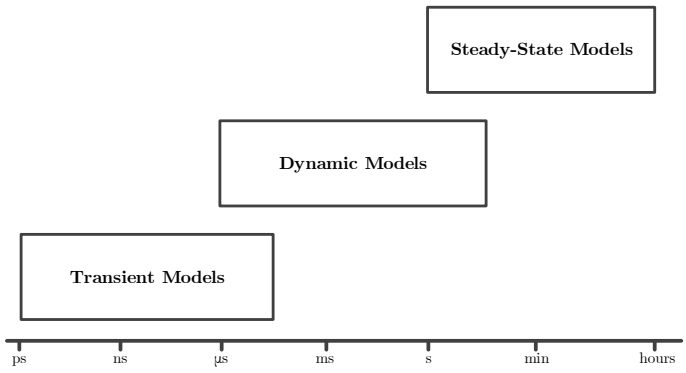

Figure 2.1: The timescales of the different types of distribution grid models

In Section 2.2, the incidence matrix and line models, which are used in this chapter to model dc distribution systems, are presented. In Section 2.3, several existing and two novel steady-state modeling methods are compared. In Section 2.4, a state-space dynamic model for dc distribution systems is presented. In Section 2.5, a symmetrical component decomposition method for bipolar dc distribution systems is proposed that further simplifies modeling. In Section 2.6, transient models for dc distribution systems are briefly discussed. Lastly, in Section 2.7, some of the models are verified using experimental results.

2.2 Generalized System Description

In essence, any dc distribution grid consists of n nodes that are interconnected by l distribution lines with m conductors. Furthermore, power electronic converters are connected to some or all of the nodes. An example of a bipolar dc distribution grid (with a metallic neutral) that has 5 nodes, 8 lines with 3 conductors, and 5 power electronic converters is shown in Figure 2.2.

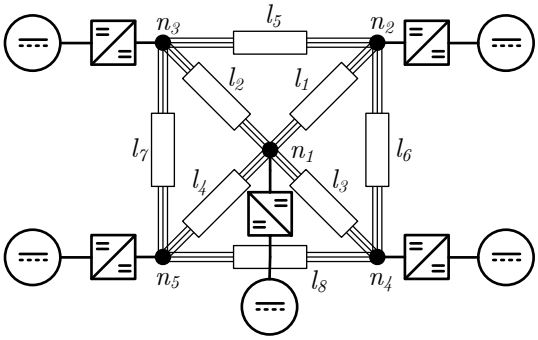

Figure 2.2: Example of a bipolar dc distribution system with 5 nodes, 8 lines with 3 conductors, and 5 power electronic converters

2.2.1 Incidence Matrix

The incidence matrix of the dc distribution depicts the connectivity of the electrical network. Strictly speaking, it represents the directed graph of the system, where each row represents a distribution line and every column represents a node in the system. The element in row j and column i of the incidence matrix, $\boldsymbol{\gamma}$, is given by

$$\boldsymbol{\gamma}(j,i) = \begin{cases} 1 & \text{if } I_j \text{ is flowing from node } i \\ -1 & \text{if } I_j \text{ is flowing to node } i \end{cases}, \tag{2.1}$$

where the indices i and j are used to indicate the nodes and lines of the system respectively. Therefore, I_j indicates the current flowing in distribution line j.

Unipolar and bipolar dc distribution systems have more than one conductor in each line. Since the conductors in the line have different potentials and carry different currents, each individual conductor must be modeled separately. Therefore, the incidence matrix is extended to be able to differentiate between conductors. The multi-conductor incidence matrix is given by

$$\boldsymbol{\Gamma}((j-1)\,m+k,(i-1)\,m+k) = \boldsymbol{\gamma}(j,i)\,, \tag{2.2}$$

where the total number of nodes, distribution lines and conductors are depicted by n, l, and m respectively. Moreover, the different indices for the nodes, distribution lines and conductors are given by i, j, and k respectively.

Figure 2.3: DC distribution system with 3 nodes and 2 lines with 3 conductors

To illustrate how the incidence matrix is composed, the bipolar distribution system shown in Figure 2.3 is used. Since this system contains 2 lines and 3 nodes the incidence matrix will have 2 rows and 3 columns respectively. The first line connects n_1 and n_2 and the second line connects n_2 and n_3, therefore the incidence matrix is given by

$$\boldsymbol{\gamma} = \begin{bmatrix} 1 & -1 & 0 \\ 0 & 1 & -1 \end{bmatrix}. \tag{2.3}$$

It is important that realize that in this example the conventions of the currents in the lines are chosen from n_1 to n_2 and from n_2 to n_3. However, the chosen convention is arbitrary and inconsequential to the results of models, which utilize this incidence matrix.

In this example, the dc distribution system is bipolar and therefore has 3 conductors in every line. Therefore, since there are $2 \cdot 3$ individual currents and $3 \cdot 3$ individual voltages, the multi-conductor incidence matrix has 6 rows and 9 columns. By utilizing (2.2) and cycling through all the indices, the multi-conductor incidence matrix is derived to be

$$\boldsymbol{\Gamma} = \begin{bmatrix} 1 & 0 & 0 & -1 & 0 & 0 & 0 & 0 & 0 \\ 0 & 1 & 0 & 0 & -1 & 0 & 0 & 0 & 0 \\ 0 & 0 & 1 & 0 & 0 & -1 & 0 & 0 & 0 \\ 0 & 0 & 0 & 1 & 0 & 0 & -1 & 0 & 0 \\ 0 & 0 & 0 & 0 & 1 & 0 & 0 & -1 & 0 \\ 0 & 0 & 0 & 0 & 0 & 1 & 0 & 0 & -1 \end{bmatrix}. \tag{2.4}$$

The multi-conductor incidence matrix orders the nodes first according to the different conductors (positive, neutral and negative), and then according to their numbering. Therefore, the columns represent the nodes of the system according to

$$\begin{bmatrix} n_{1+} & n_{1n} & n_{1-} & n_{2+} & n_{2n} & n_{2-} & n_{3+} & n_{3n} & n_{3-} \end{bmatrix}. \tag{2.5}$$

Similarly, the lines are ordered first according the different conductors, and then according to their numbering. Therefore, the rows represent the lines of the system according to

$$\begin{bmatrix} l_{1+} \\ l_{1n} \\ l_{1-} \\ l_{2+} \\ l_{2n} \\ l_{2-} \end{bmatrix}. \tag{2.6}$$

2.2.2 Distribution lines

Transmission and distribution lines are usually modeled by taking their electromagnetic phenomena into account. The most common lumped element models for these lines are shown in Figure 2.4. Although the resistive, inductive and capacitive elements are usually distributed over the lines, this approach provides reasonable accuracy when the wavelength of the signals are much longer than the length of the lines [34].

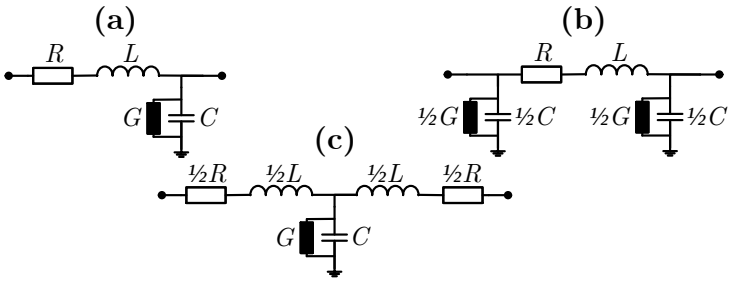

Figure 2.4: Gamma (a), pi (b), and T (c) lumped element line models

The models shown in Figure 2.4 are the models for a line in a monopolar dc system and therefore the return current flows through ground. However, in general, dc ground currents are not allowed since they cause corrosion [35]. On the other hand, the presence of multiple conductors introduces mutual couplings between the conductors in the form of mutual inductance, conductance, and capacitance. These couplings can have a significant effect on the behavior of the system. The lumped element pi model for a bipolar distribution line that includes the mutual couplings is shown in Figure 2.5.

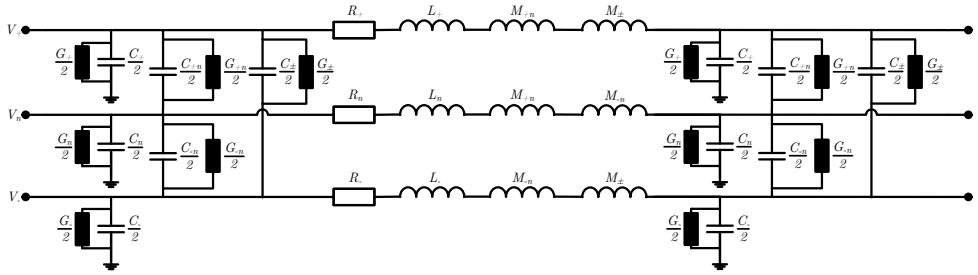

Figure 2.5: Lumped element pi model of a bipolar distribution line that includes mutual couplings

2.3 Steady-State Modeling

Steady-state methods, also sometimes called load flow or power flow methods, determine the steady-state operating point of an electrical power system. In general, the main goal of these methods is to determine all the bus voltages and line currents of a system, given the injected or consumed power of each node [36, 37]. Power flow analysis is most widely used for operation and planning of electrical power systems, but can also be used for more complex processes such as stability analysis, optimization routines, flow-based market simulations and N-1 security assessments [38].

Several methods are found in literature that are able to determine the steady-state operating point of power systems. Most commonly the power flow is found iteratively by utilizing analytical methods based on Gauss-Seidel (GS), Newton-Raphson (NR), Backward-Forward (BF) sweep methods, or by incorporating the system's equations into an Optimization Problem (OP) [37–40]. However, a Quadratic Solver (QS) can also be used to find the power flow solution by directly solving the quadratic equations [41].

In this section a steady-state model, which can be applied to any dc grid, is presented and it is shown how the power flow equations can be derived from this model. Furthermore, the most common existing power flow methods for dc grids are discussed and it is shown how they can be applied to dc grids. Moreover, two novel power flow methods are proposed which prove to be better than existing methods in terms of accuracy, convergence and computational effort.

2.3.1 Power Flow Formulation for DC Grids

In Figure 2.4 the different lumped element line models were presented for distribution lines. Conveniently all the lumped element models are reduced to the same steady-state model, which consists of a single resistor. Essentially, since the focus of this section is on the steady-state, the inductive and capacitive components can be neglected. Furthermore, the conductance G is also neglected since most systems have very high R/G ratio, which is especially true for distribution systems [42].

If all the resistances of the lines in the dc systems are put in a diagonal matrix $\boldsymbol{R}$, the currents in the system's lines are

$$\boldsymbol{I_L} = \boldsymbol{R^{-1}\Gamma U_N}, \tag{2.7}$$

where $\boldsymbol{U_N}$ is the vector containing the voltages at each node, and $\boldsymbol{I_L}$ is the vector containing the currents in each line.

According to Kirchhoff's law the sum of the currents flowing into each node must equal 0. Therefore, the current flowing from the power electronic converters into each node, defined as $\boldsymbol{I_N}$, must be equal to the current flowing out of that node via the connected lines. Accordingly,

$$\boldsymbol{I_N} = \boldsymbol{\Gamma^T I_L} = \boldsymbol{\Gamma^T R^{-1}\Gamma U_N} = \boldsymbol{Y U_N}, \tag{2.8}$$

where $\boldsymbol{Y}$ is the admittance matrix of the dc system.

From (2.8) it seems linear and simple to find the voltages in the system from the injected or consumed power at each node. However, when the power in each node is used instead of the injected current, the system's equations become

$$\boldsymbol{P_N} = \langle \boldsymbol{U_N}, \boldsymbol{Y}\boldsymbol{U_N} \rangle, \tag{2.9}$$

where $\langle \cdot, \cdot \rangle$ represents the scalar product of two vectors. From this equation it is clear that the equation becomes quadratic and can therefore not be solved directly.

More importantly, the admittance matrix is singular and can therefore not be inverted. This is because, if only the currents are defined in the system, an infinite number of solutions exist for the node voltages. Therefore, a slack node (a node with a constant voltage) is usually defined in the system to solve the power flow equations. However, any node which provides a behavior relative to a specified voltage will result in a single solution and therefore make the system solvable.

2.3.2 Power Flow Methods for DC Grids

In this subsection the most commonly used methods for solving power flow problems are discussed in detail. Furthermore, it is shown how these methods can be applied to dc grids by utilizing the notation from the previous subsection. Moreover, two novel power flow methods are presented, which arise from the dc system's equations.

Quadratic Solver (QS)

Equation (2.9) showed that the relation between the node power and the node voltages is quadratic. The expansion of this equation results in

$$P_i = U_i \sum_{j=1}^{n} Y_{ij} U_j, \tag{2.10}$$

where Y_{ij} refers to the element in row i and column j of the admittance matrix $\boldsymbol{Y}$. In matrix form this equation becomes

$$\boldsymbol{P_N} = \begin{bmatrix} U_1 & \dots & 0 \\ \vdots & \ddots & \vdots \\ 0 & \dots & U_n \end{bmatrix} \boldsymbol{Y}\boldsymbol{U_N}. \tag{2.11}$$

To solve these equations directly often Newton or Quasi-Newton methods are used to find the solution [41]. For the power flow simulations in this thesis, the Newton search algorithm is used.

Optimisation Problem (OP)

It is also possible to adapt the power flow problem into a quadratically constrained quadratic problem (QCQP). This optimization problem is defined as

$$\min \sum_{i=1}^{n} \epsilon_i^2, \tag{2.12}$$

$$\text{s.t.} \quad \epsilon_i = P_i - U_i \sum_{j=1}^{n} Y_{ij} U_j. \tag{2.13}$$

Methods to solve these types of problems include the interior point, augmented Lagrangian and the Simplex algorithms [43–45]. In this thesis the interior point solver is used to solve the optimization problem, to which the Hessian and the Gradient matrices are provided to improve convergence.

Gauss-Seidel (GS)

The Gauss-Seidel method is based on a simple fixed-point iteration process [37, 46]. It composes the equations for each individual node voltage and iterates on a node by node basis until the convergence criteria are met. The equations for the voltage at each node, for the k-th iteration, are given by

$$U_i^{k+1} = \frac{1}{Y_{ii}} \left(\frac{P_i}{U_i^k} - \sum_{j=1}^{i-1} Y_{ij} U_j^{k+1} - \sum_{j=i+1}^{n} Y_{ij} U_j^k \right). \tag{2.14}$$

In matrix form this equation becomes

$$U_i^{k+1} = \frac{1}{Y_{ii}} \left(\frac{P_i}{U_i^k} - \boldsymbol{Y_i^* U_N} \right), \tag{2.15}$$

where $\boldsymbol{Y^*}$ is the admittance matrix where the diagonal entries are removed, and $\boldsymbol{Y_i^*}$ represents the i-th row of this matrix.

In general the Gauss-Seidel method is easy to implement, but the convergence is slow compared to other methods. Therefore, an accelerating factor α is often used to improve convergence [37]. The algorithm is then appended with

$$U_i^{k+1} = U_i^k + \alpha \left(U_i^{k+1} - U_i^k \right), \tag{2.16}$$

where usually an α between 1.4 and 1.6 is used [37].

Newton-Raphson (NR)

The Newton-Raphson method and its many variations is the most widely used computational method [37, 47–49]. For this method the mismatch between the specified

power and the calculated power is composed as

$$\Delta P_{N,i} = P_i - U_i \sum_{j=1}^{n} Y_{ij} U_j. \tag{2.17}$$

In order to reduce this mismatch, the Jacobian matrix (the first derivative component in the Taylor approximation of the system) is used to determine the next iteration of the node voltages according to

$$\boldsymbol{U_N}^{k+1} = \boldsymbol{U_N}^{k} + \boldsymbol{J}^{-1} \Delta \boldsymbol{P_N}, \tag{2.18}$$

where the Jacobian, $\boldsymbol{J}$, is given by

$$\begin{aligned} \boldsymbol{J} &= \begin{bmatrix} \frac{\partial P_1}{\partial U_1} & \cdots & \frac{\partial P_1}{\partial U_n} \\ \vdots & \ddots & \vdots \\ \frac{\partial P_n}{\partial U_1} & \cdots & \frac{\partial P_n}{\partial U_n} \end{bmatrix} \\ &= \boldsymbol{Y} \begin{bmatrix} U_1 & \dots & 0 \\ \vdots & \ddots & \vdots \\ 0 & \dots & U_n \end{bmatrix} + \operatorname{diag}(\boldsymbol{Y U_N}), \end{aligned} \tag{2.19}$$

where diag() is a function that makes a diagonal matrix from the elements of a vector.

Since the partial derivatives are taken into account, the Newton-Raphson converges relatively fast. However, every iteration requires a refactorization of the Jacobian leading to increased computational effort per iteration, although strategies could be used to reduce this computational burden as is done for ac power flow techniques.

Backward-Forward (BF)

Another method that has been successfully implemented several times in literature for radial or weakly meshed dc grids is the Backward-Forward sweep method [50–52], where at every iteration, backward and forward sweeps are carried out. For the backward sweep the node voltages are considered constant and therefore the current from each converter is

$$I_i^k = \frac{P_i}{U_i^k}. \tag{2.20}$$

Next the algorithm iterates through all the lines from downstream to upstream. Then for every line j connecting node a (downstream) to node b (upstream) the current in line I_j and the current flowing in node I_a are found by

$$I_j^k = I_a^k, \tag{2.21}$$

$$I_b^k = I_b^k + I_a^k. \tag{2.22}$$

Consequently, the node current I_b is the sum of the currents in downstream lines, and the current in every line is the cumulative current in its downstream node. For the forward sweep the line currents are considered constant and the node voltages are calculated. Again the algorithm iterates through all the lines, but now from upstream to downstream, and the node voltages are given by

$$U_a^{k+1} = U_b^{k+1} - I_j^k R_j. \tag{2.23}$$

The main advantages of the Backward-Forward method are its simplicity and convergence. However, a downstream-upstream hierarchy of the lines in the system is required and the method only converges for radial or weakly meshed dc grids.

Direct Matrix - Current Approximation (DM-CA)

Here, a novel power flow method is presented that combines the strengths of the NR, BF and interior point methods to solve the quadratic problem. For every iteration, the constant power loads are linearized as a constant current load, utilizing the node voltages from the previous iteration. The resulting system is linear and the resulting node voltages can be solved explicitly.

It was mentioned before that for the admittance matrix to be invertible one or more of the voltages in the system must be referenced to a pre-determined voltage. If one or more of the nodes in the system are a slack node (have a constant voltage), the currents in the lines are given by

$$\boldsymbol{I_L} = \boldsymbol{R^{-1}\check{\Gamma}\check{U}_N} + \boldsymbol{R^{-1}\hat{\Gamma}\hat{U}_N}, \tag{2.24}$$

where $\boldsymbol{\check{U}_N}$ contains the unknown node voltages and $\boldsymbol{\hat{U}_N}$ contains the known node voltages. Furthermore, $\boldsymbol{\check{\Gamma}}$ contains the columns of the incidence matrix referring to the unknown node voltages and $\boldsymbol{\hat{\Gamma}}$ contains the columns of the incidence matrix referring to the known node voltages.

The currents flowing from the converters into nodes which voltage is not defined must therefore be equal to

$$\boldsymbol{\check{I}_N} = \boldsymbol{\check{\Gamma}^T R^{-1}\check{\Gamma}\check{U}_N} + \boldsymbol{\check{\Gamma}^T R^{-1}\hat{\Gamma}\hat{U}_N} = \boldsymbol{\check{Y}\check{U}_N} + \boldsymbol{I_0}. \tag{2.25}$$

By taking inspiration from the Backward-Forward method, and utilizing (2.25), the (unknown) voltages for each iteration can be calculated by

$$\boldsymbol{\check{U}_N^{k+1}} = \boldsymbol{\check{Y}^{-1}} \left(\begin{bmatrix} \frac{P_1}{U_1^k} \\ \vdots \\ \frac{P_n}{U_n^k} \end{bmatrix} - \boldsymbol{I_0} \right). \tag{2.26}$$

This method directly uses the system's matrices instead of the Jacobian, and approximates the constant power nodes as a current source. Therefore, this method is referred here as the Direct Matrix - Current Approximation (DM-CA) method.

The main advantage of this method is that the matrix $\check{\boldsymbol{Y}}$ remains constant during the iterations and therefore only has to be factorized once. Only the injected current for each node, $\frac{P_i}{U_i}$, and the product with the factorized admittance matrix has to be determined every iteration. Therefore, the complexity of this method mostly depends on one factorization of the admittance matrix and multiple matrix multiplications.

Direct Matrix - Impedance Approximation (DM-IA)

Another novel power flow technique is proposed here, where the constant power converter model is modified by adding a parallel impedance. Therefore, the current flowing from each constant power converter is given by

$$I_i^{k+1} \approx \frac{2P_i}{U_i^k} - \frac{P_i}{\left(U_i^k\right)^2} U_i^{k+1} = \frac{2P_i}{U_i^k} - Z_i^k U_i^{k+1}. \tag{2.27}$$

Consequently, the current flowing from the converters into each node is

$$\check{\boldsymbol{I}}_{\boldsymbol{N}} = \check{\boldsymbol{Z}}^{-\mathbf{1}} \check{\boldsymbol{U}}_{\boldsymbol{N}} + \check{\boldsymbol{Y}} \check{\boldsymbol{U}}_{\boldsymbol{N}} + \boldsymbol{I_0}, \tag{2.28}$$

where $\check{\boldsymbol{Z}}$ is a diagonal impedance matrix which elements are determined from (2.27). The voltages at each iteration can then be determined by utilizing

$$\check{\boldsymbol{U}}_{\boldsymbol{N}}^{\boldsymbol{k+1}} = \left(\left(\check{\boldsymbol{Z}}^{\boldsymbol{k}} \right)^{-1} + \check{\boldsymbol{Y}} \right)^{-1} \left(\begin{bmatrix} \frac{2P_1}{U_1^k} \\ \vdots \\ \frac{2P_n}{U_n^k} \end{bmatrix} - \boldsymbol{I_0} \right). \tag{2.29}$$

Since this method adds an impedance to the approximation of the constant power nodes, this method is referred here as the DM-IA method. The main advantage of this method over the DM-CA is that its iterations converge faster, since it also takes into account the gradient from the constant power converters' behavior. However, this comes at the cost of having to factorize $(\check{\boldsymbol{Z}}^{\boldsymbol{k}})^{-1} + \check{\boldsymbol{Y}}$ at every iteration, thus increasing the complexity of every iteration. Both the DM-CA and DM-IA methods give a numerical approximation of the power flow solution with an error dependent on the convergence criteria.

An advantage of both DM methods is that they can deal with a broader set of grids than those with only slack and constant power nodes. In this case, any linear node behavior can be modeled by a linear combination of a constant voltage, impedance, or current node. Furthermore, non-linear behavior can be approximated by a constant current and a constant impedance that are updated every iteration, as was done for the constant power nodes. However, for the sake of convergence, every grid has to have at least one slack node, or a node with an impedance.

2.3.3 Comparison of the Power Flow Methods

In this subsection, the power flow methods presented in the previous section are compared with respect to accuracy, convergence, and computational effort. Accuracy

is defined here as a Root Mean Square Error (RMSE) with respect to the actual solution of the power flow problem. For the iterative methods, the convergence is given by the number of iterations that are required to achieve a convergence criteria, with computational effort being measured as the required computational time to converge.

For the iterative power flow methods, the iterative process stops when the solution converges with a desired tolerance according to

$$\left| \frac{U_i^{k+1} - U_i^k}{U_i^k} \right| < \epsilon \qquad \forall i, \tag{2.30}$$

where ϵ is the desired tolerance. Note that a set tolerance does not always guarantee a similar accuracy for all methods, which will be shown later.

The results in this section are obtained by implementing the power flow methods in Matlab 2017b, and run on a computer with Windows 7, an Intel Xeon E5-1620 processor, and 8 GB of RAM.

IEEE Test Feeder

To compare the power flow methods the IEEE European Low Voltage Test Feeder [53] is used, as is illustrated in Figure 2.6, and consists of 111 nodes and 112 lines. The ac feeder is a representative neighborhood grid that includes household load profiles and line parameters, and it is assumed here to be a dc feeder with the same line parameters. In this case, 10.000 simulations of one day are carried out, where a day consists of 96 time steps of 15 minutes. In addition to the 55 households included in the test feeder, 15 photovoltaic (PV) systems and 15 electric vehicles (EVs) are randomly distributed among the households for every simulation. A convergence tolerance of 10^{-6} is used.

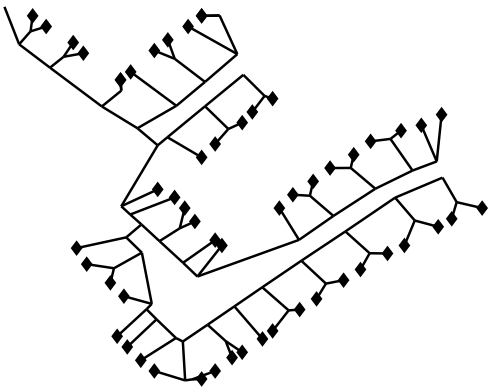

Figure 2.6: IEEE European Low Voltage Test Feeder that is used for the comparison of the power flow methods [53]

The power consumption from each household is randomly determined, assuming a uniform Probability Density Function (PDF) from the provided load profiles in the test feeder at every time step. Furthermore, the PV production is simulated using a Gaussian PDF, with a variance of 1/6 of the expected value. Additionally, the arrival time of the EVs is simulated by a Gaussian PDF with a mean at 18:00 and a standard deviation of 1.2 hours, while the charging time is defined as a Weibull distribution with $k = 2.022$ and $\lambda = 2.837$ [54, 55], resulting in a Gaussian-like PDF for the probability that a vehicle is charging with a constant power of 3 kW. The expected power for all these grid elements are shown in Figure 2.7.

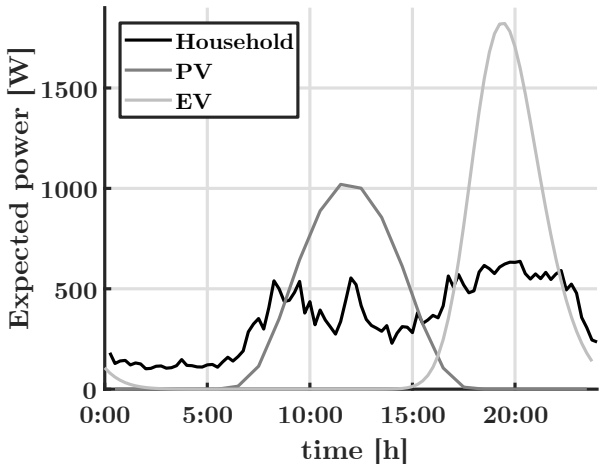

Figure 2.7: Expected power for the IEEE test feeder load profiles, photovoltaic systems, and electric vehicles

Numerical Results

For the first step in the power flow calculations, an initial guess of 350 V is used at all nodes. Furthermore, the solution of each time step t is used as initial guess for the next time step $(t + 1)$. Note that, because this system is relatively large and the matrices are sparse, LU factorization significantly reduces the average computation times.

The RMSE, average number of iterations, and average computation time (per simulation of a day) for the various power flow methods applied to the IEEE test feeder are shown in Table 2.1. Observe that the OP and DM-IA methods converge faster (have less iterations on average), since both these methods incorporate the non-linear behavior of the constant power loads. Besides the GS method (which is notorious for slow convergence) and QS method (which is not an iterative method), the other methods exhibit similar convergence.

Notice that the DM methods require the least computational effort of all the power

Method	RMSE [p.u.]	Average Iterations	Average Time [s]
GS	0.000189	367	2.87
NR	$1.1 * 10^{-9}$	2.74	0.0445
BF	$3.0 * 10^{-9}$	2.88	0.109
DM-CA	$2.9 * 10^{-9}$	2.87	0.0031
DM-IA	$2.7 * 10^{-14}$	2.00	0.0175
QS	$5.3 * 10^{-15}$	N/A	240
OP	$4.1 * 10^{-10}$	2.00	9.54

Table 2.1: Computational metrics with $\epsilon = 10^{-6}$

flow methods. Moreover, even though the DM-IA converges faster than the DM-CA method, the DM-CA method requires the least computational effort of all methods. This is because, for the DM-CA method, the factorized admittance matrix is re-used for every iteration and every time step. Also note that, due to the slow convergence and many iterations of the GS method, the GS does not achieve the level of accuracy that one would expect with these convergence criteria. Consequently, these criteria should be adjusted for the GS method if higher levels of accuracy are required.

For the previous simulation, a convergence tolerance $\epsilon = 10^{-6}$ was used. However, to ensure that a comprehensive comparison of the different power flow methods is given, the RMSE, average number of iterations, and average computation time for the same simulation with $\epsilon = 10^{-3}$ are given in Table 2.2. Note that, as expected, for all methods, the average number of required iterations decreases when the convergence tolerance is substantially increased. Nevertheless, the results are consistent with the previous simulations.

Method	RMSE [p.u.]	Average Iterations	Average Time [s]
GS	0.00841	1.028	0.0141
NR	$5.9 * 10^{-7}$	1.684	0.0277
BF	$1.1 * 10^{-6}$	1.683	0.0705
DM-CA	$1.1 * 10^{-6}$	1.683	0.0022
DM-IA	$6.0 * 10^{-10}$	1.684	0.0141
QS	$2.4 * 10^{-12}$	N/A	240
OP	$3.4 * 10^{-10}$	2.003	9.59

Table 2.2: Computational metrics with $\epsilon = 10^{-3}$

2.4 Dynamic Modeling

Dynamic models take into account the behavior of the discrete elements (e.g., power electronic switches) and energy storage elements (e.g., capacitors and inductors) in the system. Typically this means that the model includes the behavior of, for example, the capacitors, inductors and power electronic switches in the system.

Literature presents several types of dynamic models. For example, dc distribution grids can be modeled according to their transfer functions [56–58]. Furthermore, different state-space approaches exist to the model dc distribution grids [59–62]. Additionally, specialized transient simulations environments can be employed for the dynamic modeling of these systems [63]. However, existing models only consider monopolar configurations and, when extended to other configurations, do not allow for mutual couplings to be taken into account.

In this section a flexible generalized modeling method is presented that simplifies the analysis, design, and optimization of dc distribution systems. The developed method is flexible enough to allow for the analysis of dc distribution systems with any number of nodes, distribution lines, and conductors, in any configuration. The novelty of the developed method lies in that it allows for multiple conductors, and that mutual couplings and conductance to ground can be taken into account. Furthermore, a procedure is presented how the matrices of a distribution system can be derived programmatically. Therefore, the method can be implemented in many simulation environments, and it allows for rapid analysis of different systems without the need of (re)building the model through a GUI. Commercial simulation tools could produce similar results as the model. However, the mathematical nature of the presented model offers a significant advantage over these tools. It allows for the algebraic analysis of, for example, stability and control of dc distribution systems.

The presented model is valid when the lines are much shorter than the wavelengths of the signals in the system. Therefore, the model can be used for any dc distribution or transmission system of any power rating as long as the above statement is true.

2.4.1 State-Space Approach

To model the distribution system using a state-space approach the state variables must be chosen. For this model the state variables are chosen to be the voltages at each node and the currents in each distribution line. The formula for these voltages and currents are

$$\boldsymbol{C}\dot{\boldsymbol{U}}_{\boldsymbol{N}} = \boldsymbol{I}_{\text{net}}, \tag{2.31}$$

$$\boldsymbol{L}\dot{\boldsymbol{I}}_{\boldsymbol{L}} = \boldsymbol{U}_{\boldsymbol{L}}, \tag{2.32}$$

where $\boldsymbol{U}_{\boldsymbol{N}}$ are the voltages at each node, $\boldsymbol{I}_{\text{net}}$ are the net currents flowing into each node, $\boldsymbol{I}_{\boldsymbol{L}}$ are the currents flowing in each distribution line, $\boldsymbol{U}_{\boldsymbol{L}}$ are the voltage over each distribution line's inductance, and $\boldsymbol{C}$ and $\boldsymbol{L}$ are the matrices for the capacitance and inductance of the network respectively.

The net current flowing into each node consists of the current from the connected converter(s), the current from connected distribution lines, and current leaked through admittances. Similarly, the voltage over the inductance of the distribution line relates to the voltage difference between the two connected nodes and the voltage drop over the distribution line's resistance. Therefore, by expanding (2.31) and (2.32), the differential equations become

$$\boldsymbol{C}\dot{\boldsymbol{U}}_{\boldsymbol{N}} = \boldsymbol{I}_{\boldsymbol{N}} - \boldsymbol{\Gamma}^{\boldsymbol{T}}\boldsymbol{I}_{\boldsymbol{L}} - \boldsymbol{G}\boldsymbol{U}_{\boldsymbol{N}}, \tag{2.33}$$

$$\boldsymbol{L}\dot{\boldsymbol{I}}_{\boldsymbol{L}} = \boldsymbol{\Gamma}\boldsymbol{U}_{\boldsymbol{N}} - \boldsymbol{R}\boldsymbol{I}_{\boldsymbol{L}}, \tag{2.34}$$

where $\boldsymbol{I}_{\boldsymbol{N}}$ are the currents flowing into the node from the connected converter(s), $\boldsymbol{\Gamma}$ is the multi-conductor incidence matrix presented in Section 2.2, and $\boldsymbol{G}$ and $\boldsymbol{R}$ are the matrices for the conductance and resistance of the network respectively.

With the inverses of the capacitance and inductance matrices the state-space equations can be derived to be

$$\dot{\boldsymbol{U}}_{\boldsymbol{N}} = \boldsymbol{C}^{-1}\boldsymbol{I}_{\boldsymbol{N}} - \boldsymbol{C}^{-1}\boldsymbol{\Gamma}^{\boldsymbol{T}}\boldsymbol{I}_{\boldsymbol{L}} - \boldsymbol{C}^{-1}\boldsymbol{G}\boldsymbol{U}_{\boldsymbol{N}}, \tag{2.35}$$

$$\dot{\boldsymbol{I}}_{\boldsymbol{L}} = \boldsymbol{L}^{-1}\boldsymbol{\Gamma}\boldsymbol{U}_{\boldsymbol{N}} - \boldsymbol{L}^{-1}\boldsymbol{R}\boldsymbol{I}_{\boldsymbol{L}}. \tag{2.36}$$

To solve these state-space equations they can be molded into the form of

$$\dot{\boldsymbol{x}} = \boldsymbol{A}\boldsymbol{x} + \boldsymbol{B}\boldsymbol{u}, \tag{2.37}$$

$$\boldsymbol{y} = \boldsymbol{D}\boldsymbol{x} + \boldsymbol{E}\boldsymbol{u}, \tag{2.38}$$

where $\boldsymbol{x}$ is the set of state variables, $\boldsymbol{u}$ is the set of input variables, $\boldsymbol{y}$ are the output variables, and $\boldsymbol{A}$, $\boldsymbol{B}$, $\boldsymbol{D}$ and $\boldsymbol{E}$ are the state-space matrices.

The state variables and input variables for different conductors are grouped by node or line, and are composed as

$$\boldsymbol{x} = \begin{bmatrix} U_{1,1} & U_{1,2} & \cdots & U_{n,m} & I_{1,1} & I_{1,2} & \cdots & I_{l,m} \end{bmatrix}, \tag{2.39}$$

$$\boldsymbol{u} = \begin{bmatrix} I_{N,1,1} & I_{N,1,2} & \cdots & I_{N,n,m} \end{bmatrix}, \tag{2.40}$$

where $U_{i,k}$ is the voltage of conductor k at node i, $I_{j,k}$ is the current flowing in conductor k of distribution line j, and $I_{N,i,k}$ is the total current flowing from converter(s) into conductor k of node i.

Subsequently, from (2.35) and (2.36), the $\boldsymbol{A}$, $\boldsymbol{B}$, $\boldsymbol{D}$, and $\boldsymbol{E}$ matrices for the state-space equations are then derived as

$$\boldsymbol{A} = \begin{bmatrix} -\boldsymbol{C}^{-1}\boldsymbol{G} & -\boldsymbol{C}^{-1}\boldsymbol{\Gamma}^{\boldsymbol{T}} \\ \boldsymbol{L}^{-1}\boldsymbol{\Gamma} & -\boldsymbol{L}^{-1}\boldsymbol{R} \end{bmatrix}, \tag{2.41}$$

$$\boldsymbol{B} = \begin{bmatrix} \boldsymbol{C}^{-1} \\ \boldsymbol{\emptyset} \end{bmatrix}, \tag{2.42}$$

$$\boldsymbol{D} = \boldsymbol{I}, \tag{2.43}$$

$$\boldsymbol{E} = \boldsymbol{\emptyset}, \tag{2.44}$$

where $\boldsymbol{\emptyset}$ indicates an empty matrix and $\boldsymbol{I}$ indicates an identity matrix.

The impedance matrices ($\boldsymbol{R}$ and $\boldsymbol{L}$) and the admittance matrices ($\boldsymbol{G}$ and $\boldsymbol{C}$) are formed using the impedance and admittance matrices of the distribution lines. The general form of these matrices is

$$\boldsymbol{R_{L,j}} = \begin{bmatrix} R_1 & 0 & \cdots & 0 \\ 0 & \ddots & \ddots & \vdots \\ \vdots & \ddots & \ddots & 0 \\ 0 & \cdots & 0 & R_m \end{bmatrix}, \tag{2.45}$$

$$\boldsymbol{L_{L,j}} = \begin{bmatrix} L_{11} & M_{12} & \cdots & M_{1m} \\ M_{21} & L_{22} & \ddots & \vdots \\ \vdots & \ddots & \ddots & M_{(m-1)m} \\ M_{m1} & \cdots & M_{m(m-1)} & L_{mm} \end{bmatrix}, \tag{2.46}$$

$$\boldsymbol{C_{L,j}} = \begin{bmatrix} \sum_{k=1}^{m} C_{1k} & -C_{12} & \cdots & -C_{1m} \\ -C_{21} & \sum_{k=1}^{m} C_{2k} & \ddots & \vdots \\ \vdots & \ddots & \ddots & -C_{(m-1)m} \\ -C_{m1} & \cdots & -C_{m(m-1)} & \sum_{k=1}^{m} C_{mk} \end{bmatrix}, \tag{2.47}$$

$$\boldsymbol{G_{L,j}} = \begin{bmatrix} \sum_{k=1}^{m} G_{1k} & -G_{12} & \cdots & -G_{1m} \\ -G_{21} & \sum_{k=1}^{m} G_{2k} & \ddots & \vdots \\ \vdots & \ddots & \ddots & -G_{(m-1)m} \\ -G_{m1} & \cdots & -G_{m(m-1)} & \sum_{k=1}^{m} G_{mk} \end{bmatrix}, \tag{2.48}$$

where the elements of $\boldsymbol{R_{L,j}}$ $\boldsymbol{L_{L,j}}$, $\boldsymbol{C_{L,j}}$ and $\boldsymbol{G_{L,j}}$ indicate resistance, (mutual) inductance, capacitance and conductance of the distribution lines' conductors. The elements of these matrices for a bipolar line can be found in Figure 2.5

Subsequently, since a type of π-model is used the capacitance and conductance matrices of each node can be found by summing half of the capacitance and conductance of each distribution line connected to it. Accordingly,

$$\boldsymbol{C_{N,i}} = \frac{1}{2} \sum_{j=1}^{l} \boldsymbol{C_{L,j}} \; [\boldsymbol{\gamma}(j,i) \neq 0], \tag{2.49}$$

$$\boldsymbol{G_{N,i}} = \frac{1}{2} \sum_{j=1}^{l} \boldsymbol{G_{L,j}} \; [\boldsymbol{\gamma}(j,i) \neq 0]. \tag{2.50}$$

If any external capacitance or conductance (such as grounding) is added to the network they can also be incorporated in these equations.

Finally, the impedance and admittance matrices that are used in the state-space equations are formed according to

$$\boldsymbol{R} = \begin{bmatrix} \boldsymbol{R_{L,1}} & 0 & \cdots & 0 \\ 0 & \ddots & \ddots & \vdots \\ \vdots & \ddots & \ddots & 0 \\ 0 & \cdots & 0 & \boldsymbol{R_{L,l}} \end{bmatrix}, \tag{2.51}$$

$$\boldsymbol{L} = \begin{bmatrix} \boldsymbol{L_{L,1}} & 0 & \cdots & 0 \\ 0 & \ddots & \ddots & \vdots \\ \vdots & \ddots & \ddots & 0 \\ 0 & \cdots & 0 & \boldsymbol{L_{L,l}} \end{bmatrix}, \tag{2.52}$$

$$\boldsymbol{C} = \begin{bmatrix} \boldsymbol{C_{N,1}} & 0 & \cdots & 0 \\ 0 & \ddots & \ddots & \vdots \\ \vdots & \ddots & \ddots & 0 \\ 0 & \cdots & 0 & \boldsymbol{C_{N,n}} \end{bmatrix}, \tag{2.53}$$

$$\boldsymbol{G} = \begin{bmatrix} \boldsymbol{G_{N,1}} & 0 & \cdots & 0 \\ 0 & \ddots & \ddots & \vdots \\ \vdots & \ddots & \ddots & 0 \\ 0 & \cdots & 0 & \boldsymbol{G_{N,n}} \end{bmatrix}. \tag{2.54}$$

The presented state-space method for the distribution network allows for the employment of any convenient converter model. This is achieved through the input vector $\boldsymbol{I_N}$ of the state-space model and the output vector containing the node voltages and line currents. In this thesis, the models that are depicted in Appendix B are used in conjunction with this model.

2.4.2 Simulation of a Bipolar DC Distribution Grid

For illustrative purposes, the bipolar dc distribution grid shown in Figure 2.2 is simulated in this section. During the simulation, the voltage is regulated by a droop controlled converter at node n_1 with a chosen droop constant of 1050 W/V, while the converters at the other nodes control their output power. The converters are modeled with the average model presented in Appendix B. Furthermore, the line parameters that are used for the simulation are typical values for 100 m distribution lines, which can be found in Table A.2.

The scenario for which this distribution grid is simulated is shown in Table 2.3. The reference voltage and droop constant of the droop controlled converter remain constant, while the other converters change their output power at varying times.

t [ms]	U_1^* [V]	P_2^* [W]	P_3^* [W]	P_4^* [W]	P_5^* [W]
0	700	0	0	0	0
10	700	1500	0	0	0
20	700	1500	0	0	-1500
30	700	1500	-3000	0	-1500
40	700	1500	-3000	2250	-1500
50	700	1500	-3000	2250	-1500

Table 2.3: Scenario for the simulation of the bipolar dc distribution system

The resulting node voltages and line currents for this scenario are shown in Figure 2.8. Because this system is balanced, the negative pole quantities are identical but opposite in sign to the positive pole quantities and the neutral quantities are zero, therefore for clarity's sake only the positive pole quantities are shown.

From the node voltages and line currents it is seen that the system is stable and power is exchanged according to the scenario. It is seen that, because of the droop control, the voltage in the system is closely related to the power demanded from, or supplied to, the system. Furthermore, the currents in the system show oscillations that are caused by the interaction of the converters' output capacitors and the distribution lines' inductance.

Since the network is connected in a star configuration with respect to the voltage regulated node and is otherwise symmetrical, between 0.02 s and 0.03s the steady-state current in lines l_2 and l_3 becomes negligible. Furthermore, the voltage in the system returns to around the reference voltage in this case.

Interestingly, the currents flowing in the lines connected to the droop controlled converter have a significantly longer time constant than the currents flowing in the lines between the constant power controlled converters. This is because the time constant formed by the droop impedance and the capacitance in the system is much slower than the time constants of the lines themselves.

2.4.3 Discussion

The state-space approach to modeling dc distribution systems presented in this section has a couple of distinct advantages over other methods. Firstly, the same model can be used for systems with any number of nodes, lines and conductors and in any configuration, because of the generalized approach to describing the system according to its incidence matrix. Secondly, the state-space matrices can be derived programmatically by following the procedures outlined in (2.45) to (2.54), making it possible to simplify and automate the modeling. Lastly, due to the mathematical nature of the approach, the model allows for the algebraic analysis of, for example, the stability and control of dc distribution systems.

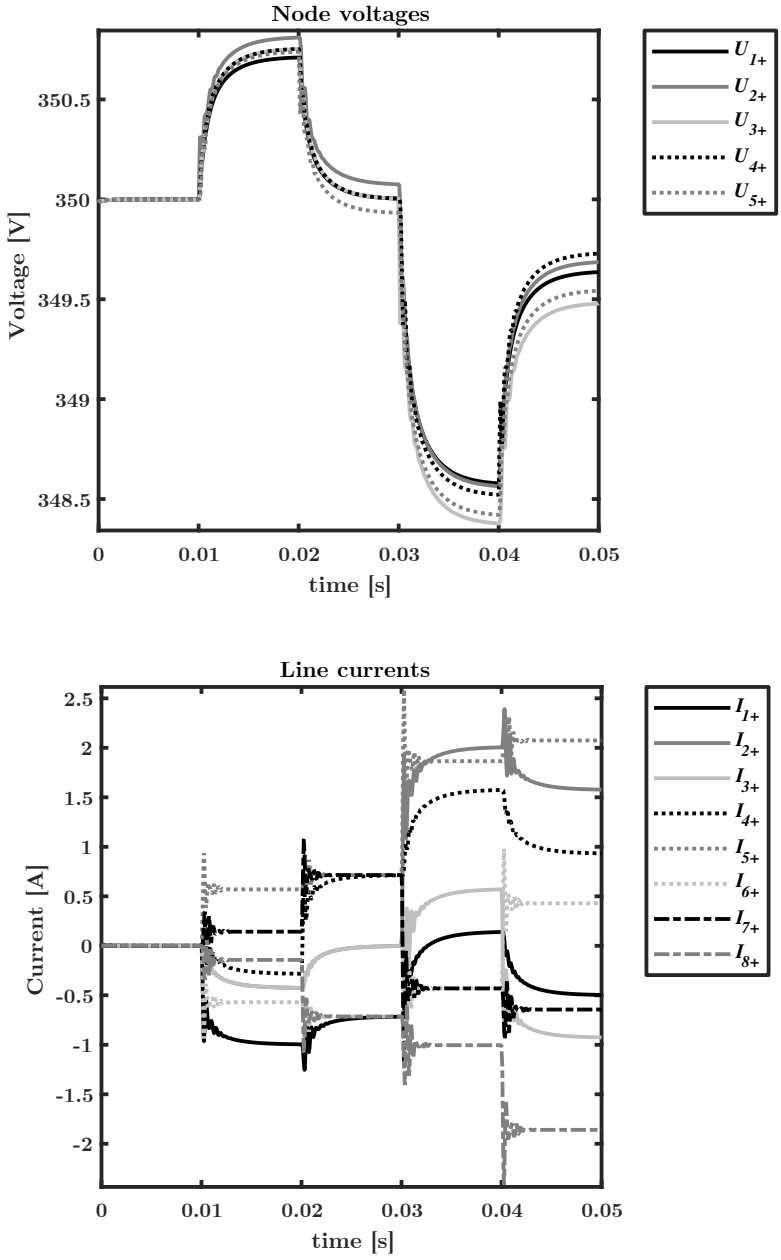

Figure 2.8: Node voltages and line currents of the bipolar dc distribution grid for the given scenario

2.5 Symmetrical Component Decomposition

Bipolar grids are becoming the norm for dc grids. The main advantages of bipolar grids are the relatively low voltage rating of the lines, flexibility and redundancy [13, 64]. However, since bipolar systems have multiple conductors there is a possibility of imbalance. If the current flowing in the positive pole is not exactly opposite to the current flowing in the negative pole, a current will flow in the neutral conductor. Consequently, a neutral conductor will be required as ground currents are generally not allowed because they cause corrosion [35].

In ac distribution systems the symmetrical component decomposition method has become a typical tool to simplify the analysis of complex power networks [65]. The symmetrical component decomposition method simplifies the analysis of (un)balanced systems, and short circuit or ground faults. Therefore, it is compelling to see if a similar technique can be applied to dc distribution grids.

Previous research decomposed bipolar dc distribution grid into a common mode and a differential mode [66, 67]. However, the transformation only takes the positive and negative pole quantities into account. Therefore, the neutral is neglected unless significant assumptions are made. Furthermore, the voltages taken for the transformation are the voltages of the poles with respect to the neutral. As a result, the information of the neutral voltage, and therefore the voltages of the poles with respect to ground, is lost in the transformation. Consequently, no capacitance or conductance to ground can be taken into account.

In this section an improved method to decompose bipolar dc distribution systems into symmetrical components is presented. The improved method inherently includes the neutral quantities, capacitance and conductance to ground, and allows for ground fault analysis. Furthermore, a generalized method is presented to transform network components to the symmetrical domain. Additionally, several equivalent circuits of various (a)symmetrical faults are presented.

2.5.1 Symmetrical Component Decomposition Background

Any asymmetrical set of N co-planar vectors can be represented by a symmetrical set of N vectors [68]. As a result, three phase ac systems are commonly decomposed into their zero sequence, negative sequence and positive sequence according to

$$\begin{bmatrix} X_0 \\ X_1 \\ X_2 \end{bmatrix} = \frac{1}{3} \begin{bmatrix} 1 & 1 & 1 \\ 1 & \alpha & \alpha^2 \\ 1 & \alpha^2 & \alpha \end{bmatrix} \begin{bmatrix} X_a \\ X_b \\ X_c \end{bmatrix}, \tag{2.55}$$

where $\alpha = e^{j2\pi/3}$ and X is any variable (e.g., current or voltage).

Firstly, the positive sequence (X_2) represents a system of 3 phases of equal magnitude that are displaced 120 degrees with respect to each other. Secondly, the negative sequence (X_1) represents a system of 3 phases that are perfectly displaced 120 degrees in the opposite (phase) direction. Lastly, the 3 phases of the zero sequence (X_0) are equal in magnitude and are in phase. This is shown schematically in Figure 2.9.

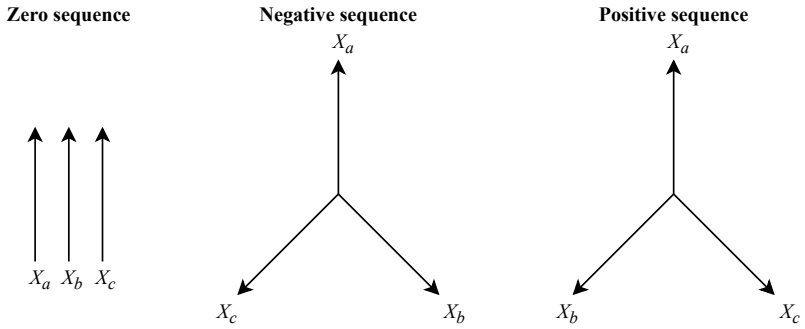

Figure 2.9: Symmetrical component decomposition of ac systems

Bipolar dc systems where the neutral is solidly grounded, although very different from the ac systems, can be seen as 2 phase systems, where the positive and negative poles are the phases. This potentially asymmetrical system can therefore be decomposed in a symmetrical set of 2 vectors.

The symmetrical set of vectors contains one vector that represents the balanced component of the system, the differential mode, and one vector that represents the unbalanced component of the system, the common mode [66,67]. By choosing $\alpha = e^{j\pi}$, this system can be decomposed into symmetrical components utilizing

$$\begin{bmatrix} X_1 \\ X_2 \end{bmatrix} = \frac{1}{2} \begin{bmatrix} 1 & 1 \\ 1 & -1 \end{bmatrix} \begin{bmatrix} X_+ \\ X_- \end{bmatrix}, \tag{2.56}$$

where X_1 and X_2 are the unbalanced and balanced symmetrical components respectively, while X_+ and X_- are the positive and negative pole quantities respectively [66, 67].

The inverse of this symmetrical components transformation is

$$\begin{bmatrix} X_+ \\ X_- \end{bmatrix} = \begin{bmatrix} 1 & 1 \\ 1 & -1 \end{bmatrix} \begin{bmatrix} X_1 \\ X_2 \end{bmatrix}. \tag{2.57}$$

However, this approach to decomposing dc distribution grids into symmetrical components has several disadvantages when a distribution system with a metallic return is modeled.

A distribution line model of a solidly grounded bipolar system is given in Figure 2.10 as an example. The series resistance ($\boldsymbol{R}_\pm$) and inductance ($\boldsymbol{L}_\pm$), and shunt

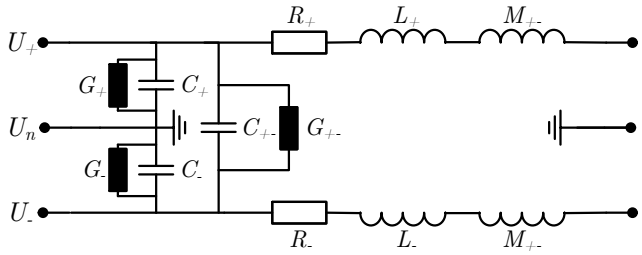

Figure 2.10: Lumped element model of a solidly grounded bipolar distribution line

capacitance ($\boldsymbol{C}_\pm$) and conductance ($\boldsymbol{G}_\pm$) matrices of this model are

$$\boldsymbol{R}_\pm = \begin{bmatrix} R_+ & 0 \\ 0 & R_- \end{bmatrix}, \tag{2.58}$$

$$\boldsymbol{L}_\pm = \begin{bmatrix} L_+ & M_{+-} \\ M_{+-} & L_- \end{bmatrix}, \tag{2.59}$$

$$\boldsymbol{C}_\pm = \begin{bmatrix} C_+ + C_{+-} & -C_{+-} \\ -C_{+-} & C_- + C_{+-} \end{bmatrix}, \tag{2.60}$$

$$\boldsymbol{G}_\pm = \begin{bmatrix} G_+ + G_{+-} & -G_{+-} \\ -G_{+-} & G_- + G_{+-} \end{bmatrix}, \tag{2.61}$$

where the diagonal elements in the series matrices arise from voltage drops caused by the current in that conductor and the diagonal elements originate from voltage drops caused by currents in other conductors (e.g., via mutual inductance). The diagonal elements of the shunt matrices stem from the sum of the connected components through which current is leaked and the diagonal elements indicate to where these components are connected.

For the distribution lines the resistance is characterized according to the voltage drop over the distribution line

$$\Delta\boldsymbol{U} = \boldsymbol{R}\boldsymbol{I}, \tag{2.62}$$

where $\Delta\boldsymbol{U}$ is the voltage drop over the distribution line.

The step by step derivation of the resistance matrix in the symmetrical domain is

$$\boldsymbol{A}^{-1}\Delta\boldsymbol{U}_{12} = \boldsymbol{R}_\pm\boldsymbol{A}^{-1}\boldsymbol{I}_{12}, \tag{2.63}$$

$$\Delta\boldsymbol{U}_{12} = \boldsymbol{A}\boldsymbol{R}_\pm\boldsymbol{A}^{-1}\boldsymbol{I}_{12}, \tag{2.64}$$

$$\boldsymbol{R}_{12} = \boldsymbol{A}\boldsymbol{R}_\pm\boldsymbol{A}^{-1}, \tag{2.65}$$

where $\boldsymbol{A}$ is the symmetrical component transformation matrix from (2.56), the $\pm$ subscript indicates the original pole domain, and the 12 subscript indicates the symmetrical domain.

In a similar fashion the inductance, capacitance and conductance matrices in the symmetrical domain are derived to be

$$\boldsymbol{L}_{12} = \boldsymbol{A}\boldsymbol{L}_{\pm}\boldsymbol{A}^{-1}, \tag{2.66}$$

$$\boldsymbol{C}_{12} = \boldsymbol{A}\boldsymbol{C}_{\pm}\boldsymbol{A}^{-1}, \tag{2.67}$$

$$\boldsymbol{G}_{12} = \boldsymbol{A}\boldsymbol{G}_{\pm}\boldsymbol{A}^{-1}. \tag{2.68}$$

Equations (2.65) to (2.68) are used to compute the system's matrices in the symmetrical domain. The matrices in the symmetrical domain of the line shown in Figure 2.10, given that the distribution lines are symmetrical (e.g., $R_+ = R_-$, $L_+ = L_-$, $C_+ = C_-$ and $G_+ = G_-$), are

$$\boldsymbol{R}_{12} = \begin{bmatrix} R_+ & 0 \\ 0 & R_+ \end{bmatrix}, \tag{2.69}$$

$$\boldsymbol{L}_{12} = \begin{bmatrix} L_+ + M_{+-} & 0 \\ 0 & L_+ - M_{+-} \end{bmatrix}, \tag{2.70}$$

$$\boldsymbol{C}_{12} = \begin{bmatrix} C_+ & 0 \\ 0 & C_+ + 2C_{+-} \end{bmatrix}, \tag{2.71}$$

$$\boldsymbol{G}_{12} = \begin{bmatrix} G_+ & 0 \\ 0 & G_+ + 2G_{+-} \end{bmatrix}. \tag{2.72}$$

From (2.69) to (2.72) it is seen that the currents and voltages in the symmetrical domain are independent. Independent means that no (mutual) coupling occurs between the two components. The independence of the symmetrical domain circuit is further illustrated by the equivalent circuit in Figure 2.11.

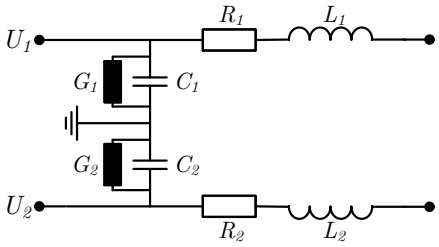

Figure 2.11: Equivalent circuit of the solidly grounded bipolar distribution line model in the symmetrical domain

2.5.2 Improved Symmetrical Component Decomposition

In the previous section it is assumed that the neutral current passes through ground. However, this is usually not allowed as this causes corrosion. Therefore, generally a metallic return (neutral conductor) is used. Under the assumption that the neutral

conductor carries both the current of the positive and negative pole, the currents can be represented by

$$\begin{bmatrix} I_+ \\ I_n \\ I_- \end{bmatrix} = \begin{bmatrix} 1 & 0 \\ -1 & -1 \\ 0 & 1 \end{bmatrix} \begin{bmatrix} I_+ \\ I_- \end{bmatrix}. \tag{2.73}$$

The assumption in (2.73) and its inverse can be used to incorporate the neutral conductor quantities into the symmetrical domain. However, in this section it is suggested to modify the transform to directly include the neutral conductor. The transform matrices then become

$$\boldsymbol{A'} = \boldsymbol{A} \cdot \frac{1}{3} \begin{bmatrix} 2 & -1 & -1 \\ -1 & -1 & 2 \end{bmatrix} = \frac{1}{6} \begin{bmatrix} 1 & -2 & 1 \\ 3 & 0 & -3 \end{bmatrix}, \tag{2.74}$$

$$\boldsymbol{A'}^{-1} = \begin{bmatrix} 1 & 0 \\ -1 & -1 \\ 0 & 1 \end{bmatrix} \boldsymbol{A}^{-1} = \begin{bmatrix} 1 & 1 \\ -2 & 0 \\ 1 & -1 \end{bmatrix}. \tag{2.75}$$

Although this modified transformation does directly take the neutral conductor into account, and allows for the inclusion of capacitance and conductance to ground, it is based on two major assumptions: it is assumed that the neutral voltage is exactly opposite to twice the unbalanced component voltage, and that the neutral current is exactly opposite to twice the unbalanced component current. These assumptions are only valid if the neutral conductor is symmetrical with both pole conductors. However, this is not the case if there are any asymmetries in the system.

Therefore, it is proposed to view the bipolar dc distribution system as a 3 vector system and accordingly decompose it into 3 symmetrical components instead of 2. The proposed transformation is

$$\begin{bmatrix} X_0 \\ X_1 \\ X_2 \end{bmatrix} = \frac{1}{\sqrt{6}} \begin{bmatrix} \sqrt{2} & \sqrt{2} & \sqrt{2} \\ 1 & -2 & 1 \\ \sqrt{3} & 0 & -\sqrt{3} \end{bmatrix} \begin{bmatrix} X_+ \\ X_n \\ X_- \end{bmatrix}, \tag{2.76}$$

where X_0, X_1 and X_2 are the bias, unbalanced and balanced symmetrical components of the system respectively.

The bias component represents an equal dc offset of the pole and neutral quantities, while the unbalanced and balanced components are the same as previously described. The inverse of this transformation is

$$\begin{bmatrix} X_+ \\ X_n \\ X_- \end{bmatrix} = \frac{1}{\sqrt{6}} \begin{bmatrix} \sqrt{2} & 1 & \sqrt{3} \\ \sqrt{2} & -2 & 0 \\ \sqrt{2} & 1 & -\sqrt{3} \end{bmatrix} \begin{bmatrix} X_0 \\ X_1 \\ X_2 \end{bmatrix}. \tag{2.77}$$

The added bias component transformation and the modification of the balanced component transformation are chosen in such a way that if there is asymmetry in the system the symmetrical domain matrices are still symmetrical. Moreover, the transformation is orthogonal and power invariant.

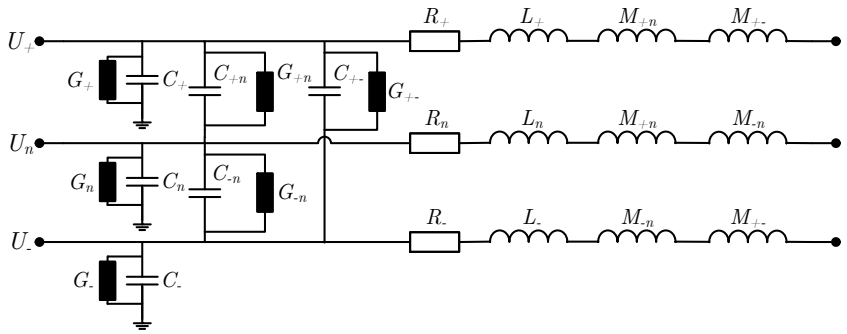

Figure 2.12: Lumped element model of a bipolar distribution line with a metallic return

An example of a bipolar distribution line model with a metallic return is given in Figure 2.12. The resistance, capacitance, inductance and conductance matrices of this line model are

$$\boldsymbol{R}_{\pm} = \begin{bmatrix} R_+ & 0 & 0 \\ 0 & R_n & 0 \\ 0 & 0 & R_- \end{bmatrix}, \tag{2.78}$$

$$\boldsymbol{C}_{\pm} = \begin{bmatrix} \sum\limits_{i=+,n,-} C_{+i} & -C_{+n} & -C_{+-} \\ -C_{+n} & \sum\limits_{i=+,n,-} C_{ni} & -C_{-n} \\ -C_{+-} & -C_{-n} & \sum\limits_{i=+,n,-} C_{-i} \end{bmatrix}, \tag{2.79}$$

$$\boldsymbol{L}_{\pm} = \begin{bmatrix} L_+ & M_{+n} & M_{+-} \\ M_{+n} & L_n & M_{-n} \\ M_{+-} & M_{-n} & L_- \end{bmatrix}, \tag{2.80}$$

$$\boldsymbol{G}_{\pm} = \begin{bmatrix} \sum\limits_{i=+,n,-} G_{+i} & -G_{+n} & -G_{+-} \\ -G_{+n} & \sum\limits_{i=+,n,-} G_{ni} & -G_{-n} \\ -G_{+-} & -G_{-n} & \sum\limits_{i=+,n,-} G_{-i} \end{bmatrix}. \tag{2.81}$$

The system's matrices in the symmetrical domain can be determined analogously to (2.65) to (2.68). For example, the series resistance matrix in the symmetrical domain is determined by

$$\boldsymbol{R}_{012} = \boldsymbol{T}\boldsymbol{R}_{\pm}\boldsymbol{T}^{-1}, \tag{2.82}$$

where the symmetrical transformation matrix $\boldsymbol{T}$ is obtained from (2.76), subscript 012 indicates the symmetrical domain, and the $\pm$ subscript still indicates the (original) pole domain.

Consequently, the system's matrices in the symmetrical domain, in the case the distribution lines are symmetrical, are

$$\boldsymbol{R}_{012} = \begin{bmatrix} R_+ & 0 & 0 \\ 0 & R_+ & 0 \\ 0 & 0 & R_+ \end{bmatrix}, \tag{2.83}$$

$$\boldsymbol{L}_{012} = \begin{bmatrix} L_+ + 2M_{+n} & 0 & 0 \\ 0 & L_+ - M_{+n} & 0 \\ 0 & 0 & L_+ - M_{+n} \end{bmatrix}, \tag{2.84}$$

$$\boldsymbol{C}_{012} = \begin{bmatrix} C_+ & 0 & 0 \\ 0 & C_+ + 3C_{+n} & 0 \\ 0 & 0 & C_+ + C_{+n} + 2C_{+-} \end{bmatrix}, \tag{2.85}$$

$$\boldsymbol{G}_{012} = \begin{bmatrix} G_+ & 0 & 0 \\ 0 & G_+ + 3G_{+n} & 0 \\ 0 & 0 & G_+ + G_{+n} + 2G_{+-} \end{bmatrix}. \tag{2.86}$$

From these matrices it can be seen that the bias, unbalanced and balanced components are again fully independent. Additionally, it can be noted that this transform exhibits similarities to the symmetrical decomposition of symmetrical 3 phase ac distribution lines.

The equivalent circuits in the symmetrical domain, in case the transmission lines are symmetrical, can be derived from (2.83) to (2.86) and are shown in Figure 2.13. The symmetrical domain parameters in this figure (e.g., R_0, L_0, C_0 and G_0) are obtained from (2.83) to (2.86).

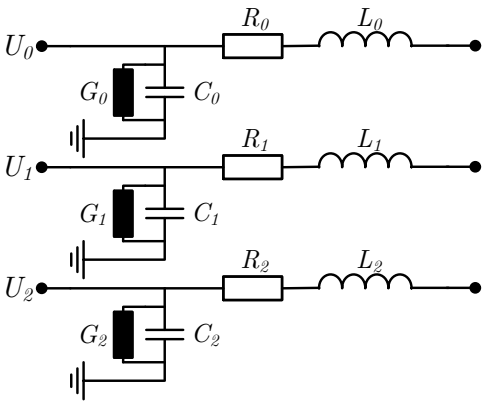

Figure 2.13: Equivalent circuit of the symmetric bipolar distribution line model with metallic return in the symmetrical domain

Consequently, the (dynamic) analysis of dc distribution systems can be significantly simplified by using the symmetrical component decomposition method. If a

balanced system is analyzed only the balanced component has to be investigated compared to the positive, neutral and negative components in the original pole domain. For simulations this means a reduction of the variables by two thirds. Similarly, for unbalanced systems only the balanced and unbalanced component have to be investigated. Moreover, the system matrices are sparse further simplifying computation for unbalanced systems.

Sources and Loads in the Symmetrical Domain

The behavior of most nodes (loads and sources) in dc distribution systems can be modeled as a combination of an output capacitance, a voltage source with a (virtual) series resistance, and current source with a (virtual) shunt resistance. This is illustrated in Figure 2.14.

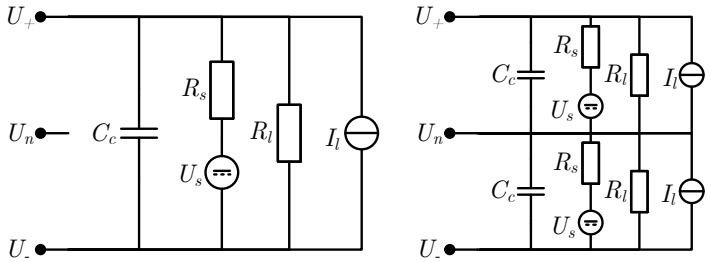

Figure 2.14: Equivalent circuits of the node behavior in the original pole domain

To find the equivalent circuits in the symmetrical domain (2.76), (2.77) and the previously derived transformation method illustrated in (2.82) are used. The equivalent circuits in the symmetrical domain are shown in Figure 2.15.

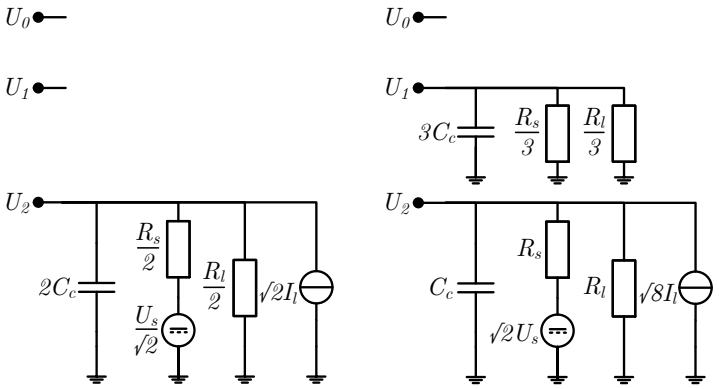

Figure 2.15: Equivalent circuits of the node behavior in the symmetrical domain

2.5.3 Analysis of (A)symmetrical Faults

The previous subsection showed how the symmetrical component decomposition can simplify the dynamic analysis of a bipolar dc distribution grid. Analogously to ac systems, the symmetrical component decomposition can also be employed to determine the fault currents of various (a)symmetrical faults. In this subsection alternative method for determining the steady-state fault currents is presented. This is done by creating Thevenin equivalent circuits of the symmetrical components at the fault location.

To arrive at the equivalent circuits in the symmetrical domain several assumptions have to be made. Firstly, it is assumed that the entire system, besides the fault, is symmetrical. Secondly, it is assumed that the superposition principle can be applied. Therefore, the system's currents, other than the fault current, can be neglected during the analysis of the fault. Thirdly, it is assumed that capacitance and inductance can be neglected in steady-state. Lastly, Thevenin's theorem is applied, which allows for the replacement of the non-faulted part of the system by an equivalent generator and a series resistance for each symmetrical component (see Figure 2.16A).

For several types of faults the circuit in the pole domain and the equivalent circuit in the symmetrical domain are shown in Figure 2.16. The derivation of the pole-to-ground (Figure 2.16B), double pole-to-ground (Figure 2.16C), and pole-to-pole (Figure 2.16D) faults will be given in this subsection.

First, the pole-to-ground fault is analyzed. It is important to differentiate the voltage at the location of the Thevenin equivalent sources (E) and at the location where the fault occurs (U). Accordingly, during the pole-to-ground fault

$$E'_+ = R'_+ I_+ + U_+ = R'_+ I_+ + R_f I_f, \tag{2.87}$$

where E'_+ and R'_+ are the Thevenin equivalents in the pole domain, I_f is the fault current and R_f is the fault resistance.

This equation can be solved without knowing the pole domain Thevenin equivalent parameters. Applying the transformations (2.76) and (2.77) to (2.87) results in

$$\frac{E_0}{\sqrt{3}} + \frac{E_1}{\sqrt{6}} + \frac{E_2}{\sqrt{2}} = R_f I_f + \frac{R_0 I_0}{\sqrt{3}} + \frac{R_1 I_1}{\sqrt{6}} + \frac{R_2 I_2}{\sqrt{2}}, \tag{2.88}$$

where the numbered subscripts denote that the quantities are in the symmetrical domain.

The fault current is equal to the current in the positive pole, while the currents in the neutral and negative pole conductor are 0 A. Therefore, using (2.76) to transform these currents to the symmetrical domain gives

$$I_f = \sqrt{3} I_0 = \sqrt{6} I_1 = \sqrt{2} I_2. \tag{2.89}$$

Substituting (2.89) into (2.88) yields

$$I_f = \frac{\frac{E_0}{\sqrt{3}} + \frac{E_1}{\sqrt{6}} + \frac{E_2}{\sqrt{2}}}{R_f + \frac{R_0}{3} + \frac{R_1}{6} + \frac{R_2}{2}}. \tag{2.90}$$

The equivalent circuit in the symmetrical domain is shown in Figure 2.16B.

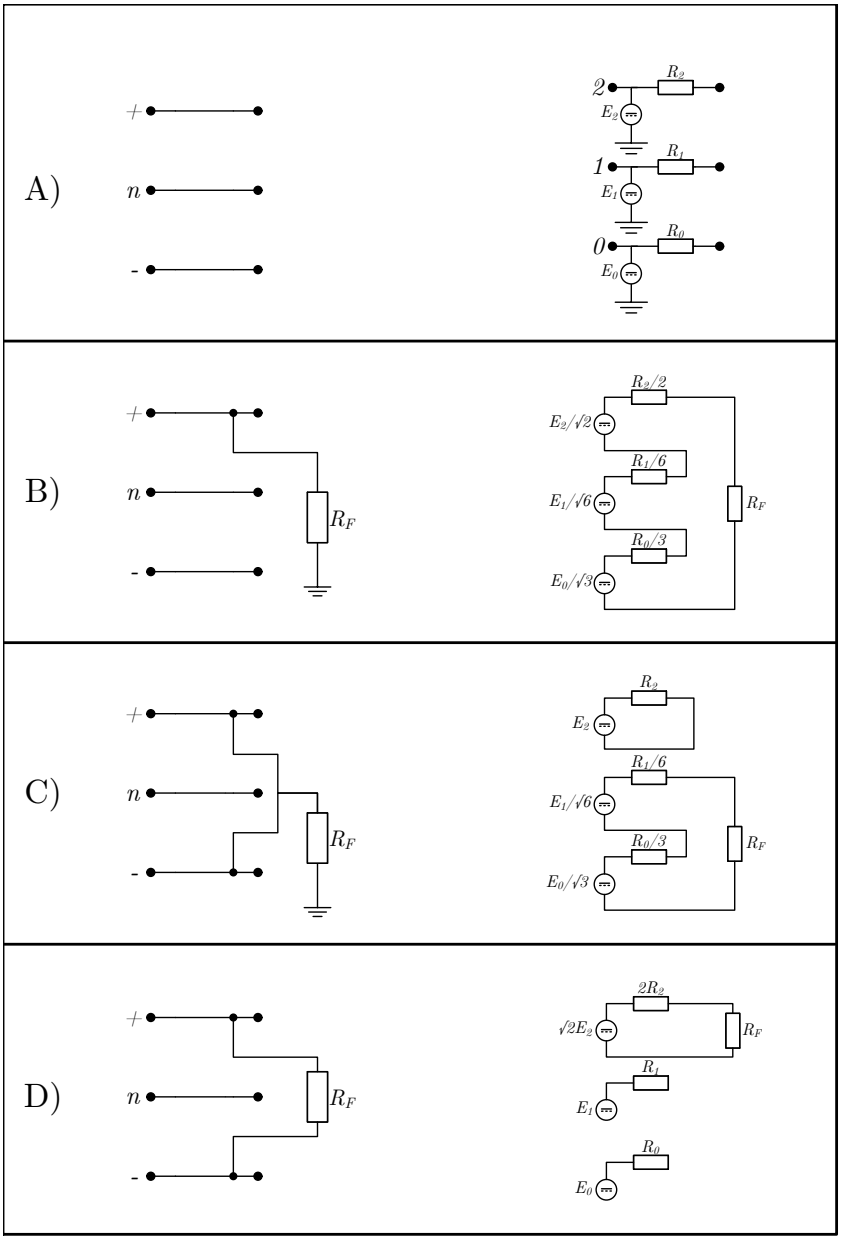

Figure 2.16: Equivalent circuits of (a)symmetrical faults and their equivalent circuits in the symmetrical domain for A) non-faulted systems, B) single phase-to-ground faults, C) double pole-to-ground faults and D) pole-to-pole faults

For the double pole-to-ground fault (2.88) still holds. However, now the fault current is the addition of both the pole currents. Moreover, since the voltages of the positive and negative pole at the fault location are equal ($U_- = U_+$) the bias component voltage U_2 is 0 V. The currents in the symmetrical domain and the fault current are therefore

$$I_f = \sqrt{3} I_0 = \sqrt{6} I_1, \tag{2.91}$$

$$I_2 = \frac{E_2}{R_2}. \tag{2.92}$$

Substituting (2.91) and (2.92) into (2.88) yields

$$I_f = \frac{\frac{E_0}{\sqrt{3}} + \frac{E_1}{\sqrt{6}}}{R_f + \frac{R_0}{3} + \frac{R_1}{6}}. \tag{2.93}$$

The equivalent circuit in the symmetrical domain is given in Figure 2.16C.

For the pole-to-pole fault the current in the positive pole is opposite to the current in the negative pole. Moreover, the voltage equation must be modified to

$$E'_+ - U_+ - I_+ R'_+ = E'_- + I_- R'_-. \tag{2.94}$$

The current in the positive and negative pole are equal but opposite in sign. Therefore, once again using the transform, the relations between the fault current and the currents in the symmetrical domain are

$$I_0 = I_1 = 0, \tag{2.95}$$

$$I_2 = \sqrt{2} I_f. \tag{2.96}$$

Using the symmetrical component transformations from (2.76) and (2.77) it can be shown that

$$\begin{aligned} &\frac{E_0}{\sqrt{3}} + \frac{E_1}{\sqrt{6}} + \frac{E_2}{\sqrt{2}} - R_f I_f - \frac{R_2 I_2}{\sqrt{2}} = \\ &\frac{E_0}{\sqrt{3}} + \frac{E_1}{\sqrt{6}} - \frac{E_2}{\sqrt{2}} + \frac{R_2 I_2}{\sqrt{2}}. \end{aligned} \tag{2.97}$$

Consequently, using (2.95), (2.96) and (2.97) the fault current is derived to be

$$I_f = \frac{\sqrt{2} E_2}{R_f + 2R_2}. \tag{2.98}$$

The equivalent circuit in the symmetrical domain is shown in Figure 2.16D.

Other faults than the ones depicted in Figure 2.16 are derived in an analogous fashion. From the derivations and equivalent circuits it can be seen that the transform can be used for the analysis of faults in a similar fashion to the ac symmetrical component decomposition method.

2.6 Transient Modeling

Non-transient models often assume a lumped element representation of the distribution line. Typically the Gamma, pi, or T models, shown in Figure 2.4, are used [69]. The lumped element models can be solved by, for example, their differential equations, transfer function, or a state-space representation.

The limitations of (most) lumped element models lie in the neglect of propagation delays and frequency dependent effects. In general, parameters such as resistance, capacitance, conductance and inductance are assumed constant, while in reality they are frequency dependent. Moreover, it is usually assumed that changes at one side of the line are instantly discernible at the other side, while in reality there are propagation delays. The validity of neglecting propagation delays depends on the wavelength of the signal

$$\lambda = \frac{c}{f\sqrt{\epsilon_r \mu_r}}, \tag{2.99}$$

where λ is the wavelength, f is the frequency of the signal, c is the speed of light, and ϵ_r and μ_r are the relative permittivity and relative permeability of the distribution line respectively. Usually it is assumed that propagation delays can be neglected when the length of the distribution line is much smaller than the wavelength of the signal [34].

To circumvent the problem of wavelengths becoming comparable to the lengths of the distribution lines the model can be broken up into smaller pieces which individually have lengths much shorter than the wavelength of the signal. However, solving such a segmented model could quickly become time consuming depending on the required number of subsections [70].

Other models directly take the propagation delay into account in their equations. Popular examples of such models are the Bergeron model and variants of the travelling wave model [70, 71]. For the latter it is required to fit the frequency response of the model to a set of rational functions.

Since transients such as short-circuits often impose high frequency oscillations on the system, models that include propagation delays are often called transient models. The most common transient models are based on distributed lumped element models or travelling wave models. Some specialized transient simulation environments that implement these methods exist such as the PSCAD-EMTDC, EMTP, and ATP software packages. Generally, transient models are more accurate than non-transients models, but are much more complex and require much more computational power and time for a simulation.

Transient models that are specifically designed and optimized for dc systems are imperative for the future research and development of the protection devices and schemes for these systems. However, due to time constraints the development of transient models for dc systems are not inside the scope of these thesis, and therefore remain an open research question.

2.7 Experimental Validation

In the previous sections the novel steady-state models were verified using established power flow methods from literature, and it was shown that the models in the symmetrical domain are mathematically equivalent to the developed dynamic models. In this section an experimental setup is used to verify the state-space modeling method proposed in Section 2.4. For this experiment three power electronic converters are interconnected via three lines in the meshed (ring) configuration, which is depicted in Figure 2.17. Detailed descriptions of the dc sources, converters and line emulation circuits that are used for the experiment are given in Appendix A.

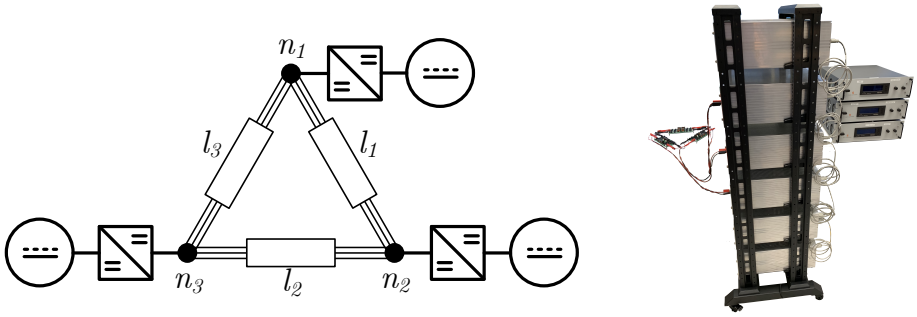

(a) Schematic (b) Picture

Figure 2.17: Experimental setup that is used to verify the state-space modeling method proposed in Section 2.4

For the experiment a droop controlled converter is located at n_1, which the reference input current is given by

$$I_i = \frac{U_d - U_o}{Z_d}, \tag{2.100}$$

where U_d is the reference output voltage and Z_d is the droop impedance. During the experiment U_d and Z_d are set to 350 V and 1 Ω respectively. Furthermore, two constant power controlled converters are located n_2 and n_3. Moreover, the input voltage for all these converters is regulated at 175 V. The reference output power and the droop parameters of these converters over time are given in Table 2.4.

t [ms]	U_d [V]	Z_d [Ω]	P_2^* [W]	P_3^* [W]
-5	350	1	0	0
0	350	1	2100	0
23	350	1	2100	2100

Table 2.4: Scenario of the experiment to verify the state-space modeling method

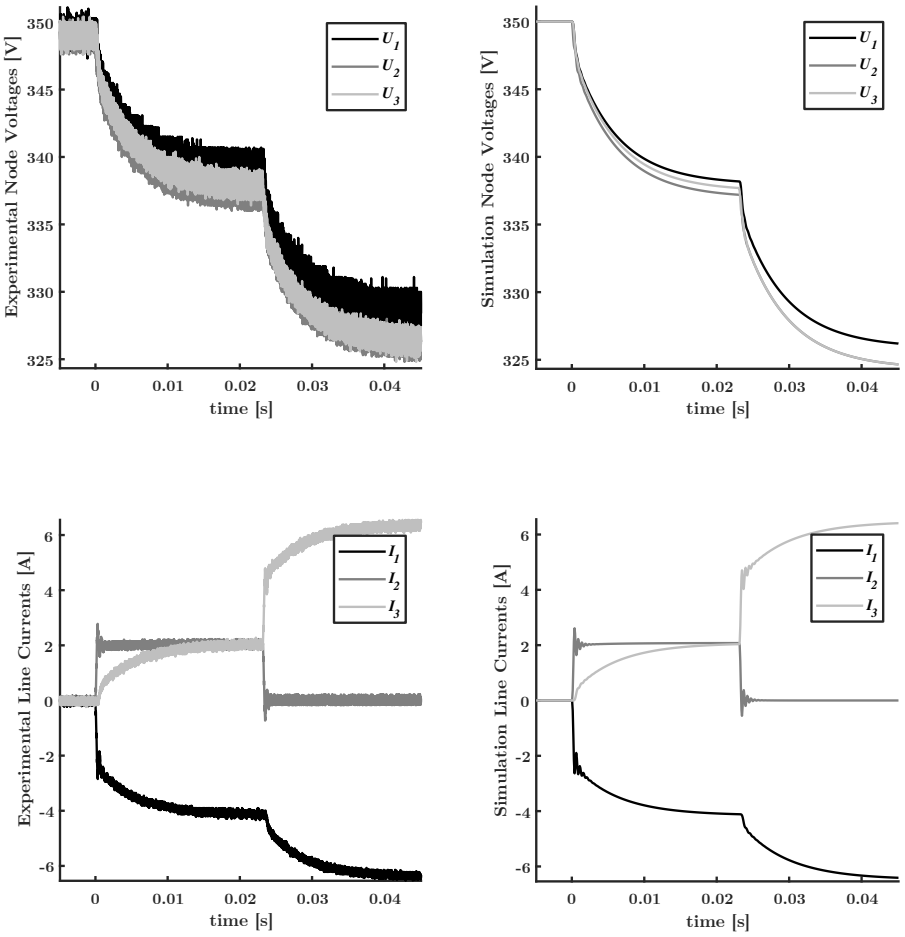

Figure 2.18: Experimental and simulation results for the dc distribution system shown in Figure 2.17 and under the scenario shown in Table 2.4

The experimental and simulation results are given in Figure 2.18. Observe that, for both the simulation and experiment, clear drops in voltage can be seen after a load step occurs, after which the system converges with a slower time constant to the steady-state voltage. Furthermore, the currents show fast current oscillations after the occurrence of a load step, which are caused by the interactions between the converters' output capacitance over the lines' inductance. The oscillations in the experimental results, which are not present in the simulation results, are caused by the voltage and current probes' measurement errors. Overall, the experimental results show that the state-space modeling method and the converter models presented in Appendix B are adequate for modeling larger interconnected systems.

2.8 Conclusions

Models of dc distribution systems are required for the analysis, design and optimization of the markets, stability, control and protection in these systems. In this chapter existing steady-state, dynamic and transient distribution grid models were discussed, and novel and improved models were presented.

It was examined how the power flow of dc distribution systems can be determined by using the Gauss-Seidel, Newton-Rhapson and Backward-Forward methods, and by solving it as a quadratic or optimization problem. Furthermore, two novel iterative methods were presented, which model the non-linear converters as current sources (Direct Matrix - Current Approximation method) or as a current source with an impedance in parallel (Direct Matrix - Impedance Approximation method) and then perform linear iterations to arrive at the power flow solution. It was shown that the Direct Matrix methods require up to 93 % less computational effort than the established methods, while providing similar or better accuracy and convergence. In the future the Direct Matrix methods can be used to significantly reduce the computational effort required for the operation and planning of dc power systems. Moreover, they can be used for stability analysis, optimization routines, market simulations and N-1 security assessments.

The dynamic behavior of dc distribution systems is often modeled via the system's transfer functions or state-space matrices. In this chapter a new approach to composing the state-space models via its nodes, lines, conductors and incidence matrix was presented. In contrast to the dynamic models found in literature, the presented modeling method differentiates between the different conductors in each line and takes their mutual couplings into account. Furthermore, due to the mathematical nature of the model, it allows for the algebraic analysis of, for example, the stability and control of dc distribution systems. Additionally, rapid analysis of various systems can be achieved, since the derivation of the state-space matrices can be automated by utilizing the incidence matrix. Moreover, experimental results showed that the model can accurately predict the dynamic behavior of dc distribution systems.

Previously proposed symmetrical component decomposition methods for bipolar dc distribution systems assume that the neutral is solidly grounded, and decompose the system into two components. Consequently, these models are not able to appropriately model bipolar systems with a metallic neutral, and they cannot be used to perform (ground) fault analysis. To resolve these limitations, it is proposed to decompose the system into three components with transformation matrices that are orthogonal and power invariant. It was demonstrated that the proposed method reduces the number of variables (degrees of freedom) that are required to model dc distribution systems by up to a factor of three. Furthermore, it was shown that it substantially simplifies the analysis of (ground) faults in these systems.

Although solutions were presented in this chapter for the steady-state and dynamic modeling of dc distribution systems, a novel transient model was not presented. For future research and development of protection devices and schemes it is still imperative that a transient model, which is optimized for dc systems, is developed.

Chapter 3

Algebraic and Plug-and-Play Stability

The increasing share of renewable energy generation and constant power loads pose significant challenges on the stability of distribution systems. Therefore, literature on the stability of dc distribution systems is reviewed and novel methods to analyze and ensure stability are developed. In this chapter an algebraic method to analyze the stability of any dc distribution system is presented, which allows for some generalized conclusions on the systems' sensitivity towards system parameters. Furthermore, plug-and-play stability guidelines are derived for dc distribution systems, such that a communication infrastructure and knowledge about the system's topology are not required to achieve global (i.e., system-wide) stability. Experiments showed that additional research into the impedance characteristic of power electronic converters is still vital.

This chapter is based on

- N. H. van der Blij, L. M. Ramirez-Elizondo, M. T. J. Spaan and P. Bauer, "Stability of DC Distribution Systems: An Algebraic Derivation", Energies, vol. 10, Jul. 2017.
- N. H. van der Blij, L. M. Ramirez-Elizondo, M. T. J. Spaan and P. Bauer, "Stability and Decentralized Control of Plug-and-Play DC Distribution Grids", IEEE Access, vol. 6, 2018.

3.1 Introduction

In this chapter, dc distribution systems are considered to be stable if all the voltages and currents in the system converge to a steady-state and all oscillations/disturbances are eventually damped out.

Traditionally speaking, stability is ensured by regulating the supply of conventional generators, which also provide a significant amount of inertia to the grid. However, with the increasing share of renewable energy sources, the inertia of transmission grids and consequently distribution grids is significantly decreased [19]. Therefore, in grids with a substantial share of renewable energy sources, the balance of supply and demand must be ensured on a much shorter time scale than in conventional grids.

Another challenge for the stability is the increasing amount of tightly regulated load converters that behave as constant power loads. Constant power loads have the voltage-current characteristic shown in Figure 3.1. The slope of the characteristic is negative at all currents, which is shown in Figure 3.1 for one operating point. Consequently, when the voltage at the converter's node decreases, the current that the converter draws from the node increases. This behavior can cause voltage instability, but also amplifies oscillations in the grid [20].

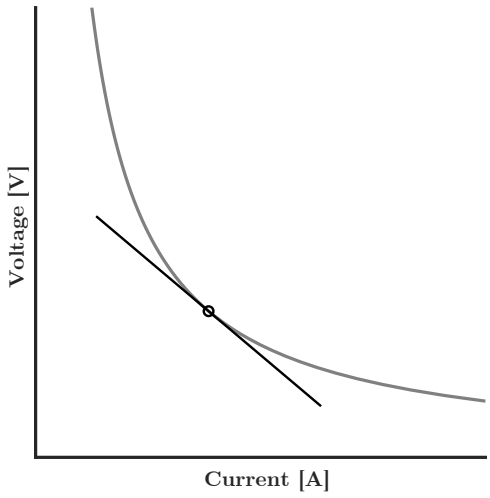

Figure 3.1: Voltage-current characteristic of a power electronic converter with constant power control

In Section 3.2, the small-signal converter models that are used for the stability analysis are presented. In Section 3.3, it is shown how the stability of any dc distribution grid can be determined algebraically. In Section 3.4, stability requirements are derived for plug-and-play grids, utilizing a Brayton-Moser representation. Lastly, in Section 3.5, some of the findings are experimentally verified.

3.2 Small-Signal Converter Model

Several models of power electronic converters have been reported in literature in order to analyze the stability of dc distribution systems. Large-signal models fully describe the non-linear behavior of the system, while small-signal models linearize components at a certain operating point. Since deriving stability from large-signal models for larger dc distribution systems is intractable, small-signal models of power electronic converters are utilized. Most small-signal methods average and/or linearize the power electronic converters, which is reasonably accurate on time frames longer than the switching period of the semiconductors. Furthermore, the bandwidths of these converters are typically lower than one-tenth of the switching frequency. Therefore, inside the control bandwidth, it can be assumed the converters react instantaneously to disturbances in the system [29, 72].

3.2.1 Norton Equivalent Small-Signal Model

In one operating point, the higher level control of power electronic converters can be characterized as a linear combination of constant voltage, current, impedance, or constant power behaviors. While the constant voltage controlled converter can be modeled by an ideal voltage source, other converters can be modeled by the Norton equivalent small-signal model shown in Figure 3.2. This Norton equivalent small-signal model consist of a constant current source I_c, a parallel impedance Z_c and the output capacitance C_c.

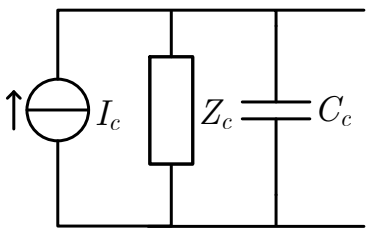

Figure 3.2: Norton equivalent small-signal models for power electronic converters

For example, constant current controlled converters can be implemented by letting the impedance go to infinity, while constant impedance controlled converters can be implemented by letting the current source go to zero.

3.2.2 Droop and Constant Power Controlled Converters

Since it is assumed that power electronic converters react instantaneously within their control bandwidths, droop and constant power controlled converters can be modeled according to their ideal equivalent circuits shown in Figure 3.3 on the left.

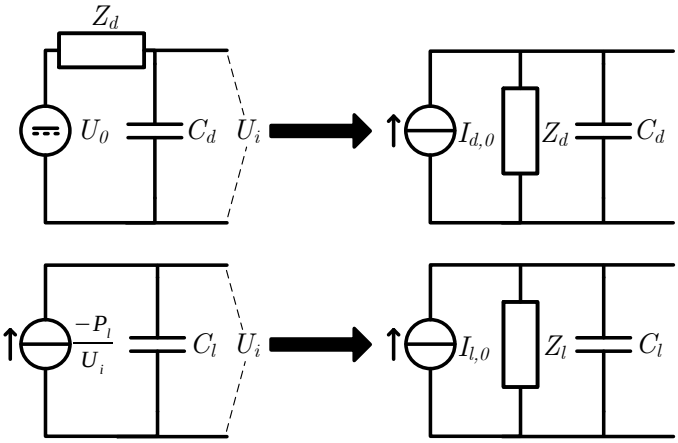

Figure 3.3: Ideal (left) and linearized Norton equivalent circuits (right) for droop (top) and constant power (bottom) controlled converters

The currents flowing from the droop and constant power controlled converters into the nodes they are connected to are respectively given by

$$I_d = \frac{U_0 - U_i}{Z_d}, \tag{3.1}$$

$$I_l = -\frac{P_l}{U_i}, \tag{3.2}$$

where U_0 is the reference voltage, U_i is voltage of the node the converter is connected to, Z_d is the (virtual) impedance of the droop controller, and P_l is the load's power.

The derivation of the Norton equivalent of the droop controlled converter is trivial, while the constant power controlled converter needs to be linearized around the voltage $\overline{U}$. Consequently, the first component of the Taylor series approximation for these converters are given by

$$I_d = \frac{U_0}{Z_d} - \frac{U_i}{Z_d} = I_{d,0} - \frac{U_i}{Z_d}, \tag{3.3}$$

$$I_l = -\frac{2P_l}{\overline{U}} + \frac{P_l}{\overline{U}^2} U_i = I_{l,0} - \frac{U_i}{Z_l}, \tag{3.4}$$

where Z_l is the equivalent impedance of the constant power load converter and $\overline{U}$ is the voltage at which the constant power load is linearized. The equivalent circuits of these (small-signal) models of droop sources and constant power loads are shown in Figure 3.3 on the right.

3.3 Algebraic Derivation of Stability

Four main approaches to analyze the stability of dc distribution grids can be identified. Firstly, the minor loop gain (the relationship between the complex load and source impedance) can be evaluated. Different limits on the minor loop gain have been proposed to ensure stability. However, this approach assumes unidirectional power flow and measurements are essential for accurate impedance estimations [29, 73–75]. Secondly, a root locus analysis of the system can be done and the locations of the poles can be investigated [57, 61, 76–78]. Nevertheless, this approach does not provide mathematical insight into the origin of the (in)stability. Thirdly, an analysis based on Lyapunov methods can be conducted [79–82]. However, these are not easily applied and require a suitable construction of the Lyapunov storage function. Lastly, the roots of the system can be derived from the eigenvalues of its state-space matrix [83–87]. The disadvantage of this method is that the converters need to be linearized.

Previous research often only analyzes specific systems or uses oversimplified models and therefore no generalized conclusions can be derived. For example, only star type systems with a source at the central node are analyzed [86], the node capacitance is not considered in the equations [59], or no (general) conclusions regarding stability are provided [77]. Therefore, any verdicts on the effect of system parameters (e.g. inductance, capacitance and droop coefficients) on the distribution system's stability cannot be generalized.

In this section a generalized method to algebraically analyze the stability of dc distribution systems, regardless of configuration, is presented. The method can be used to derive necessary and sufficient conditions for the stability by determining the system's eigenvalues algebraically.

3.3.1 Stability of Simple DC Distribution Systems

The simplest (potentially unstable) dc distribution grid is a converter that controls the voltage that is connected to a constant power controlled converter via a distribution line. This simple grid, where the constant power load is replaced by its Norton equivalent circuit, is shown in Figure 3.4.

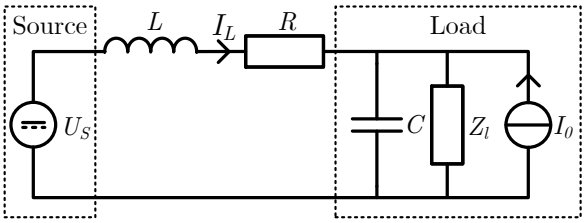

Figure 3.4: Simple dc distribution grid containing a constant voltage source and a constant power load connected via a distribution line

The voltage of the constant power load's output capacitor U_C relates to the net current flowing into the capacitor, and the line current I_L relates to the voltage over its inductor. Therefore, the differential equations are

$$C\dot{U}_C = I_L + I_0 - \frac{U_C}{Z_l}, \tag{3.5}$$

$$L\dot{I}_L = U_S - U_C - RI_L. \tag{3.6}$$

Consequently, the state-space formulation of this system is derived to be

$$\begin{bmatrix} \dot{U}_C \\ \dot{I}_L \end{bmatrix} = \begin{bmatrix} \frac{-1}{CZ_l} & \frac{1}{C} \\ -\frac{1}{L} & -\frac{R}{L} \end{bmatrix} \begin{bmatrix} U_C \\ I_L \end{bmatrix} + \begin{bmatrix} \frac{1}{C} & 0 \\ 0 & \frac{1}{L} \end{bmatrix} \begin{bmatrix} I_0 \\ U_S \end{bmatrix}. \tag{3.7}$$

The characteristic equation and eigenvalues of any matrix $\boldsymbol{A}$ can be found by solving $|\boldsymbol{A} - \lambda \boldsymbol{I}|$ and $(|\boldsymbol{A} - \lambda \boldsymbol{I}| = 0)$ respectively. The determinant of the left-hand matrix, and therefore the characteristic equation of this system, is

$$\lambda^2 + \lambda \left(\frac{R}{L} + \frac{1}{CZ_l} \right) + \frac{1}{LC} + \frac{R}{LCZ_l}. \tag{3.8}$$

Consequently, the poles of the simple example system are given by

$$\lambda = -\frac{R}{2L} - \frac{1}{2CZ_l} \pm \frac{1}{2}\sqrt{\left(\frac{R}{L} + \frac{1}{CZ_l} \right)^2 - 4\left(\frac{1}{LC} + \frac{R}{LCZ_l} \right)}. \tag{3.9}$$

Since any system is considered stable if all poles have negative real parts, this system is considered stable if and only if

$$\frac{R}{L} + \frac{1}{CZ_l} > 0, \tag{3.10}$$

$$\frac{1}{R} + \frac{1}{Z_l} > 0. \tag{3.11}$$

Note that (3.10) ensures that the time constant (or damping) of the line is more than the time constant (or amplification) of the constant power load. Furthermore, (3.11) makes sure that, when the load voltage fluctuates, the change in current from the source is more than the change in current of the load

Another simple dc distribution grid is shown in Figure 3.5. In this case a droop controlled converter is connected to a constant power load converter. The state-space formulation of this dc distribution system is given by

$$\begin{bmatrix} \dot{U}_1 \\ \dot{U}_2 \\ \dot{I}_L \end{bmatrix} = \begin{bmatrix} \frac{-1}{Z_1 C_1} & 0 & \frac{-1}{C_1} \\ 0 & \frac{-1}{Z_2 C_2} & \frac{1}{C_2} \\ \frac{1}{L} & \frac{-1}{L} & \frac{-R}{L} \end{bmatrix} \begin{bmatrix} U_1 \\ U_2 \\ I_L \end{bmatrix} + \begin{bmatrix} \frac{1}{C_1} & 0 \\ 0 & \frac{1}{C_2} \\ 0 & 0 \end{bmatrix} \begin{bmatrix} I_{1,0} \\ I_{2,0} \end{bmatrix}. \tag{3.12}$$

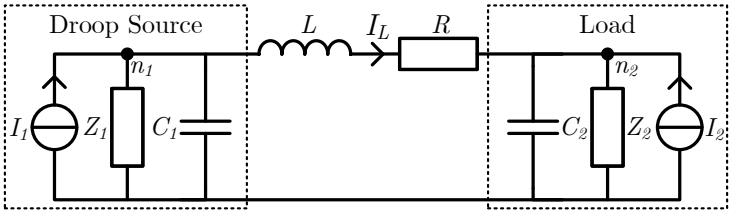

Figure 3.5: Simple dc distribution grid containing a droop controlled source and a constant power load connected via a distribution line

Via the determinant of the state matrix, the characteristic equation is derived to be

$$\lambda^3 + \lambda^2\left(\frac{R}{L} + \frac{1}{C_1 Z_1} + \frac{1}{C_2 Z_2}\right) + \lambda\frac{1}{LC_1C_2}\left(\frac{L}{Z_1Z_2} + \frac{C_2R}{Z_1} + \frac{C_1R}{Z_2} + C_2 + C_1\right) + \frac{1}{LC_1C_2}\left(\frac{R}{Z_1Z_2} + \frac{1}{Z_1} + \frac{1}{Z_2}\right). \tag{3.13}$$

To ensure that all of this system's poles have negative real parts, it is required that all coefficients of the characteristic equation are positive. Therefore, to ensure stability it is required that

$$\frac{R}{L} + \frac{1}{C_1Z_1} + \frac{1}{C_2Z_2} > 0, \tag{3.14}$$

$$\frac{L}{Z_1Z_2} + \frac{C_2R}{Z_1} + \frac{C_1R}{Z_2} + C_2 + C_1 > 0, \tag{3.15}$$

$$\frac{R}{Z_1Z_2} + \frac{1}{Z_1} + \frac{1}{Z_2} > 0. \tag{3.16}$$

In this third order case, one additional condition will make the set of conditions required and sufficient. This additional condition is that the product of the second and third coefficients is greater than the fourth.

If, for the sake of simplicity, the resistance R is neglected and the source is located at n_1, the system presented in Figure 3.5 is stable if and only if

$$|Z_2| > |Z_1|, \tag{3.17}$$

$$C_2|Z_2| > C_1|Z_1|, \tag{3.18}$$

$$C_2 + C_1 > \frac{L}{|Z_1Z_2|}, \tag{3.19}$$

$$\frac{L}{C_2Z_1Z_2^2} + \frac{C_2}{C_1Z_1} > \frac{L}{C_1Z_1^2|Z_2|} + \frac{C_1}{C_2|Z_2|}. \tag{3.20}$$

Observe that these conditions again relate to the time constants in the system and the impedances of the source and load.

3.3.2 Stability of Any DC Distribution System

The approach used in the previous subsection is in this subsection extended for any dc distribution system. To generalize the model for power electronic converters, the current flowing from any converter into the grid is assumed to have the form of

$$I_i = I_{i,0} - \frac{1}{Z_i} U_i, \tag{3.21}$$

where U_i is the voltage at the input terminals, Z_i is the (linearized) impedance and $I_{i,0}$ is the (linearized) output current of the converter. For instance, $I_{i,0}$ and Z_i are positive for droop controlled sources, and negative for constant power loads.

By combining (2.33), (2.34) and (3.21) the state-space formulation for any dc distribution consisting of nodes, distribution lines, and (linearized) power electronic converters is derived to be

$$\begin{bmatrix} \dot{\boldsymbol{U}}_{\boldsymbol{N}} \\ \dot{\boldsymbol{I}}_{\boldsymbol{L}} \end{bmatrix} = \begin{bmatrix} -\boldsymbol{C}^{-1}\boldsymbol{Z}^{-1} & -\boldsymbol{C}^{-1}\boldsymbol{\Gamma}^{\boldsymbol{T}} \\ \boldsymbol{L}^{-1}\boldsymbol{\Gamma} & -\boldsymbol{L}^{-1}\boldsymbol{R} \end{bmatrix} \begin{bmatrix} \boldsymbol{U}_{\boldsymbol{N}} \\ \boldsymbol{I}_{\boldsymbol{L}} \end{bmatrix} + \begin{bmatrix} \boldsymbol{C}^{-1} \\ \boldsymbol{\emptyset} \end{bmatrix} \boldsymbol{I}_{\boldsymbol{N,0}}, \tag{3.22}$$

where $\boldsymbol{Z}$ is the matrix containing the impedances of the power electronic converters and $\boldsymbol{I_{N,0}}$ is the vector of the constant term currents ($I_{i,0}$) from the converters connected to each node.

The Location of the Equilibrium

Besides the stability, the equilibrium (steady-state) of the system can be derived from the state-space equations. In steady-state the time derivatives in the system are zero. The steady-state node voltages and line currents can therefore be determined by

$$\begin{bmatrix} \boldsymbol{U}_{\boldsymbol{N}} \\ \boldsymbol{I}_{\boldsymbol{L}} \end{bmatrix} = \begin{bmatrix} -\boldsymbol{C}^{-1}\boldsymbol{Z}^{-1} & -\boldsymbol{C}^{-1}\boldsymbol{\Gamma}^{\boldsymbol{T}} \\ \boldsymbol{L}^{-1}\boldsymbol{\Gamma} & -\boldsymbol{L}^{-1}\boldsymbol{R} \end{bmatrix}^{-1} \begin{bmatrix} -\boldsymbol{C}^{-1} \\ \boldsymbol{\emptyset} \end{bmatrix} \boldsymbol{I}_{\boldsymbol{N,0}}. \tag{3.23}$$

The inverse of the left-hand state matrix ($\boldsymbol{A}$) can be decomposed as

$$\boldsymbol{A}^{-1} = \begin{bmatrix} \boldsymbol{Z}^{-1} & \boldsymbol{\Gamma}^{\boldsymbol{T}} \\ \boldsymbol{\Gamma} & -\boldsymbol{R} \end{bmatrix}^{-1} \begin{bmatrix} -\boldsymbol{C} & 0 \\ 0 & \boldsymbol{L} \end{bmatrix}. \tag{3.24}$$

Consequently, by substituting (3.24) into (3.23), the steady-state node voltages and line currents are derived to be

$$\begin{bmatrix} \boldsymbol{U}_{\boldsymbol{N}} \\ \boldsymbol{I}_{\boldsymbol{L}} \end{bmatrix} = \begin{bmatrix} \boldsymbol{Z}^{-1} & \boldsymbol{\Gamma}^{\boldsymbol{T}} \\ \boldsymbol{\Gamma} & -\boldsymbol{R} \end{bmatrix}^{-1} \begin{bmatrix} \boldsymbol{I}_{\boldsymbol{N,0}} \\ \boldsymbol{\emptyset} \end{bmatrix}. \tag{3.25}$$

Identifying that the matrix of (3.25) is a block matrix, the node voltages at the equilibrium are

$$\boldsymbol{U}_{\boldsymbol{N}} = (\boldsymbol{Z}^{-1} + \boldsymbol{\Gamma}^{\boldsymbol{T}}\boldsymbol{R}^{-1}\boldsymbol{\Gamma})^{-1}\boldsymbol{I}_{\boldsymbol{N,0}}, \tag{3.26}$$

which is equivalent to multiplying the constant term currents by the equivalent impedance of the network.

Stability from the Characteristic Equation

The stability of dc distribution systems can be evaluated by determining the eigenvalues of the state matrix. For the sake of simplicity it is rewritten as

$$\boldsymbol{A} = \begin{bmatrix} -\boldsymbol{C}^{-1}\boldsymbol{Z}^{-1} & -\boldsymbol{C}^{-1}\boldsymbol{\Gamma}^{\boldsymbol{T}} \\ \boldsymbol{L}^{-1}\boldsymbol{\Gamma} & -\boldsymbol{L}^{-1}\boldsymbol{R} \end{bmatrix} = \begin{bmatrix} \boldsymbol{E} & \boldsymbol{F} \\ \boldsymbol{G} & \boldsymbol{H} \end{bmatrix}, \tag{3.27}$$

where $\boldsymbol{F}$ and $\boldsymbol{G}$ are not necessarily square matrices.

The characteristic equation of this matrix ($|\boldsymbol{A} - \lambda \boldsymbol{I}|$) will always have the form of

$$a_1\lambda^{N+L} + a_2\lambda^{N+L-1} + a_3\lambda^{N+L-2} \ldots a_{N+L}, \tag{3.28}$$

where N and L are the number of nodes and number of distribution lines respectively. Therefore, this characteristic equation has $N + L$ coefficients and $N + L$ zeros.

The coefficients of the characteristic equation can be determined from the state matrix by utilizing traces of powers or the principal minors of the matrix [88, 89]. Therefore, they can by found by

$$a_1 = 1, \tag{3.29}$$

$$a_{1+k} = -\frac{1}{k}\sum_{m=1}^{m=k} a_m \,\mathrm{Tr}(\boldsymbol{A}^{k-m+1}), \tag{3.30}$$

$$a_{1+k} = (-1)^k \sum \Delta_k, \tag{3.31}$$

where Tr is the trace of a matrix, and Δ_k is the k-th order principal minor of $\boldsymbol{A}$.

Utilizing (3.27) and (3.30) the algebraic representation of the first five coefficients of the characteristic equation are determined to be

$$a_1 = 1, \tag{3.32}$$

$$a_2 = -\sum_i \boldsymbol{A}_{ii}, \tag{3.33}$$

$$a_3 = \frac{1}{2}\sum_{i\neq j} \boldsymbol{A}_{ii}\boldsymbol{A}_{jj} - \sum_i (\boldsymbol{FG})_{ii}, \tag{3.34}$$

$$a_4 = -\frac{1}{6}\sum_{i\neq j\neq k} \boldsymbol{A}_{ii}\boldsymbol{A}_{jj}\boldsymbol{A}_{kk} + \frac{1}{2}\sum_{i\neq j} \boldsymbol{E}_{ii}(\boldsymbol{FG})_{jj} + \frac{1}{2}\sum_{i\neq j} \boldsymbol{H}_{ii}(\boldsymbol{GF})_{jj}, \tag{3.35}$$

$$\begin{aligned} a_5 =& \frac{1}{24} \sum_{i\neq j\neq k\neq l} \boldsymbol{A}_{ii}\boldsymbol{A}_{jj}\boldsymbol{A}_{kk}\boldsymbol{A}_{ll} - \frac{1}{6} \sum_{i\neq j\neq k} \boldsymbol{E}_{ii}\boldsymbol{E}_{jj}(\boldsymbol{FG})_{kk} \\ & - \frac{1}{6} \sum_{i\neq j\neq k} \boldsymbol{H}_{ii}\boldsymbol{H}_{jj}(\boldsymbol{GF})_{kk} - \frac{1}{6} \sum \boldsymbol{E}_{ii}\boldsymbol{H}_{jj}(\boldsymbol{FG})_{kk} \\ & - \frac{1}{2} \sum (\boldsymbol{EFHG})_{ii} - \frac{1}{2} \sum (\boldsymbol{HGEF})_{ii} \\ & + \frac{1}{2} \sum \boldsymbol{E}_{ii}(\boldsymbol{FHG})_{jj} + \frac{1}{2} \sum \boldsymbol{H}_{ii}(\boldsymbol{GEF})_{jj} \\ & - \frac{1}{2} \sum (\boldsymbol{FG})_{ii}^2 + \frac{1}{4} \sum (\boldsymbol{FG})_{ii}(\boldsymbol{FG})_{jj}. \end{aligned} \tag{3.36}$$

From (3.32) to (3.36) it becomes apparent that the coefficients relate to the combinations of the sources', loads' and distribution lines' time coefficients, of increasing order with each subsequent coefficient (without creating loops).

For these systems to be stable it is required, but not sufficient, that all coefficients are larger than zero [90]. To make the conditions sufficient $n + l - 2$ additional coefficients need to be added [91]. These so-called Routh coefficients can be found in the leftmost column of the Routh array, which is given by

$$\boldsymbol{B} = \begin{bmatrix} a_1 & a_3 & a_5 & \dots & a_{N+L} \\ a_2 & a_4 & a_6 & \dots & a_{N+L} \\ b_{1,1} & b_{1,2} & b_{1,3} & \dots & b_{1,(N+L)/2} \\ b_{2,1} & b_{2,2} & b_{2,3} & \dots & b_{2,(N+L)/2} \\ \vdots & \vdots & \vdots & \vdots & \vdots \\ b_{N+L-2,1} & b_{N+L-2,2} & b_{N+L-2,3} & \dots & b_{N+L-2,(N+L)/2} \end{bmatrix}, \tag{3.37}$$

where the $b_{i,j}$ elements are recursively determined by

$$b_{i,j} = \frac{B_{1+i,1}B_{i,1+j} - B_{i,1}B_{1+i,1+j}}{B_{1+i,1}}. \tag{3.38}$$

For example, the first two Routh coefficients are

$$b_{1,1} = a_2a_3 - a_4, \tag{3.39}$$

$$b_{2,1} = a_2a_3a_4 + a_2a_6 - a_2^2a_5 - a_4^2. \tag{3.40}$$

Any dc distribution system is stable if and only if all the coefficients of the characteristic equation and the relevant Routh coefficients ($b_{1,j}$) are larger than zero.

3.3.3 Stability Analysis of Example Systems

To demonstrate the utility of the presented method the stability of three dc distribution systems in different configurations is analyzed. For these examples it is assumed that the source is located at node n_1 of each configuration, however, moving the

source to a different node yields similar results. Furthermore, a sensitivity analysis is done and a few general misconceptions concerning the stability of dc distribution systems are discussed.

Bus Configuration

An example of a dc distribution system in a bus configuration is shown in Figure 3.6. The idea of such a configuration is one "bus", or set of distribution lines, without branches or meshes. For the shown example it is assumed that a source is situated at n_1 and two loads are situated at n_2 and n_3. However, the derivation for other configurations is analogous. For the sake of simplicity the resistance of the distribution lines is neglected.

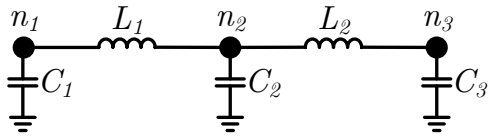

Figure 3.6: Example of a dc distribution grid with three nodes and two lines in a bus configuration

Using (3.27) and (3.30) the coefficients of the characteristic equation are derived to be

$$a_1 = 1, \tag{3.41}$$

$$a_2 = \frac{1}{C_1 Z_1} + \frac{1}{C_2 Z_2} + \frac{1}{C_3 Z_3}, \tag{3.42}$$

$$a_3 = \frac{1}{C_1 L_1} + \frac{1}{C_2 L_1} + \frac{1}{C_2 L_2} + \frac{1}{C_3 L_2} + \frac{1}{C_1 Z_1 C_2 Z_2} + \frac{1}{C_1 Z_1 C_3 Z_3} + \frac{1}{C_2 Z_2 C_3 Z_3}, \tag{3.43}$$

$$a_4 = \frac{1}{C_1 Z_1 C_2 Z_2 C_3 Z_3} + \frac{1}{C_1 L_1 C_2 Z_2} + \frac{1}{C_1 L_1 C_3 Z_3} + \frac{1}{C_2 L_1 C_3 Z_3} + \frac{1}{C_2 L_1 C_1 Z_1} + \frac{1}{C_2 L_2 C_1 Z_1} + \frac{1}{C_2 L_2 C_3 Z_3} + \frac{1}{C_3 L_2 C_2 Z_2} + \frac{1}{C_3 L_2 C_1 Z_1}, \tag{3.44}$$

$$a_5 = \frac{1}{C_1 Z_1 C_2 Z_2 C_3 L_2} + \frac{1}{C_1 Z_1 C_3 Z_3 C_2 L_1} + \frac{1}{C_1 Z_1 C_3 Z_3 C_2 L_2} + \frac{1}{C_2 Z_2 C_3 Z_3 C_1 L_1} + \frac{1}{C_1 L_1 C_2 L_2} + \frac{1}{C_1 L_1 C_3 L_2} + \frac{1}{C_2 L_1 C_3 L_2}, \tag{3.45}$$

$$a_6 = \frac{1}{C_1 Z_1 C_2 L_1 C_3 L_2} + \frac{1}{C_2 Z_2 C_1 L_1 C_3 L_2} + \frac{1}{C_3 Z_3 C_1 L_1 C_2 L_2}. \tag{3.46}$$

Now if, for simplicity, it is assumed that the capacitance in each node (C_i) and inductance in each distribution line (L_j) are equal, two simple requirements for the stability of this system result, which are given by

$$Z_1 < \frac{-1}{\frac{1}{Z_2} + \frac{1}{Z_3}}, \tag{3.47}$$

$$Z_1 > \frac{-2Z_2 - Z_3}{1 + \frac{3CZ_2Z_3}{L}}, \tag{3.48}$$

where the first requirement is derived from the even coefficients, and the second requirement follows from the odd coefficients.

Interestingly, from these requirements a constraint on the capacitance and inductance is derived to be

$$\frac{3C}{L} > \frac{2}{Z_3^2} + \frac{1}{Z_2^2} + \frac{2}{Z_2 Z_3}, \tag{3.49}$$

which depicts a minimum on the ratio between the capacitance and inductance for stability to be feasible.

The derived requirements are necessary but not sufficient for stability. To make the set of requirements sufficient additional constraints can be derived from the Routh coefficients. In general, the requirements derived from the Routh coefficients are more complex, but the result is similar to the requirements from the characteristic equation's coefficients, as is shown in (3.20). Utilizing (3.37) and (3.38), if the ratio between the capacitance and inductance is large enough, it is sufficient for stability if

$$Z_1 < \frac{-1}{\frac{1}{Z_2} + \frac{4}{Z_3}}, \tag{3.50}$$

which is a stricter versions of (3.47) that was derived from the characteristic equation's coefficients.

Ring Configuration

The second example is a dc distribution system in a "ring" configuration shown in Figure 3.7. In this case the ring configuration does not have any branches but it has a single mesh. In this example the source is located at n_1 and loads are located at n_2 and n_3.

Analogously to the bus configuration, the requirements on the source's impedance for the stability of this system can be derived from the characteristic equation. These requirements are derived to be

$$\frac{-Z_2 - Z_3}{1 + \frac{9CZ_2Z_3}{2L}} < Z_1 < \frac{-1}{\frac{1}{Z_2} + \frac{1}{Z_3}}. \tag{3.51}$$

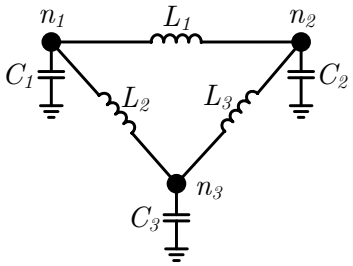

Figure 3.7: Example of a dc distribution grid with three nodes and three lines in a ring configuration

Star Configuration

The last example is a dc distribution system in a "star" configuration, which is shown in Figure 3.8. In this case the star configuration has branches, but no meshes. Since in most cases the source is situated in the center node, it is assumed that the system has a source placed at n_1 and a load is placed at n_2, n_3 and n_4.

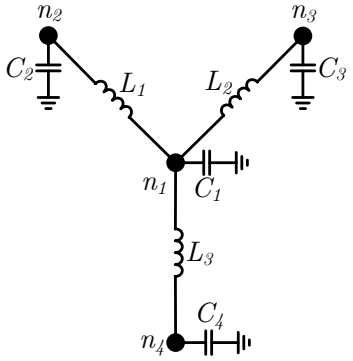

Figure 3.8: Example of a dc distribution grid with four nodes and three lines in a star configuration

Analogously to the previous examples, the requirements on the source's impedance to ensure the stability of this system are derived to be

$$\frac{\frac{1}{2}(-Z_2Z_3 - Z_2Z_4 - Z_3Z_4)}{Z_2 + Z_3 + Z_4 + \frac{2CZ_2Z_3Z_4}{L}} < Z_1 < \frac{-3}{\frac{5}{Z_2} + \frac{5}{Z_3} + \frac{5}{Z_4}}. \tag{3.52}$$

The stability requirements for the three examples show strong congruence with respect to the sensitivity towards, for example, inductance and capacitance. Therefore, it becomes viable to make some general conclusions.

Sensitivity Analysis

Similar results with respect to previous work are found for some of the parameters. With respect to inductance the results of this section are congruent with previous works [57, 59], where a decrease in inductance leads to improved stability. Furthermore, from the equations in the previous section, it can be observed that the impedance of the droop controlled source has an upper and lower bound. The upper bound is related to the power drawn by the loads in the system, while the lower bound is related to the oscillations in the system. These oscillations originate from the interaction of capacitance at different nodes through the lines' inductance. These results are also congruent with the literature [92, 93].

Generally, it is thought that increasing the capacitance is beneficial for the stability of the system. From (3.49), (3.51) and (3.52) it is clear that indeed there is a minimum required capacitance in order to achieve stability, and increasin the capacitance further improves the damping of the system. However, (3.42) and (3.46) suggest a negative effect on the overall damping of the system. The second (a_2) and last (a_{N+L}) coefficients are the sum and product of all eigenvalues respectively. Therefore, when the capacitance is increased the sum and product of all eigenvalues are decreased leading to decreased damping in the system.

Interestingly, (3.42) and (3.46) suggest that decreasing the source capacitance compared to the load capacitance has a positive influence on the damping in the system. However, this not necessarily always true since the decrease of source impedance also has a negative effect on some of the coefficients (e.g. a_3). As validation of this observation the maximum real part of the eigenvalues as function of the source capacitance for the bus example is shown in Figure 3.9. For this sensitivity analysis it is assumed that the resistance and inductance of the lines are 0 Ω and 0.36 μH respectively. Furthermore, the converters' output capacitance source impedance and load impedance are given by 50 μF, 5 Ω and -125 Ω respectively.

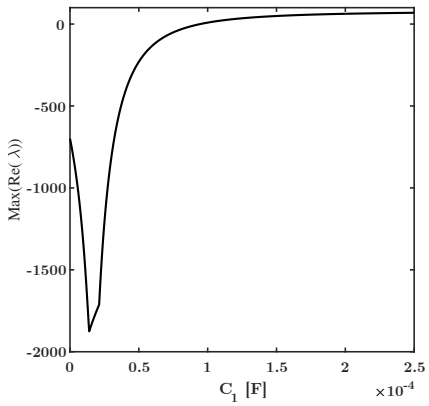

Figure 3.9: Maximum real part of the eigenvalues as function of the line resistance for the bus example shown in Figure 3.6

3.4 Plug-and-Play Stability

Previous studies into the stability of dc distribution grids often do not ensure global stability, or only apply to well defined systems (i.e., systems with known topology and/or parameters) or systems that utilize some form of communication. For example, (non-)linear droop based strategies are commonly used for many systems [94–99]. Although droop based strategies do not require any communication they do not ensure global stability unless the system's parameters and topology are known. Furthermore, several strategies exist that adapt the virtual impedance or operating mode of the converters depending on system parameters [100–106]. These methods further improve stability when flexibility is available in the system, but still rely on well defined system parameters (e.g., load power) or communication for global stability.

In this section easy-to-use global (small-signal) stability guidelines are presented for plug-and-play dc distribution grids that are without communication. The global stability guidelines are derived using a Brayton-Moser representation of the system to arrive at a suitable Lyapunov candidate function. The derived guidelines only pose requirements on the output capacitors of constant power loads and the total load of the constant power loads in the system.

3.4.1 DC Distribution System Equilibrium

As was shown in Section 3.3, the equilibrium can be found by assuming that all time derivatives in the system are zero. Therefore, from (3.23) the state variables at the equilibrium are given by

$$\begin{bmatrix} \boldsymbol{U_N} \\ \boldsymbol{I_L} \end{bmatrix} = \begin{bmatrix} -\boldsymbol{C}^{-1}\boldsymbol{Z}^{-1} & -\boldsymbol{C}^{-1}\boldsymbol{\Gamma}^T \\ \boldsymbol{L}^{-1}\boldsymbol{\Gamma} & -\boldsymbol{L}^{-1}\boldsymbol{R} \end{bmatrix}^{-1} \begin{bmatrix} -\boldsymbol{C}^{-1} \\ \boldsymbol{\emptyset} \end{bmatrix} \boldsymbol{I_{N,0}}. \tag{3.53}$$

Moreover, the node voltages are found to be

$$\boldsymbol{U_N} = (\boldsymbol{Z}^{-1} + \boldsymbol{\Gamma}^T\boldsymbol{R}^{-1}\boldsymbol{\Gamma})^{-1}\boldsymbol{I_{N,0}}, \tag{3.54}$$

which is equivalent to finding equivalent impedance of the network topology. Nevertheless, providing sufficient and necessary conditions for the existence of this inverse for any topology is not feasible, since $\boldsymbol{\Gamma}$ is unknown.

However, sufficient conditions for the existence of an equilibrium are available. According to [82, 107] an equilibrium is guaranteed to exist if the total load power of the network is bound by

$$P_\Sigma \leq \frac{U_0^2}{4R_\Sigma}, \tag{3.55}$$

where P_Σ is the total load power of the network, U_0 is the reference voltage of source(s) in the system and R_Σ is the total resistance of the network.

This sufficient condition for the existence of an equilibrium can be substantiated and slightly appended by utilizing a simple example circuit shown in Figure 3.10.

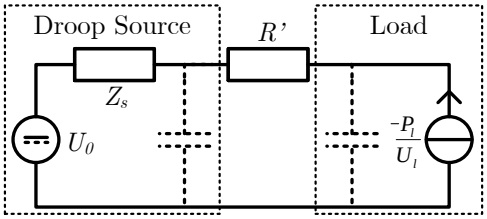

Figure 3.10: Equivalent steady-state circuit of a droop controlled source connected to a constant power load via an arbitrary dc distribution network

This figure depicts the steady-state circuit of a droop controlled source connected to a constant power load via an arbitrary dc distribution network. The voltage at the load side's output capacitance is given by

$$U_l = U_0 - \frac{P_l Z_s}{U_l} - \frac{P_l R'}{U_l}, \tag{3.56}$$

where R' is the equivalent resistance of the arbitrary dc distribution network between the source and the load.

For this system an equilibrium exists if and only if

$$P_l \leq \frac{U_0^2}{4(Z_s + R')}. \tag{3.57}$$

For an arbitrary dc distribution system with an arbitrary number of loads, in the worst case, all the currents from all the constant power loads flow through all line resistances. Consequently, the existence of an equilibrium can be ensured by

$$P_\Sigma \leq \frac{U_0^2}{4(Z_s + R_\Sigma)}. \tag{3.58}$$

Adequacy of the Equilibrium

Equation (3.58) ensures the existence of an equilibrium, but it does not ensure that the voltage in the system remains within preferred limits. Therefore, it must be ensured that the voltage remains above the minimum voltage $U_{\min}$.

In the worst (allowed) case the load current is given by $I_l = \frac{P_l}{U_{\min}}$. Therefore, using the example circuit from Figure 3.10, the equilibrium has voltages that are above the minimum voltage if and only if

$$U_0 - \frac{P_l Z_s}{U_{\min}} - \frac{P_l R'}{U_{\min}} \geq U_{\min}. \tag{3.59}$$

Equivalently to the existence of the equilibrium, in the worst case scenario all the load currents flow through all the resistances in the network. Therefore the adequacy

of the equilibrium in the worst case scenario is ensured by

$$P_\Sigma \leq \frac{U_{\min}(U_0 - U_{\min})}{Z_s + R_\Sigma}, \tag{3.60}$$

which, as long as the minimum voltage is not chosen to be exactly half of the reference voltage, is stricter than (3.58).

3.4.2 Brayton-Moser Stability

To assess the asymptotic stability the Lyapunov's method is used. From the system's state-space representation (3.23), the natural Lyapunov function candidate is given by

$$\Phi_0 = G_0 - \frac{1}{2}\boldsymbol{I_L}^T \boldsymbol{R}\boldsymbol{I_L} + \boldsymbol{I_L}^T \boldsymbol{\Gamma}\boldsymbol{U_N}, \tag{3.61}$$

$$G_0 = \sum_i \left(P_{l,i} \ln U_i - \frac{2U_iU_0 - U_i^2}{2Z_{s,i}} + \frac{U_i^2}{2Z_{z,i}} - U_i I_{I,i} \right), \tag{3.62}$$

where G_0 is the resistive co-content of the sources and loads [82]. The different terms in (3.62) are for constant power, droop, constant impedance and constant current converters that are connected to each node respectively.

Utilizing the natural Lyapunov candidate function and the resistive co-content, the dynamic equations of the system can be rewritten as

$$\boldsymbol{Q_0}\dot{\boldsymbol{X}} = -\partial_{\boldsymbol{X}}\Phi_0, \tag{3.63}$$

$$\boldsymbol{Q_0} = \begin{bmatrix} \boldsymbol{C} & \boldsymbol{\emptyset} \\ \boldsymbol{\emptyset} & -\boldsymbol{L} \end{bmatrix}. \tag{3.64}$$

However, Lyapunov function candidate Φ_0 is not suitable to ensure stability of the system, since it is not sign definite. Therefore, a closely related Brayton-Moser potential Φ is defined, which is given by

$$\Phi = \frac{\tau_{\max}}{2}(\partial_{\boldsymbol{X}}\Phi_0)^T \begin{bmatrix} \boldsymbol{C} & \boldsymbol{\emptyset} \\ \boldsymbol{\emptyset} & \boldsymbol{L} \end{bmatrix}^{-1} (\partial_{\boldsymbol{X}}\Phi_0) + \Phi_0, \tag{3.65}$$

where $\tau_{\max}$ is the maximum time constant (L/R) of all the distribution lines in the dc distribution system [82, 108, 109].

Subsequently, by substituting $\dot{\boldsymbol{X}} = -{\boldsymbol{Q_0}}^{-1}\partial_{\boldsymbol{X}}\Phi_0$ into (3.65) and utilizing $\boldsymbol{Q}\dot{\boldsymbol{X}} = -\partial_{\boldsymbol{X}}\Phi$, the Brayton-Moser potential Φ and the matrix $\boldsymbol{Q}$ corresponding to the Brayton-Moser potential Φ are found to be

$$\partial_{\boldsymbol{X}}\Phi = \tau_{\max}(\partial^2_{\boldsymbol{X}}\Phi_0)^T \begin{bmatrix} \boldsymbol{C} & \boldsymbol{\emptyset} \\ \boldsymbol{\emptyset} & \boldsymbol{L} \end{bmatrix}^{-1} \partial_{\boldsymbol{X}}\Phi_0 + \partial_{\boldsymbol{X}}\Phi_0, \tag{3.66}$$

$$\boldsymbol{Q} = \begin{bmatrix} \tau_{\max}\partial_{\boldsymbol{X}}\partial_{\boldsymbol{X}}G_0 + \boldsymbol{C} & \tau_{\max}\boldsymbol{\Gamma}^T \\ -\tau_{\max}\boldsymbol{\Gamma} & \tau_{\max}\boldsymbol{R} - \boldsymbol{L} \end{bmatrix}. \tag{3.67}$$

The Lyapunov function V that follows from this Brayton-Moser representation is given by

$$V = \dot{\boldsymbol{X}}^T \boldsymbol{Q} \dot{\boldsymbol{X}}, \tag{3.68}$$

which according to LaSalle's invariance principle makes the system asymptotically stable if

$$\dot{V} = \dot{\boldsymbol{X}}^T (\dot{\boldsymbol{Q}} - \partial_{\boldsymbol{X}} \partial_{\boldsymbol{X}} \Phi) \dot{\boldsymbol{X}} \leq 0, \tag{3.69}$$

$$\boldsymbol{Q} \succ 0, \tag{3.70}$$

where $\boldsymbol{Q} \succ 0$ indicates that the matrix $\boldsymbol{Q}$ is positive definite.

System Convexity

The first condition for asymptotic stability is given by (3.69) and it can be shown that this equation reduces to

$$(\dot{\boldsymbol{Q}} - \partial_{\boldsymbol{X}} \partial_{\boldsymbol{X}} \Phi) \leq 0, \tag{3.71}$$

where $\dot{\boldsymbol{Q}}$ is zero when the system is at rest, and negative or negligible otherwise [82].

Therefore, the system is convex if $\partial_{\boldsymbol{X}} \partial_{\boldsymbol{X}} \Phi \geq 0$, which is valid when

$$\sum_j R_j I_j^2 + \sum_i \left(-\frac{P_{l,i}}{U_i^2} + \frac{1}{Z_{s,i}} + \frac{1}{Z_{z,i}} \right) \geq 0. \tag{3.72}$$

In the worst case scenario all currents flow through all the lines, there is only one droop source, and constant power loads all operate at the minimum voltage $U_{\min}$. Therefore, convexity is ensured if

$$P_\Sigma \leq \frac{U_{\min}^2}{Z_s + R_\Sigma}, \tag{3.73}$$

which is less strict than (3.60) as long as the minimum voltage is more than half the reference voltage.

The same result can be obtained using a more intuitive approach. Figure 3.11 shows a linearized version of the example circuit shown in Figure 3.10, where the constant power load is replaced by a current source and a parallel impedance (see Section 3.2). This equivalent circuit converges to the equilibrium if a perturbation on the load voltage causes a larger change in the source current than a change in the load current. In other words, if

$$\frac{1}{Z_s + R'} \geq \frac{1}{Z_l}, \tag{3.74}$$

$$Z_s + R' \leq \frac{U_l^2}{P_l}, \tag{3.75}$$

$$P_l \leq \frac{U_l^2}{Z_s + R'}, \tag{3.76}$$

which, in the worst case scenario, is equivalent to (3.73).

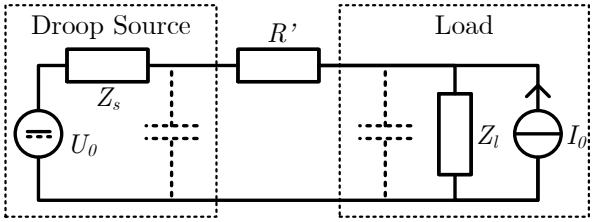

Figure 3.11: Incremental steady-state circuit of a droop controlled source connected to a constant power load via an arbitrary dc distribution network

Asymptotic Stability

The second condition for asymptotic stability is given by (3.67). Clearly, the choice of $\tau_{\max}$ ensures that $\tau_{\max}\boldsymbol{R} - \boldsymbol{L} \succ 0$. Therefore, it can be derived that $\boldsymbol{Q} \succ 0$ when the diagonal entries of $\boldsymbol{Q}$ are positive definite [82]. Furthermore, $\tau_{\max}\partial_{\boldsymbol{X}}\partial_{\boldsymbol{X}}G_0 + \boldsymbol{C}$ is positive definite if (for each node) it is true that

$$-\frac{\tau_{\max}P_{l,i}}{U_i^2} + \frac{\tau_{\max}}{Z_{s,i}} + \frac{\tau_{\max}}{Z_{z,i}} + C_i > 0, \tag{3.77}$$

which is always true for nodes to which no constant power nodes are connected (or other converters with negative incremental impedance). Furthermore, for nodes to which only constant power nodes are connected it is required that

$$C_i > \frac{\tau_{\max}P_{l,i}}{U_{min}^2}. \tag{3.78}$$

Intuitively this requirement can be explained by the time constants and damping of the system. If (3.78) is true, then the damping of each distribution line is more than the amplification caused by the constant power loads with respect to oscillations in the system.

3.4.3 Stability Guidelines

Any dc distribution system is stable if all four guidelines, (3.58), (3.60), (3.73) and (3.77), are adhered to. These guidelines are simple, robust and sufficient for stability and can be valuable for designing dc distribution systems that exhibit changes in components, topology and/or power. Usually, when the minimum allowed voltage is more than half the reference voltage, only (3.60) and (3.77) have to be taken into account. This is because, in this case, (3.58) and (3.73) are less strict variants of (3.60).

With the direct application of the guidelines, the constraints on the power electronic converters can become rather conservative, especially for larger systems. Therefore, it can be beneficial to take a different approach to applying these guidelines. A decentralized control strategy which incorporates the stability guidelines is proposed in Chapter 4.

3.5 Experimental Results

The previous sections showed how the stability of dc distribution systems can be derived algebraically, and how the plug-and-play stability of these grids can be ensured. In this section an experimental setup is used to provide practical insight into the stability of dc distribution grids. For the experiments, the bus configuration depicted in Figure 3.12 is used. Specifications for all the components in this experimental setup can be found in Appendix A.

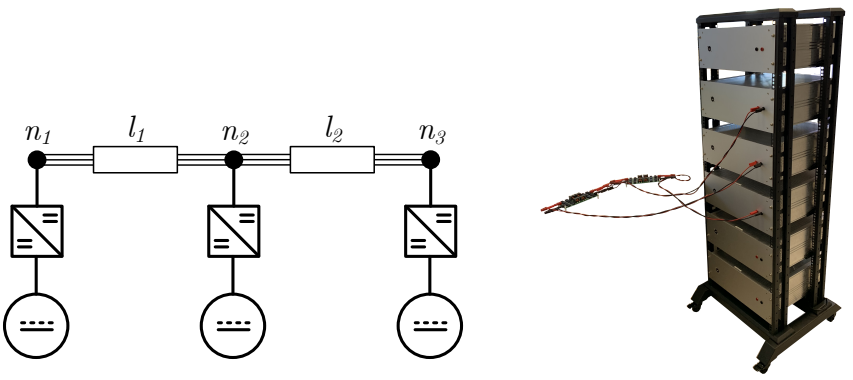

(a) Schematic (b) Picture

Figure 3.12: Setup that is used to analyze the stability of dc distribution systems

For the experiment a droop controlled converter is located at n_1, which reference input current is given by

$$I_i = \frac{U_d - U_o}{Z_d}, \tag{3.79}$$

where the reference droop voltage U_d is set to 350 V, and the droop impedance Z_d is set to either 0.2, 1.0 or 8.3 Ω. Furthermore, two constant power controlled converters are located at n_2 and n_3. Moreover, the input voltage of all the converters is regulated at 100 V. The reference output power over time of the constant power load converters are given in Table 3.1. The experimental results, for the different droop impedances, are shown in Figure 3.13.

t [ms]	U_d [V]	P_2^* [W]	P_3^* [W]
-5	350	0	0
0	350	1200	0
20	350	1200	1200

Table 3.1: Scenario for the stability experiments

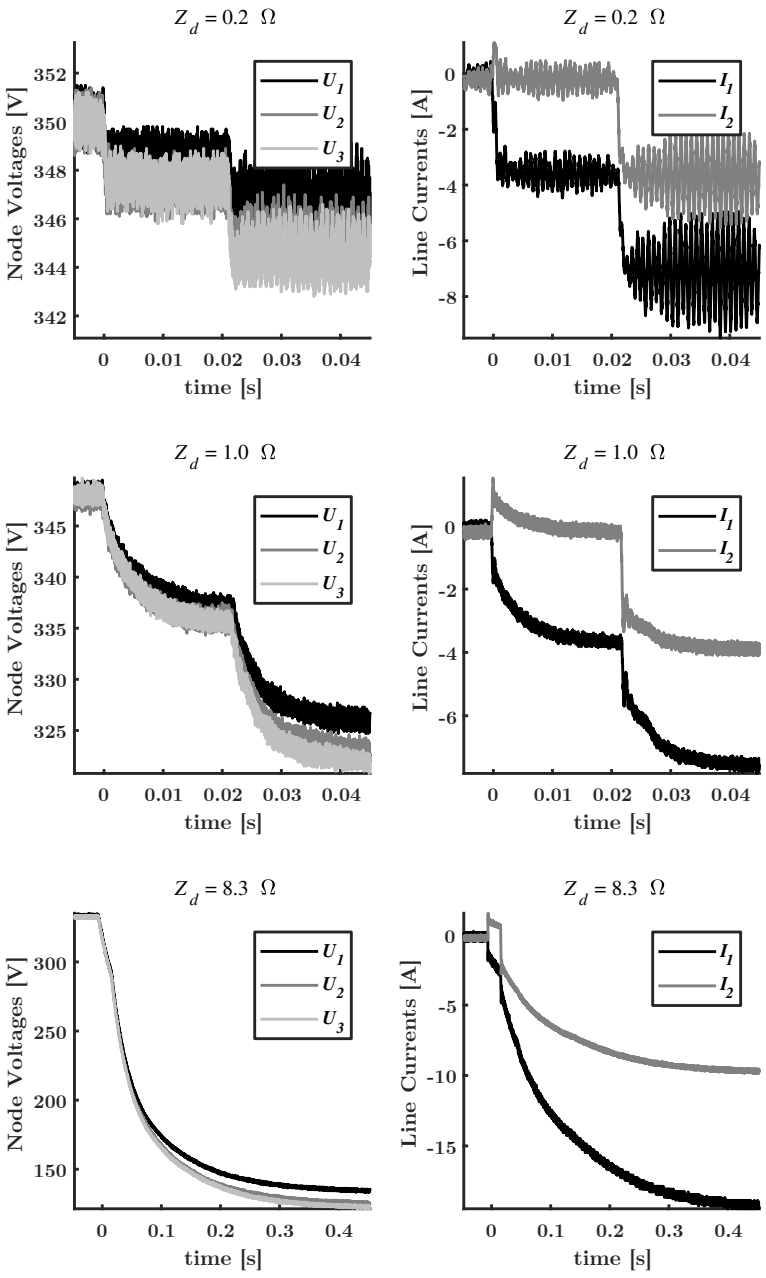

Figure 3.13: Experimental results for the dc distribution system shown in Figure 3.12 and under the scenario shown in Table 3.1, for different values of the droop impedance

From Figure 3.13 it is seen that, when the droop impedance Z_d is 1.0 Ω, the system behaves as expected from the theoretical analysis developed in the previous sections. Even though the natural oscillation frequencies of the system, 1150 and 2300 Hz, are just outside of the control bandwidth of the converters (1000 Hz), the system is stable. However, the system does not fully damp the oscillations when the droop impedance is 0.2 Ω, and does not go unstable when the voltage drops below half the reference voltage.

Given a line inductance of 32 μH, a line resistance of 120 mΩ, a desired minimum system voltage of 315 V, and an output capacitance of 288 μF, according to (3.78), the maximum power that each load can draw from the grid without causing oscillatory instability is around 100 kW. However, it is seen from Figure 3.13 that the system is unstable when the droop impedance is 0.2 Ω. Moreover, the line currents show significant oscillations even before the constant power load converters draw power from the grid.

In this case the oscillatory behavior is caused by the practical limitations of the converter compared to the idealized model. When the droop constant decreases the (virtual) RC time constant of the converter decreases. In this case, when the droop constant is 0.2 Ω, the RC time constant becomes lower than the time constant of the voltage measurement circuits. Consequently, the converter itself is operating outside of its control bandwidth.

Note that the system is stable even when the droop impedance is 8.3 Ω and the voltage goes below half the reference voltage (i.e., 175 V). Initially, this seems contradictory with the findings of Section 3.4. However, in this case the input current is drooped and not the output current, and the output current is given by

$$I_o = \frac{U_i}{U_o}\frac{U_d - U_o}{Z_d}. \tag{3.80}$$

Assuming that the input voltage remains constant the output power of this system is then given by

$$P_o = U_i\frac{U_d - U_o}{Z_d}, \tag{3.81}$$

which in contrary to the output current droop provides more power to the grid even if the voltage drops below half of the reference voltage. The output power of output current droop is given by

$$P_o' = U_o\frac{U_d - U_o}{Z_d}. \tag{3.82}$$

Therefore, it might be that input current droop, or output power droop, is more suitable for ensuring voltage stability in dc distribution grids.

3.6 Conclusions

The stability of distribution systems faces challenges such as decreasing inertia due to the increasing share of renewable energy, and the increasing number of constant power load converters that exhibit negative incremental impedance. In this chapter a method was presented to algebraically derive the stability of any dc distribution system, and global stability guidelines were derived using a Brayton-Moser representation of the system.

Deriving the stability of larger dc distribution systems, using large-signal models, is intractable. Therefore, to analyze the stability in these systems, a Norton equivalent small-signal converter model was used to approximate any (non-)linear behavior via a constant current source with an impedance in parallel. This simplification is reasonably accurate within the control bandwidth of the converters.

It was discussed that the stability of dc distribution systems can be derived by utilizing minor loop gain, root locus, Lyapunov or eigenvalue methods. However, previous research only analyzed specific systems or used oversimplified models and therefore no generalized conclusions could be drawn. This chapter showed how the stability of dc distribution systems can be algebraically derived from their state-space matrices, which, unlike other techniques, does not neglect node capacitance or line inductance. Utilizing this method it was confirmed that increasing line inductance and decreasing line resistance has a negative effect on the system's stability. Moreover, it was shown that increasing the capacitance of source converters can deteriorate the stability, in contrast with increasing the capacitance of load converters.

No guidelines were provided in literature for the global stability of dc distribution grids, without using communication or knowing the topology of the system. A Brayton-Moser representation of dc distribution systems was used to arrive at a suitable Lyapunov candidate function, and subsequently guidelines were derived for global plug-and-play stability. The guidelines ensure that an equilibrium exists, the voltages in the system are above the desired minimum voltage, the system converges to the equilibrium and oscillations are damped. To prevent instability, the capacitance of constant power loads needs to be sized appropriately and the voltage drops in the system need to be limited.

Experimental results confirmed that two modes of instability exist in dc distribution grids; voltage instability and oscillatory instability. Furthermore, they showed that the practical limitations of converters need to be taken into account for the stable operation of dc distribution systems. Although idealized representations of the converters lead to convenient stability guidelines, the impedance of the converters must be analyzed at all relevant frequencies to ensure stability.

When designing a dc distribution system, the results from this chapter can be used to ensure and analyze its stability. However, future research into the impedance characteristics of various converter topologies and their control is still essential.

Chapter 4

Decentralized Control Strategy and Algorithm

Decentralized control is essential to deal with the decentralization and segmentation of the distribution grid, and the potential absence of a communication infrastructure. In this chapter, literature on the decentralized control of dc grids is surveyed, and a decentralized control scheme is proposed that ensures global stability and voltage propriety for plug-and-play dc distribution systems. Furthermore, it is shown that voltage dependent demand or supply response can cause inadequate energy utilization. Therefore, the Grid Sense Multiple Access (GSMA) algorithm is proposed, which relies on an exponential backoff mechanism to improve system and energy utilization. Several simulations and experiments are carried out, validating the decentralized control strategy and algorithm.

This chapter is based on

- N. H. van der Blij, L. M. Ramirez-Elizondo, M. T. J. Spaan and P. Bauer, "Stability and Decentralized Control of Plug-and-Play DC Distribution Grids", IEEE Access, vol. 6, 2018.
- N. H. van der Blij, L. M. Ramirez-Elizondo, M. T. J. Spaan and P. Bauer, "Grid Sense Multiple Access: A Decentralized Control Algorithm for DC Grids", International Journal of Electrical Power & Energy Systems, 2020.

4.1 Introduction

Different strategies can be used to control, for example, the power flow, stability and unit commitment in dc distribution systems. The different approaches are frequently divided into centralized, decentralized and distributed control strategies [29,110]. For centralized control, a central controller determines the behavior of all the actors in the system. On the other hand, in decentralized control, each individual actor determines its own actions without communicating with other devices. Furthermore, distributed control is characterized by actors that communicate only with close neighbors to reach a consensus on their actions.

For dc distribution systems, a hierarchical control scheme is often used, which is a combination of the different control approaches [26,29]. The typical different layers of a hierarchical control system are shown in Figure 4.1. First, the physical layer consists of the converters, distribution lines and other components of the network. Second, the decentralized control layer only uses locally available information. Third, the coordinated control is characterized by control schemes that utilize communication for providing functionalities such as voltage restoration, power sharing and stability. Last, the management layer pursues complex auxiliary objectives, which are often executed on a slower time frame, such as power flow control and economic optimization.

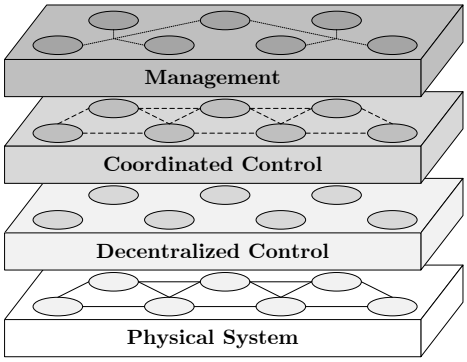

Figure 4.1: Typical layers in the hierarchical control of dc distribution systems

The hierarchical approach to controlling dc distribution system is well researched, especially when communication is used [26, 111, 112]. Furthermore, decentralized control is the foundation for any control architecture, since the grid must remain operational even if the communication infrastructure is (temporarily) unavailable. Therefore, this chapter focuses on the decentralized control of dc distribution grids. In Section 4.2, a decentralized control strategy is proposed that ensures global stability for any dc distribution system. In Section 4.3, a decentralized control algorithm is proposed that improves energy utilization. Last, in section 4.4, experiments are carried out to validate the proposed strategy and algorithm.

4.2 Decentralized Control Strategy

Several decentralized strategies are presented in literature in order to improve the stability, power quality and power sharing of dc grids. Droop based control strategies are commonly used for many systems [96, 113, 114]. Further efforts improve power quality and stability by adapting the converters' virtual impedance or operating mode depending on measured parameters [103, 115, 116].

Some plug-and-play strategies have also been proposed [117, 118]. For example, local controllers can be updated after a change in the system occurs [117, 118]. Alternatively, a (centralized) power management strategy can specify the set points of the converters in the grid [27]. Moreover, global stability can be ensured when a well-defined topology is used [103, 119, 120]. Overall, these control strategies require some form of communication, or require well-known system topologies and parameters, to ensure global stability.

In Section 3.4 the global stability guidelines were derived using a Brayton-Moser representation of the system to arrive to a Lyapunov candidate function. In this section, a decentralized control strategy is proposed that implements these stability guidelines, and supplementary converter guidelines for plug-and-play dc distribution grids that are (temporarily) without communication.

4.2.1 Decentralized Control for Stability

From Section 3.4 it is clear that, to ensure voltage propriety and a damped system, any dc distribution system must adhere to (3.60) and (3.77). It is straightforward to ensure sufficient damping on oscillations in the system, by requiring that the output capacitances of all constant power loads in the system are sized using (3.78). Note that $\tau_{\max}$ is independent on the length and configuration of the distribution lines, and therefore only depends on the ratio of inductance and resistance of the lines or, in other words, the type of lines that are used.

It is less straightforward to ensure voltage propriety from (3.60), since the total load power, total resistance of the network and the droop impedance are often variable or unknown for plug-and-play systems. Therefore, to ensure that the voltage stays within its minimum and maximum voltage, a decentralized control strategy is proposed, instead of applying (3.60) directly.

The converters in dc distribution grids can be categorized as source, load or hybrid converters. Although renewable energy sources are variable and uncertain by nature, due to maximum power point tracking algorithms, they exhibit constant power behavior in time frames shorter than seconds [121]. Load converters exhibit behaviors such as constant impedance, constant power, constant current or a combination of these behaviors [122]. Hybrid converters are able to both supply and consume power, and often exhibit constant power behavior or mimic constant impedance behavior.

To guarantee global stability and propriety of the voltage, it must be ensured that the voltage never goes below the minimum voltage or above the maximum voltage. Previous research showed the advantages of dividing the acceptable voltage range into

regions where the converters' mode of operation is varied [103–105,119,120]. However, no concrete strategies were presented for voltage propriety or global stability. It is proposed here to divide the acceptable voltage range into supply response, absorption, emission and demand response regions. An example of such division of voltages is given in Figure 4.2, although the different regions do not necessarily need to be divided with identical proportions.

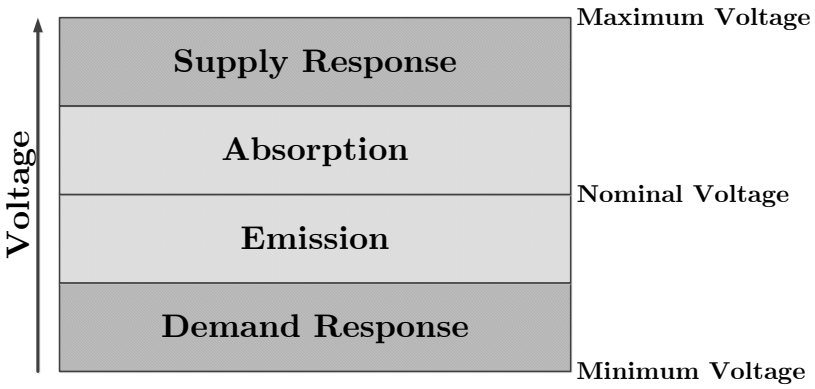

Figure 4.2: The division of the acceptable voltage range into supply response, absorption, emission and demand response voltage regions

The absorption and emission regions are the naturally desired regions of operation of the dc distribution grid. In these regions the load and source converters operate at constant power, while the hybrid converters (e.g., batteries) regulate the voltage. In the emission region, when the voltage is below the nominal voltage, the hybrid converters supply power to the grid. In this region, the hybrid converters ramp up their supplied current as the voltage reduces. In the absorption region, when the voltage is above the nominal voltage, the hybrid converters consume power from the grid. Analogously, the hybrid converters ramp up their consumed current as the voltage increases. When there are no hybrid converters in the network the system will always operate in the supply or demand response regions.

If the voltage enters the demand response region it means that the source and hybrid converters cannot cope with the power demand. Therefore, in the demand response region the load must be decreased. Loads either decrease their power gradually (e.g., by dimming lights) or switch off when a specified voltage is reached. The voltage at which the loads are switched off determines their priority. However, no load is allowed to consume power when the voltage is below the minimum voltage.

If the voltage reaches the supply response region the loads and hybrid converters cannot consume the power supplied by the sources. Therefore, in this region the power supply must be reduced. Similar to the demand response, the sources either gradually decrease their output power or switch off at a specified voltage. However, no source is allowed to supply power when the voltage is above the maximum voltage.

An example of the behavior in the voltage regions for source, load and hybrid converters is shown in Figure 4.3. In this example the source and load converters' power is ramped down in the supply and demand response regions.

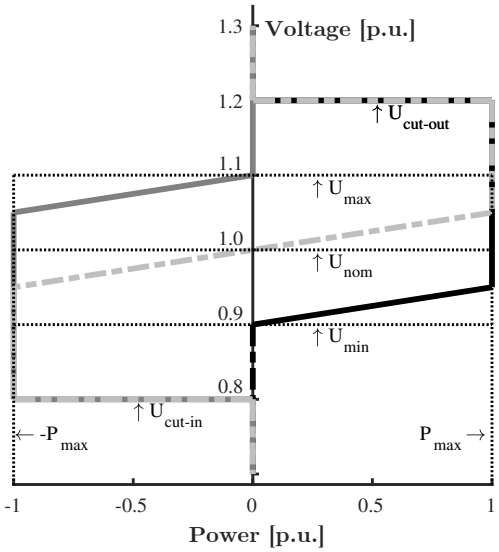

Figure 4.3: Example of a source (grey), load (black) and hybrid (dashed) converters' voltage-current characteristic that complies with the decentralized control strategy

4.2.2 Converter Guidelines

Applying the decentralized control strategy from the previous subsection ensures global stability and voltage propriety. However, it is preferable to define additional constraints on the behavior of the converters in dc distribution systems. To illustrate this, the simple system shown in Figure 4.4 is used. For this example, the source's voltage U is assumed to be constant, while the load's current I is variable.

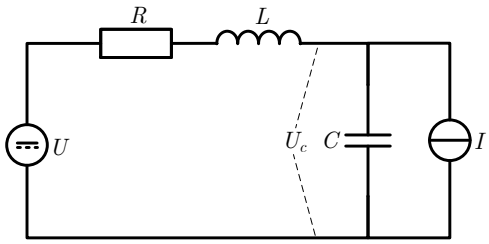

Figure 4.4: Example dc distribution system used to derive the converter guidelines

Because it is used in the load's control decisions, the voltage of the capacitor U_c is of interest. The transfer function $H(s)$ for the capacitor voltage as function of the load current I is given by

$$H(s) = \frac{-1}{sC + \frac{1}{sL+R}}, \tag{4.1}$$

and the poles are found to be

$$p_{1,2} = \frac{-R}{2L} \pm \sqrt{\frac{R^2}{4L^2} - \frac{1}{CL}}. \tag{4.2}$$

When the capacitance or inductance is neglected, the poles are respectively approximated by

$$p_{1,2} \approx \frac{-R}{L}, \tag{4.3}$$

$$p_{1,2} \approx \frac{-1}{RC}. \tag{4.4}$$

Consequently, the transients in the system are bounded by the time constants of the distribution line ($\tau = L/R$) and capacitance ($\tau = RC$). To prevent transients significantly affecting control decisions, it is recommended that, any change is ramped over a significantly longer period than the slowest time constant of the system.

When the current source I is ramped with a ramp rate a the dynamic response of the capacitor's voltage can be found by using the inverse Laplace transformation

$$U_c(t) = \mathcal{L}^{-1}\left(\frac{a}{s^2} \cdot \frac{-1}{sC + \frac{1}{sL+R}}\right), \tag{4.5}$$

$$U_c(t) = U_c(0) + a(-Rt - L + CR^2 + e^{-\frac{Rt}{2L}} f(t)), \tag{4.6}$$

$$f(t) = \frac{\sqrt{C}R\left(3L - CR^2\right)\sinh\left(\frac{t\sqrt{CR^2-4L}}{2\sqrt{C}L}\right)}{\sqrt{CR^2-4L}} + \left(L - CR^2\right)\cosh\left(\frac{t\sqrt{CR^2-4L}}{2\sqrt{C}L}\right). \tag{4.7}$$

In (4.6), $e^{-\frac{Rt}{2L}} f(t)$ represents the transients in the system which are damped out over time. Furthermore, $U_c(0) - aRt$ represents the steady-state of the system for the load current $I(0) + at$. Moreover, $-aL + aCR^2$ represents the offset between the steady-state of the system and the perceived voltage during the ramping of the current.

In the worst case, the offset of the capacitor's voltage with respect to the steady-state value can therefore be approximated by aL. Therefore, a desired accuracy of the converter's controller can be achieved by choosing an appropriate ramp rate a. For more complex systems, the accuracy can be ensured by assessing the equivalent inductance (in the worst case the total inductance) of the system.

4.3 Grid Sense Multiple Access Algorithm

Literature presents several decentralized strategies to ensure stability, power quality and power sharing for smart grids. Droop based control strategies are commonly used for many systems [96, 113, 114]. Further efforts improve power quality and stability by adapting the converters' virtual impedance or operating mode depending on the measured parameters [103, 115, 116]. Moreover, several plug-and-play strategies are presented [117, 118]. Often, an overarching hierarchical control is used to control the power flow [111, 112, 123].

Decentralized control strategies often implement demand and supply response based on local measurements. It is shown in this section that, when voltage dependent demand and supply response is implemented in dc systems with converters that exhibit discrete behavior (that do not ramp their output power, but switch on or off entirely), the system and energy utilization can become inadequate. In these cases it must be determined, with or without communication, which subset of the converters remain operational in order to improve system and energy utilization. Furthermore, the Grid Sense Multiple Access algorithm is proposed to improve system and energy utilization, without employing communication. The algorithm enables a subset of the converters to remain connected to the grid, by introducing an exponential backoff time between connection attempts. Moreover, it is shown that the priority of the converters and behavior of the algorithm can be influenced by altering the algorithm's parameters.

4.3.1 Decentralized Control and Discrete Behavior

To ensure stability and power quality of dc grids, the voltages between the maximum and minimum allowed voltage are divided into supply response, absorption, emission and demand response regions, as is shown in Figure 4.2. In the supply and demand response regions, the respective sources and loads are disconnected before the maximum or minimum voltage is reached. This is done to prevent the voltage from exceeding the maximum voltage or becoming less than the minimum voltage, but also to ensure stability. The change in output power can either be ramped or abruptly switched at a specified voltage.

Sources and Loads with Discrete Behavior

Sources and loads, such as photovoltaic panels and resistive heating, can easily ramp their output power. However, not all applications have that capability. Furthermore, many current standards indicate a fixed voltage to switch off, instead of a region over which it can be ramped. They exhibit so-called discrete behavior, since these sources and loads can only be switched on or off.

For the sources and loads with discrete behavior, the voltage at which it is disconnected determines its priority. In larger systems such as distribution systems, it is likely that there are multiple converters with the same priority. For example, multiple

houses in a neighborhood with photovoltaic panels, or multiple street lights in a street lighting system.

The combination of this form of decentralized control and discrete behavior can reduce the energy utilization in smart grids. To illustrate this, a dc system consisting of a photovoltaic panel and two loads, which are switched off at a specified voltage, is investigated. When the photovoltaic panel is only producing enough power to supply one load, the voltage will eventually drop below the voltage threshold and both loads will switch off. However, in this case one of the loads could have remained operational.

Experimental Results for Loads with Discrete Behavior

To demonstrate this behavior, the experimental set-up shown in Figure 4.5 is used. The set-up is discussed in more detail in Section 4.4, but in essence it consists of a droop controlled converter and two constant power load controlled converters.

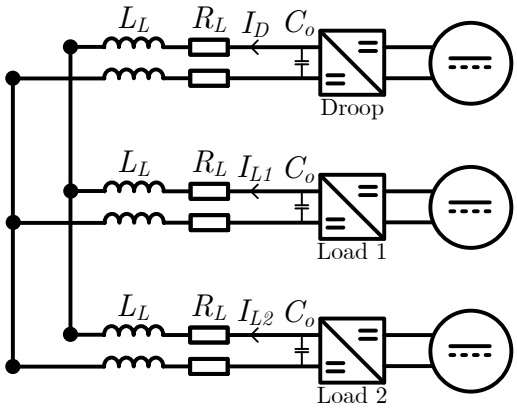

Figure 4.5: Schematic of the experimental dc microgrid set-up consisting of one droop controlled converter and two constant power controlled converters

The droop converter is first operating with a reference voltage of 350 V and a droop constant of 250 W/V, while the two load converters are consuming a constant power of 2.5 kW and switch off when the voltage drops below 325 V. Subsequently, at t = 0.05 s, the droop constant is reduced to 125 W/V. The output voltage of the droop converter and the output currents of the converters are shown in Figure 4.6. Observe that both loads detect an undervoltage and switch off, although one of the loads could have consumed 2.5 kW without the voltage dropping below 325 V. Ideally, only one load should switch off, while the other remains operational. However, since no central controller or communication link is available to ensure that one of the loads remains operational, the system and the available energy are not fully utilized.

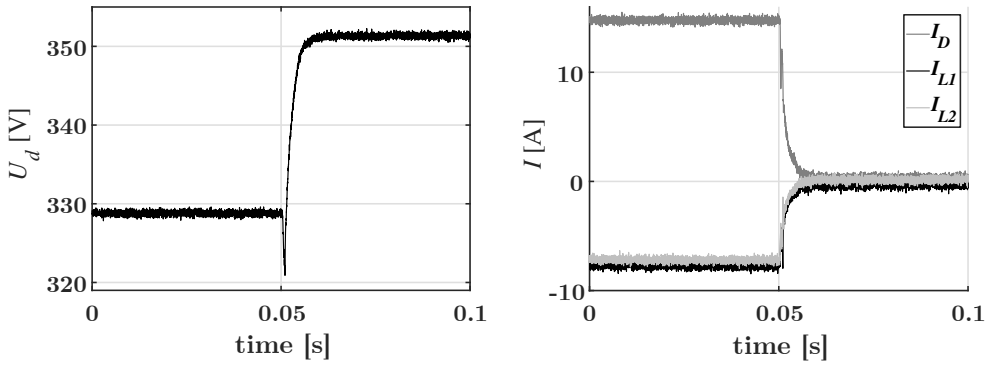

Figure 4.6: Experimental results for two identical loads with discrete behavior and a reduction in the droop converter's droop constant

4.3.2 Grid Sense Multiple Access Algorithm

It was shown that converters, which have identical priority and exhibit discrete behavior, can cause inadequate system and energy utilization. Intuitively, a simple solution might seem to reconnect the converters when the voltage crosses a certain threshold. However, even if the number of connection attempts are limited, both converters detect the same number of failures and eventually both abort attempting connection.

The Grid Sense Multiple Access Voltage Detection (GSMA/VD) algorithm is proposed, which is inspired by the Carrier Sense Multiple Access Collision Detection (CSMA/CD) algorithm, used for local area networking in the beginning of Ethernet [124]. In the CSMA/CD algorithm, data is only sent if the carrier is available and, when a collision is detected during transmission, a jamming signal is sent and the sender waits for a random time interval before re-attempting transmission. Similarly, in the GSMA/VD algorithm, converters connect to a grid when the voltage is above its threshold and, when an undervoltage is detected, the connection is aborted and the converter waits for a random time before re-attempting connection.

The GSMA algorithm uses exponential backoff to make it unlikely that different converters repeatedly attempt reconnection simultaneously. When a converter is connected to the grid, its number of connection attempts N is set to the start value S and the converter is put in an off state. From the off state, if the number of attempts is less than the maximum number of attempts K, the voltage at the converter's output is measured until an acceptable level is reached. Subsequently, the converter will wait a random time between 0 and $\tau \cdot E^N$, where τ is the base time constant and E is the exponential base. Afterwards, the number of attempts is incremented and the converter is switched on. Finally, the grid is continuously sensed and the converter is disconnected if the voltage threshold is crossed. Furthermore, the number of attempts is set to the reset value R if the converter remains successfully connected for at least the reset time T_r.

The GSMA/VD algorithm for loads in dc grids is shown in Figure 4.7, but a similar approach can be used for source converters.

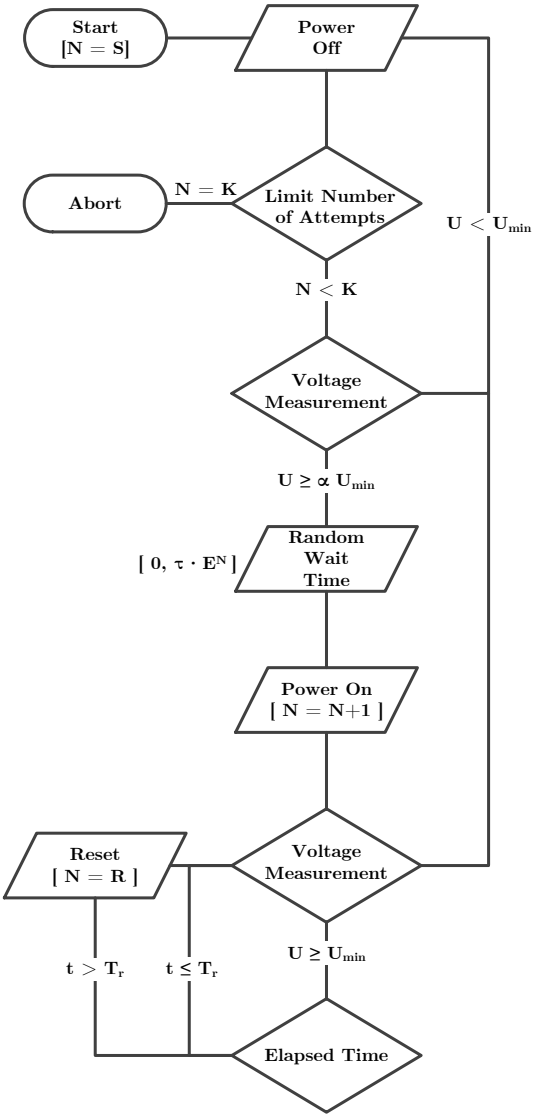

Figure 4.7: The GSMA/VD algorithm for loads in dc smart grids with discrete behavior

GSMA/VD Parameters

The GSMA/VD parameters, which are used for the simulations and experiments in this section, are summarized in Table 4.1. In this subsection, the significance of these parameters is discussed, but the optimization of the exponential backoff component of the GSMA/VD algorithm is beyond of the scope of this thesis, partly because it is dependent on the system and application of the algorithm, presented in [125, 126].

τ [ms]	T_r [ms]	E	S	R	K	α
1	25	2	3	1	8	1

Table 4.1: GSMA/VD parameters, which are used in the simulations and experiments

The base time constant τ determines the time scaling of the control algorithm, which will mostly be determined by the response time of the system. The dc grids in this chapter have a total capacitance of around 1 mF, and a droop impedance of maximally 1 Ω. Therefore, the RC time constants of these systems are around 1 ms.

The reset time T_r determines when a connection attempt is deemed successful. Therefore, T_r should be significantly larger than the base time constant to ensure that the system has reached steady-state, but as low as possible to speed up the decision making process. In this chapter, a conservative reset time of 25 ms is chosen.

The exponential base E dictates how quickly the waiting time increases for consecutive connection attempts. A high base reduces the number of connection attempts as the waiting time increases rapidly, increasing the chance of reaching the reset time. However, the probability of long decision making times are relatively high. On the other hand, a low base generally ensures lower overall decision making times, but may result in many failed connection attempts. Since the objective of the algorithm is to improve energy utilization, and the fluctuations in voltage are deemed acceptable, a base of 2 is chosen.

The start parameter S and the reset parameter R determine if the algorithm prioritizes converters that are attempting connection, or converters that are already successfully connected. If $S < R$ connecting converters have priority over already connected converters, when $S = R$ all converters have equal priority, and when $S > R$ connected converters have priority. Assuming the priority of connected converters and an exponential base of 2, S is chosen as 3 and R is chosen as 1. In this case, the probability that the connected converters reach the reset time in one of the attempts before the connecting converters is high.

The maximum number of attempts K determines how many attempts the converter will take, before connection will be aborted. It must be large enough to make the probability that a converter incorrectly aborts is sufficiently small. However, smaller values of K reduce the number of voltage fluctuations (caused by the failed attempts) and therefore improve the power quality of the system. In this chapter, K is chosen as 8, leading to a final connection attempt with a random time between 0 and 256 ms, making it likely that one of the converters reaches the reset time.

The factor α regulates the hysteresis margin between the voltage at which the converter is disconnected and the voltage at which the converter attempts connection. For loads, the voltage margin α is always equal to or larger than 1, while for sources α is always equal to or lower than 1. In this chapter, hysteresis is not required and therefore α is chosen to be 1.

4.3.3 GSMA/VD Simulation Examples

In this subsection several simulations are performed to illustrate the behavior of the GSMA/VD algorithm. For most of the simulations a reduction in droop constant mostly causes the need for demand response. However, changes in system topology, generation or consumption can also provoke supply or demand response.

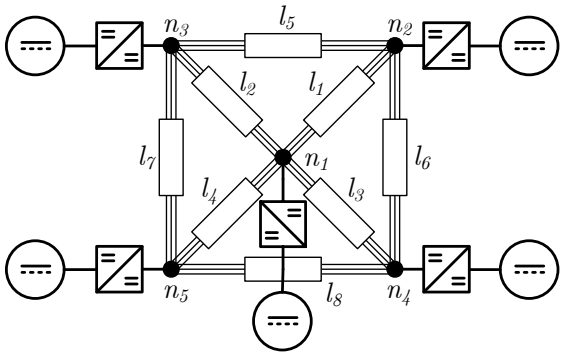

Figure 4.8: Example dc system for the simulations of the GSMA/VD algorithm

For the simulation the bipolar dc smart grid shown in Figure 4.8, and the state-space models from Section 2.4 are used. The resistance, inductance and capacitance of the lines, which are used in the simulations, are 1.0 Ω, 0.25 mH and 0.5 μF respectively.

A droop source is situated at n_1, which has a reference voltage of ±350 V and a droop impedance of 140 W/V. Furthermore, two constant power loads, controlled with the GSMA/VD algorithm, are situated at the other nodes and their reference powers over time are given in Table 4.2.

t [ms]	P_2^* [W]	P_3^* [W]	P_4^* [W]	P_5^* [W]
0	0	0	0	0
50	1500	0	0	1500
100	1500	3000	0	1500
150	1500	3000	2250	1500

Table 4.2: Load powers for the GSMA/VD simulations

Scenario without Demand Response

For the first simulation, the pole-to-pole voltage at which the constant power load converters switch off is configured as 630 V (±315 V). The node voltages, as a result of the given scenario, are shown in Figure 4.9. For clarity's sake, and because the system is symmetrical, only the positive pole quantities are displayed. In the figure, the loads at nodes n_2 to n_5 are indicated with L_2 to L_5.

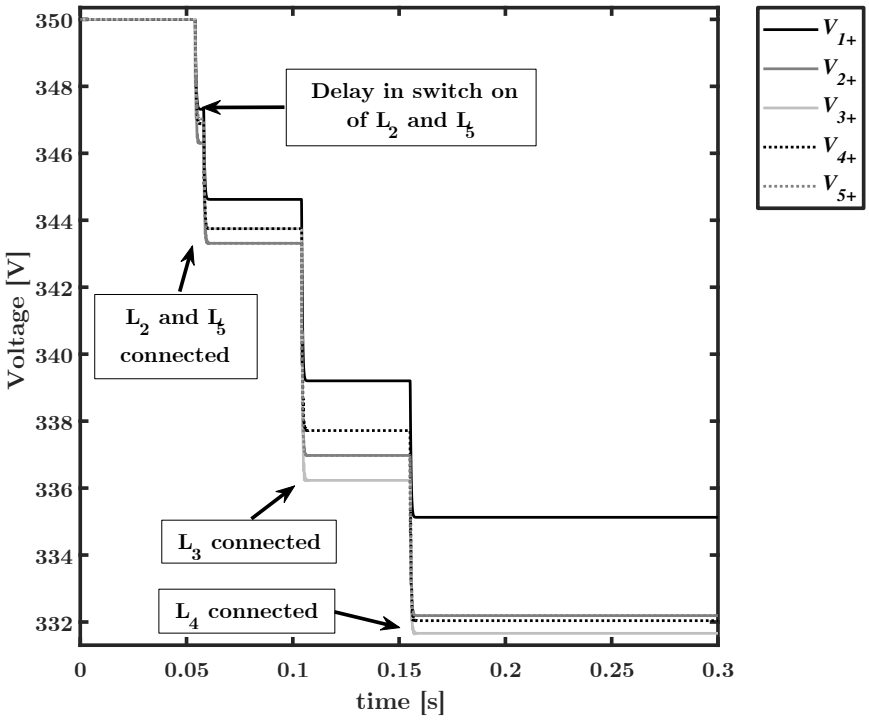

Figure 4.9: Node voltages for the system in Figure 4.8 and the scenario in Table 4.2, when demand response is not required

From Figure 4.9, it is seen that the system remains stable, and that the voltage remains above the 315 V voltage limit. In this case, no demand response is required from any of the GSMA/VD controllers. The only visible effect of the GSMA/VD controllers is the difference of the (short) initial delay at around 50 ms when loads L_2 and L_5 are switched on. This difference is caused by the stochastic nature of the GSMA/VD controllers.

Scenario with Demand Response

For the second simulation, the pole to pole voltage at which the load converters are disconnected is changed to 675 V (±337.5 V). The simulation results for the positive pole node voltages are shown in Figure 4.10. In this scenario, demand response is required to ensure that the system remains above the desired minimum voltage. In this case, load L_3 cannot connect to the grid as this would lead to unacceptably low voltages.

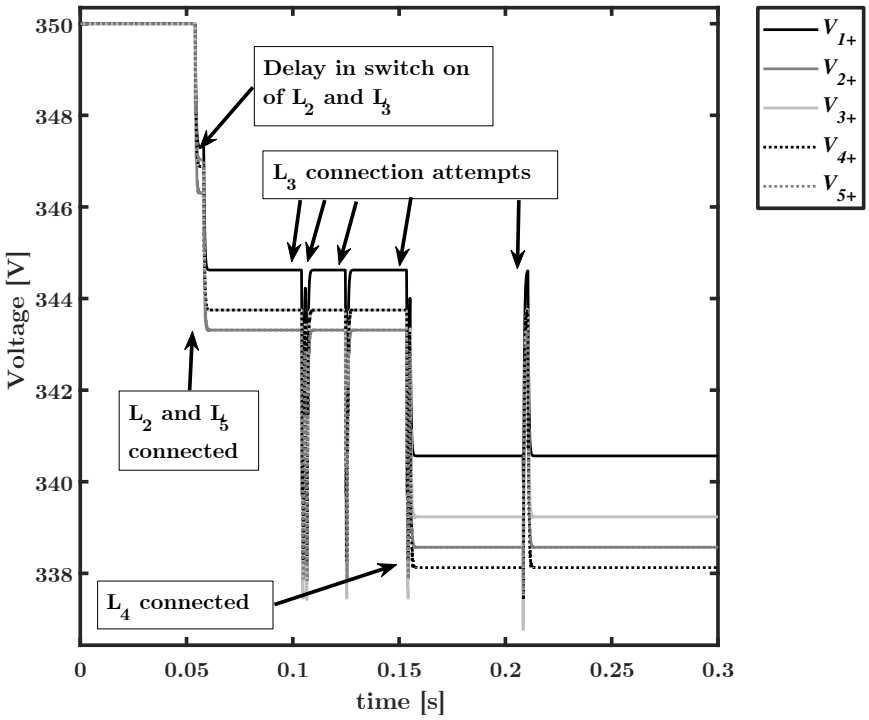

Figure 4.10: Node voltages for the system in Figure 4.8 and the scenario in Table 4.2, when demand response is required

From Figure 4.10, several observations can be made on the algorithm's behavior in a scenario where demand response needs to be applied. First, a small difference in the delay of loads L_2 and L_5 can again be seen around 50 ms. Second, at around 100 ms, the load at n_3 cannot be switched on since this brings the voltage at n_3 below ±337.5 V. Therefore, this load attempts to connect 5 times at increasing intervals, after which the connection is aborted. Third, the source can supply power to load L_4 without the voltage dropping below ±337.5 V. Load L_4 is shortly interrupted at 210 ms because of the last attempted connection of load L_3. However, load L_4 recovers quickly since the time it was connected exceeds the reset time, T_r, of 25 ms.

Scenario with Simultaneous Connection

The last simulation is designed to illustrate the behavior of the GSMA/VD algorithm when two loads, which have the same voltage threshold, attempt connection at the same time. Such a scenario can occur, for example after a blackout. For this simulation, only loads L_2 and L_5 are operated, and the pole to pole voltage at which the loads are disconnected is changed to 690 V (±345 V). Under these conditions, only one of these identical loads can be supplied by the source. Since both loads have the same priority, which converter remains connected to the grid is random. The simulation results for the positive pole node voltages are shown in Figure 4.11.

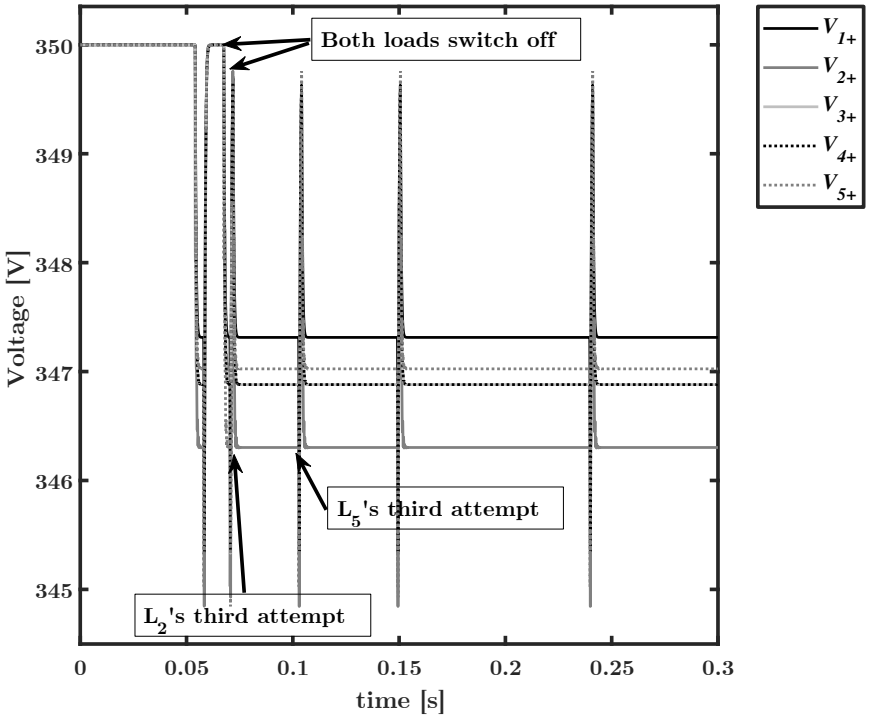

Figure 4.11: Node voltages for the system in Figure 4.8 and the scenario in Table 4.2, when two loads are connected simultaneously

At 50 ms, the converters attempt connections at roughly the same time twice and therefore both fail to connect. However, at around 75 ms the load L_2 attempts connection significantly earlier than load L_5 and therefore the reset time is exceeded. Consequently, after the next three connection attempts of load L_5, load L_2 recovers quickly and remains connected. Nonetheless, the last three unsuccessful connection attempts of load L_5 cause short interruptions in the operation of load L_2.

4.4 Experimental Results

In this section the behavior of the GSMA/VD algorithm is validated by conducting experiments on a laboratory scale dc distribution grid. Four experiments are conducted to show the algorithm's behavior in different scenarios. The experimental set-up consists of three power electronic converters, which are connected to a dc bus via line emulation circuits. More detailed information on the power electronic converters and the line emulation circuits can be found in Appendix A. A simplified schematic and a picture of the experimental set-up is shown in Figure 4.12.

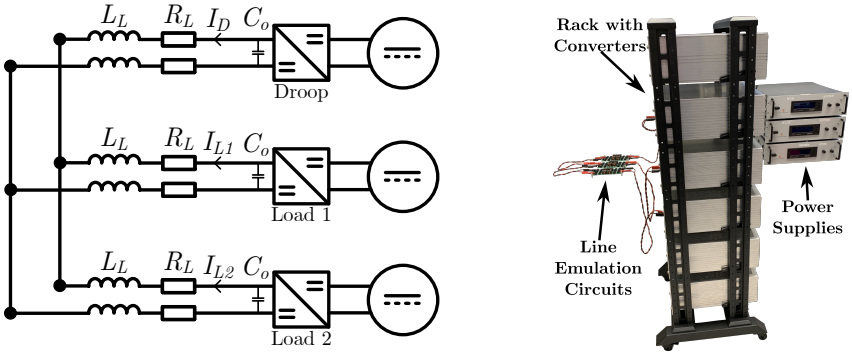

(a) Schematical overview (b) Picture

Figure 4.12: Experimental setup that is used to validate the behavior of the GSMA algorithm

During the experiments, the three converters are operated as dc/dc interleaved boost converters. One of the converters, labeled throughout the section as "Droop", implements a power droop control with a reference voltage of 350 V. The two other converters, labeled "Load 1" and "Load 2", are programmed to exhibit constant power load behavior with a power of 2.5 kW each.

In this section, the droop converter is operated with a reference voltage of 350 V and a droop constant of 250 W/V, unless otherwise specified. Furthermore, the two load converters are operated as 2.5 kW constant power loads with GSMA/VD controllers. Moreover, the voltage at which the GSMA/VD algorithm disconnects the load converters is set to 325 V.

4.4.1 Disconnection of a Single Load

For the first experiment only one load is connected to the dc microgrid, while the other load remains non-operational. The droop constant of the droop converter is then reduced from 250 W/V to 75 W/V at $t = 0.1$ s. The resulting output voltage of the droop converter and the output currents from all the converters are shown in Figure 4.13.

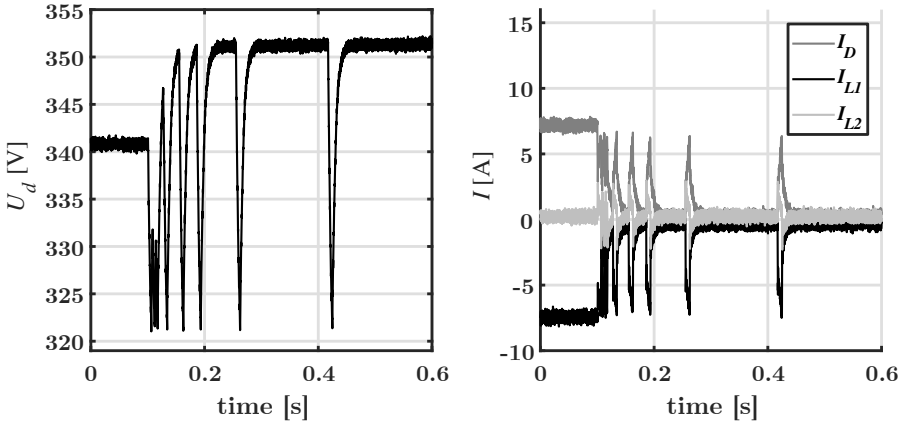

Figure 4.13: Experimental results for one load utilizing the GSMA/VD algorithm

Observe that, at $t = 0.1$ s, Load 1 attempts reconnection up to seven times with increasing intervals between attempts. Finally, the connection is completely aborted and the system is left in steady-state without the load connected at a voltage of 350 V.

4.4.2 Demand Response of Two Loads with Equal Priority

For the second experiment, both loads are connected to the dc microgrid. Subsequently, the droop constant is reduced from 250 W/V to 125 W/V at $t = 0.1$ s. The experimental results for this scenario are shown in Figure 4.14.

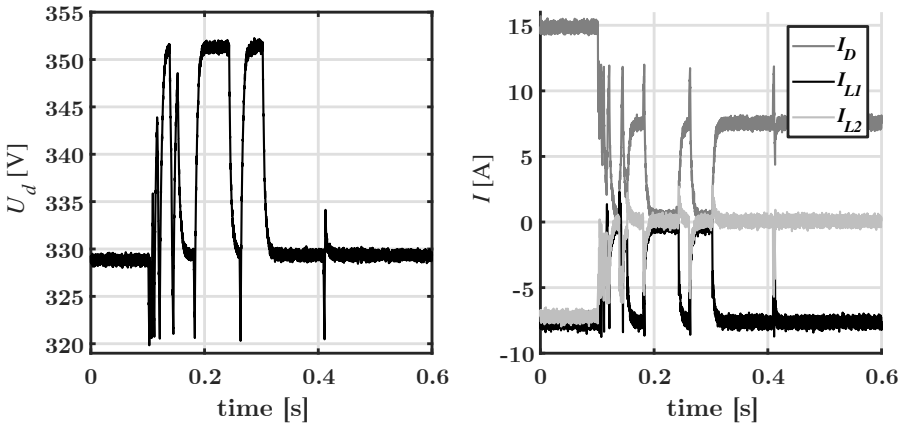

Figure 4.14: Experimental results for two loads with the GSMA/VD algorithm of which only one can remain connected to the grid

When the droop constant reduces at t = 0.1 s neither of the converters are able to connect successfully to the grid at first. However, at around 0.3 s Load 1 is successfully connected for more than 25 ms. Therefore, the number of connection attempts for Load 1 is reset and it remains connected after Load 2 reaches its maximum number of attempts.

4.4.3 Priority According to the Connection Status

For the third experiment, the droop constant of the droop converter is kept at 125 W/V during the experiment. Load 2 is successfully connected to the grid, after which Load 1 attempts connection at t = 0.1 s. The droop converter's output voltage and all the converters output currents are shown in Figure 4.15.

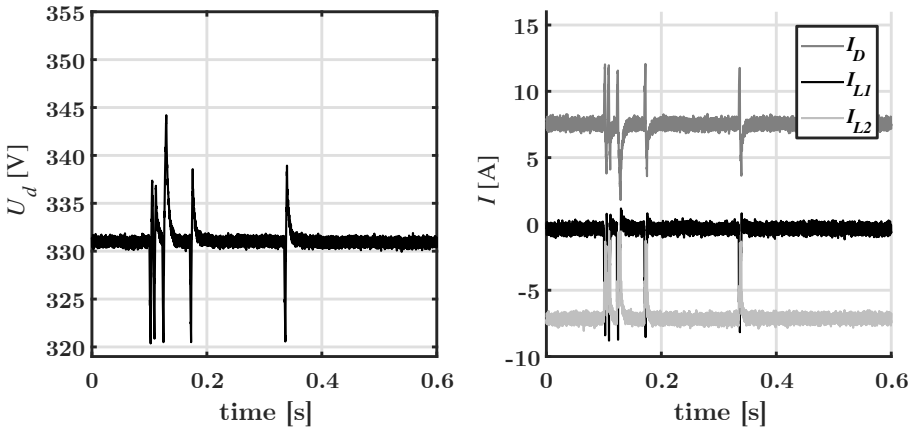

Figure 4.15: Experimental results for two loads with the GSMA/VD algorithm showing the priority of an already connected converter

Note that, due to the choice in S and R, the GSMA algorithm gives priority to converters which are already connected to the grid. Consequently, Load 1 is unsuccessful in connecting to the grid, while Load 2 remains connected. However, it is important to note that this is only the case if they have the same priority in terms of the voltage at which they switch off, which will be shown in the last experiment.

4.4.4 Priority According to the Voltage Limit

For the last experiment, the droop constant of the droop converter is again kept at 125 W/V during the experiment. The threshold voltage at which Load 2 switches off is changed to 320 V, while that of Load 1 remains at 325 V. Load 1 is successfully connected to the dc microgrid first, after which Load 2 is switched on at t = 0.1 s. The results of this experiment are shown in Figure 4.16.

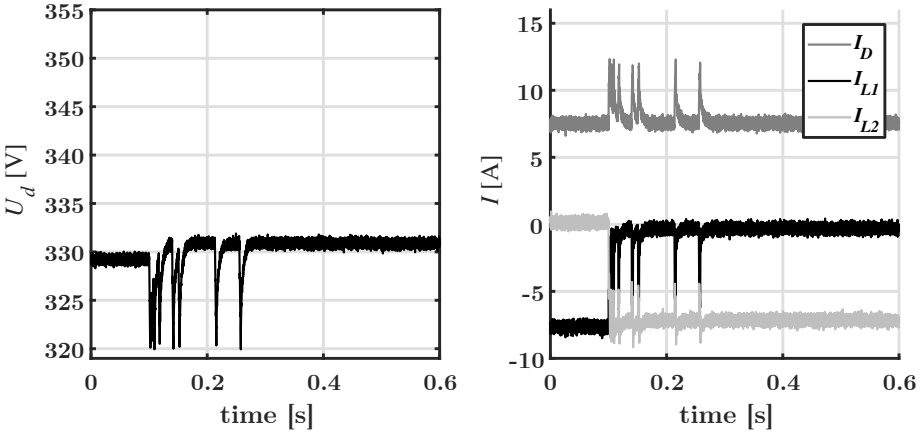

Figure 4.16: Experimental results for two loads with the GSMA/VD algorithm when the priority is set by the voltage at which they switch off

Observe that, although the GSMA algorithm enables decisions to be made when converters of equal priority are connected, the priority of converters is still primarily determined by the voltage at which they switch off. In the experiment, Load 1 detects an undervoltage when Load 2 attempts connection, while Load 2 does not. Therefore, Load 1 attempts to reconnect until its maximum number of attempts is reached, after which connection is aborted.

Advantages and Challenges of GSMA

The GSMA algorithm has several advantages. First, the algorithm is suitable for grids which (temporarily) do not have a communication infrastructure. Second, the priority of loads and sources is still primarily determined by the chosen voltage at which the converter disconnects. Third, the priority between connected converters and connecting converters with the same thresholds can be selected via R and S. Last, when converters have equal priority, it is randomly decided which subset of converters remain connected to the grid.

There are also a few drawbacks related to the GSMA algorithm. First, due to the local measurement of the grid, the priorities of the converters can be distorted due to the effects of the grid topology. However, this is not a consequence of the algorithm but a general consequence of decentralized control. Second, although fluctuations do not occur endlessly, up to K fluctuations occur for every significant change in the system where a decision must be made. Nevertheless, the fluctuations occur within the set minimum and maximum voltage. Third, during the decision-making process (which takes up to τE^{K+1}), converters equal in priority can experience intermittent operation. For the chosen parameters, a decision is made within 500 ms.

4.5 Conclusions

Because of the decentralization and segmentation of the grid, and in order to sustain operation when the communication infrastructure is (temporarily) unavailable, decentralized control is essential for dc distribution systems. The decentralized controllers must ensure that the system is stable and a balance between supply and demand is found, without utilizing any form of communication.

It was discussed that droop control is the most commonly applied strategy in dc distribution systems, and that stability and power quality can further be improved by adapting the controller according to the state of the system. However, the methods from literature only guarantee stability for well defined systems or if communication is used. In this chapter a decentralized control strategy was proposed that ensures global plug-and-play stability and voltage propriety, without using communication. First, the area between the desired maximum and minimum voltage was divided into demand response, emission, absorption and supply response regions. Second, it was described how source, load and hybrid converters should behave in these regions. In general, converters should ramp their output power or switch on/off when the locally measured voltage changes. Last, to ensure precise control decisions, it was discussed that the ramp time and ramp rate of converters are bound by the system's time constants and desired accuracy.

It was experimentally shown that decentralized control strategies, which implement voltage dependent supply or demand response, can cause inadequate energy utilization. For example, when a source is only able to supply the power for one of two loads and both loads detect an undervoltage and switch off. To solve this issue, the GSMA algorithm was proposed, which measures the local voltage and implements an exponential backoff when the voltage crosses the set threshold. Simulations showed that the GSMA algorithm allows a subset of converters, which have the same voltage threshold, to remain connected to the grid, improving the energy utilization in the grid. Moreover, the priority between several converters can be controlled via the algorithm's parameters.

Several experiments were performed, which confirmed that the decentralized control strategy ensures stability and voltage propriety. Furthermore, the experiments showed that the GSMA algorithm works in practice and the priority of converters can be set according to their connection status and voltage thresholds.

The results from this chapter can be used to build a foundation for the control of dc distribution systems. However, it is recommended to also implement some form of coordinated control in order to improve, for example, the economic viability of the systems. Distributed control can achieve complex objectives, without requiring or depending on an expensive communication infrastructure.

Chapter 5

Decentralized Protection Framework and Scheme

The protection of low voltage dc grid is challenging due to the lack of a natural zero crossing, low inertia, meshed topologies and bi-directional power flows. In this chapter, the literature is reviewed, and a decentralized protection framework is presented that offers entities interacting with different parts of the grid insight on the dangers and requirements. Furthermore, a decentralized protection scheme is proposed, which ensures selectivity via a distinct solid-state circuit breaker topology and time-current characteristic for the protection devices. Experiments showed that the protection scheme is effective at ensuring security and selectivity for radial and meshed low voltage DC grids. However, future research into the grounding, overvoltage protection and residual current detection is still recommended.

This chapter is based on

- N. H. van der Blij, P. Purgat, T. B. Soeiro, L. M. Ramirez-Elizondo, M. T. J. Spaan and P. Bauer, "Protection Framework for Low Voltage DC Grids", 19th Power Electronics and Motion Control Conference (PEMC), 2020.
- N. H. van der Blij, P. Purgat, T. B. Soeiro, L. M. Ramirez-Elizondo, M. T. J. Spaan and P. Bauer, "Decentralized Plug-and-Play Protection Scheme for Low Voltage DC Grids", Energies, vol. 13, Jun. 2020.

5.1 Introduction

In this chapter, a nanogrid refers to a grid inside a building or property that is able to be operated independently, which typically have a power rating of up to 10 kW. Furthermore, microgrids refer to (independent) low voltage grids that have a power rating of up to 500 kW. Microgrids interconnect several nanogrids and/or higher power production, consumption and storage. Additionally, when this chapter refers to macrogrid it refers to any distribution or transmission grid that is not low voltage [127]. An example of a system that is defined in this way is shown in Figure 5.1.

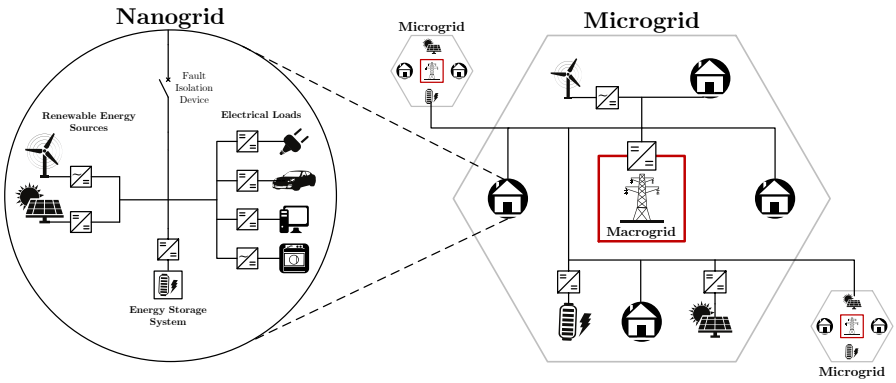

Figure 5.1: A microgrid that consists of several nanogrids, production, and storage that is connected to other microgrids and the macrogrid [127]

In general, the protection system of low voltage dc grids must ensure that:

- It is **safe** for devices and individuals to interact with the grid.
- The detection methods are **sensitive** to the different types of faults.
- The protection devices are **secure**, such that they do not unnecessarily trip.
- The protection scheme is **selective** and isolates only the faulted section.
- The fault is cleared **fast**, to prevent damage and blackouts.
- The protection of the system is **cost-effective**.

Moreover, the protection system must adhere to each of these requirements under non-faulted, overvoltage, overcurrent and fault clearing conditions [128–130].

In Section 5.2, a zonal decentralized protection framework is presented for low voltage dc grids, which partitions the grid according to short-circuit potential and the provided degree of protection. In Section 5.3, a decentralized plug-and-play protection scheme is proposed that utilizes a distinct SSCB topology and time-current characteristic to achieve selectivity. In Section 5.4, several experiments are carried out to validate the findings.

5.2 Decentralized Protection Framework

For personnel and devices it is crucial to know the dangers and requirements for interacting with different parts of the grid. Therefore, the grid is partitioned into different protection zones, where the protection is able to galvanically isolate the zones from each other. The suggested zones differentiate between sections of the grid according to their short-circuit potential or equivalently to their voltage. The various protection zones for low voltage dc grids are shown in Fig. 5.2.

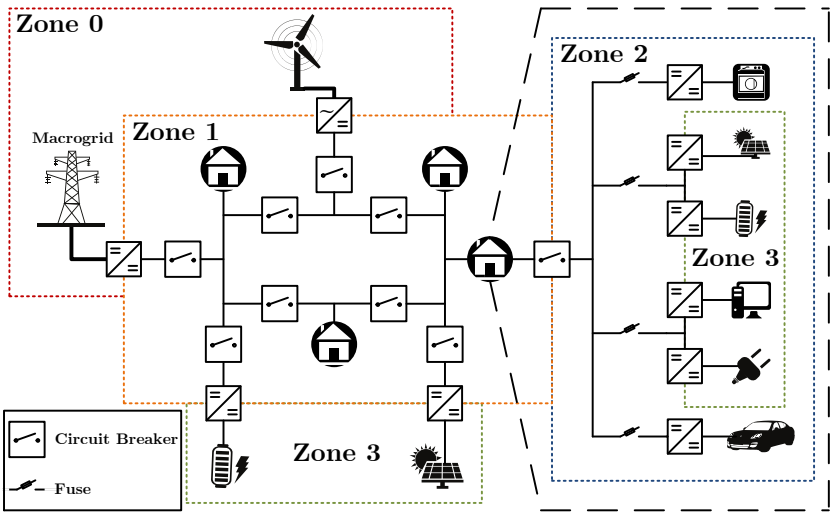

Figure 5.2: Protection zones for low voltage dc grids where the zones are distinguished according to their short-circuit potentials

Zone 0 occurs at the interfaces of the low voltage grid(s) and the macrogrid, or other medium or high voltage applications (for example, a wind turbine). Among all the zones Zone 0 has the highest potential short-circuit currents and therefore is conceivably the most harmful to entities and devices interacting with it.

Zone 1 is mostly situated on a microgrid level where the voltage between the conductors and ground ranges from 350 to 1500 V (often in unipolar or bipolar configuration). This region mostly interfaces different nanogrids, generation, storage and the macrogrid, and therefore is likely to have a relatively high short-circuit potential but relatively low inertia. Therefore, this zone has the potential for high short-circuit currents, but which will only persist for several microseconds to milliseconds.

Zone 2 is found in nanogrids with voltages between 42 and 350 V, which are mostly in monopolar or unipolar configurations. Nanogrids can be interfaced to a microgrid via a converter, or via a (solid-state) circuit breaker. This zone is characterized by relatively low short-circuit potential, but high inertia due to the low voltage and combined capacitance of the many converters in this grid.

Zone 3 arises on the application or device level and in this zone the standards for Safety/Protected Extra Low Voltage (SELV/PELV) should be adhered to. Therefore, the voltage should be kept below 42 V and it should be safe to touch everywhere in the system. This zone is likely to occur at, for example, photovoltaic panels and USB-C interfaces.

It is important to emphasize that zones can only be crossed by protection that provides provide galvanic isolation. Therefore, solid-state circuit breakers must include an auxiliary mechanical switch in order to cross different zones. Furthermore, in this chapter it is assumed that the nanogrids are interfaced to microgrids via a circuit breaker, and not via a power electronic converter. This is because most nanogrids, such as households, only operate at their peak power a fraction of the time they are operational. Consequently, it is both more cost and energy efficient to utilize a circuit breaker at the entrance of a house instead of a fully rated power electronic converter (which is also a common practice for low voltage ac grids).

5.2.1 Protection Tiers for Low Voltage DC Grids

The previous subsection divided low voltage dc grids into several zones according to their (short-circuit) potential. However, not only this determines how safe a grid section is, but also the provided level of protection in that area. Therefore, in this subsection the zones are further divided into tiers of protection.

The parts of the zone that do not provide any protection for faults and/or short-circuits fall under **Tier A**. This tier occurs, for example, at the terminals of source and storage devices. Since this tier does not provide any guarantee on the safety or survivability of entities and devices interacting with the tier, the probability for serious injury or damage can be high. Therefore, any possibility for interaction with this tier should be minimized.

In **Tier B** no autonomous protection devices are present, but devices are individually protected. In this tier short-circuits and faults are not interrupted, but connected devices are not destroyed due to internal or external transient events. This protection can be provided by specialized protection circuitry, or by the power electronic converters and the control thereof. However, the probability for the injury of personnel can still be high in this tier.

Faults in **Tier C** are interrupted when a specified current persists for a specified amount of time. Additionally, connected devices in this tier should also be protected from damage due to faults. The protection required for this tier could be provided by, for example, fuses, converters and/or circuit breakers.

Tier D ensures that faults are interrupted before significant current can flow. Since fault currents in this tier are the lowest, this tier provides the lowest probability for damage and/or injury. In the following sections it will be explained that, in most cases, solid-state protection devices with an internal fault limiting inductance are preferred for this tier of protection.

To illustrate the different tiers a simplification of the current path from the household battery to the macrogrid from the Fig. 5.2 is considered. If we assume that the

power electronic converters in the low voltage dc grid provide overcurrent protection (but not fault current prevention) and the circuit breakers provide Tier D protection, the different tiers of this system are shown in Fig. 5.3.

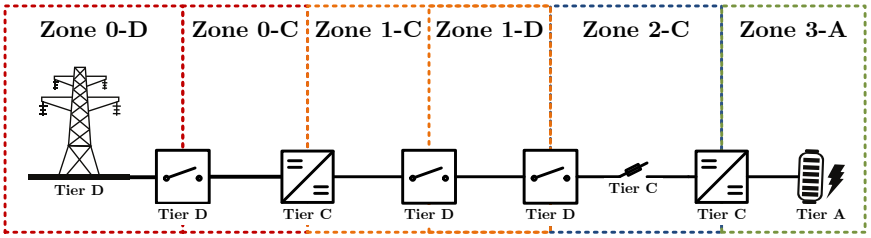

Figure 5.3: Protection tiers for low voltage dc grids where the tiers are distinguished according to their levels of fault propagation

From Fig. 5.3 it is clear that, if the power electronic converters only provide overcurrent protection, a Tier D circuit breaker should be placed near it to ensure Tier D protection. Overall, the protection tier of a zone is determined by the device with the lowest protection grade connected to it. Therefore, it is likely beneficial to standardize a minimum protection tier for devices in each zone. Moreover, since loads can only provide limited energy to the fault, there will likely be different requirements for source/storage converters and load converters for acquiring the same protection tier.

5.2.2 Protection Recommendations for Low Voltage DC Grids

For all zones, possibilities for interaction with Tier A sections of the grid should be minimized as much as possible. Furthermore, to ensure the survivability of devices in the system when short-circuits occur, the capacitors of the converters should be able to survive (a limited number of) short-circuit discharges.

In Zone 3 the grid is touch-safe and therefore, additional protection is not necessarily required. However, it is recommended that each device in this zone is able to withstand a short-circuit at its terminal. Therefore, it is advisable that extra low voltage devices are interconnected utilizing a Zone 3-B configuration.

Zone 2 is not touch-safe, but the short-circuit potentials and inductances are relatively low. Therefore, it is sensible that fault currents are limited by using a Zone 2-C configuration. Different sections in Zone 2-C can be isolated with fuses (or a current limiter), and sources and storage devices should not feed into the fault indefinitely.

For Zone 0 and Zone 1 the short-circuit potential and inductance in the grid are typically large. Protection in accessible portions of these zones should be of at least Tier D. Tier D protection is required in these grids to prevent blackouts and to ensure selectivity.

5.3 Plug-and-Play Protection Scheme

Because of the limited overload capability of power electronic converters, being able to withstand short-circuit conditions for milliseconds leads to oversized components in terms of current-carrying capability [32,128,131]. Furthermore, for dc systems with low inertia, a blackout is inevitable when a fault is sustained for a longer period of time. Therefore, although fuses, electromechanical devices and hybrid circuit breakers provide solutions for clearing faults in the order of milliseconds to seconds, much faster fault detection and interruption is required for low voltage dc systems [32, 132–134]. In this chapter, the low voltage dc distribution systems are protected with SSCBs that can detect and interrupt faults within microseconds [135, 136].

Several non-unit and unit protection schemes for low voltage dc grids have been reported in literature [110,137,138]. Non-unit protection schemes utilize local measurements in order to detect faults. Many of these protection schemes measure the current and current rate-of-change, and circuit breakers are opened when preset thresholds are exceeded, but the utilization of higher order derivatives of the current and the grid's voltage are also reported [139–141]. The main advantages of non-unit protection schemes are their simplicity, and their resilience to the failure of protection devices when a hierarchical structure of circuit breakers is used. However, these schemes have difficulty isolating only the faulted areas of the grid and thus achieving selectivity. Therefore, protection schemes were proposed that utilize knowledge about the system's topology in order to achieve selectivity. For example, faults can be located by measuring the grid's impedance and comparing it to known line parameters, or a wavelet transform can be used to identify faults by comparing them to simulations of the system [142–146]. Furthermore, a handshaking protection scheme was introduced, which locates and isolates a fault by temporarily powering down the dc system [147]. Nevertheless, these methods struggle to ensure selectivity when system parameters are uncertain or the system topology is changing. On the other hand, unit protection schemes achieve selectivity by utilizing a communication infrastructure. For instance, differential protection schemes locate faults by comparing the currents at different locations in the system, and event-based protection schemes ensure selectivity by combining local detection with central decision-making [148–154] However, since fast fault detection and interruption is required in low voltage dc grids, utilizing a communication infrastructure is not desirable.

In this section it is experimentally demonstrated that fast fault propagation and the commutation of inductive currents are two challenges for the selectivity of decentralized protection schemes. Furthermore, a decentralized plug-and-play protection scheme is presented, which ensures selectivity without utilizing communication and with minimal knowledge about the system. The protection scheme is plug-and-play in the sense that selective protection is provided on both sides of the circuit breakers in the system, regardless of the system's configuration or where the circuit breakers are located in the system and without requiring (re)configuration of the circuit breakers. Moreover, the protection scheme is experimentally validated, showing the effectiveness of the protection scheme for different low voltage dc systems under various conditions.

5.3.1 Short-Circuit Fault Currents in Low Voltage DC Grids

In low voltage dc grids overvoltages can occur when, for instance, lightning strikes one of the conductors. Therefore, surge arresters such as Metal Oxide Varistors (MOVs) or spark gaps should be used to clamp the voltage. Furthermore, short-circuits can occur when, for example, a tree falls on one of the overhead lines or the insulation deteriorates in one of the underground lines. In those cases, one or more conductors are short-circuited to each other or to the ground [155].

To calculate the short-circuit fault current in a monopolar dc grid, the equivalent circuit in Figure 5.4 is used [137, 139, 143]. The fault current is highest when the voltage on the non-faulted part of the system remains constant, and therefore this part of the system is modeled by a voltage source U_{dc}. Furthermore, the SSCB is modeled by an ideal switch, its on-state resistance R_{CB} and its (intrinsic) inductance L_{CB}. Therefore, the overhead or underground line(s) between the SSCB and the short-circuit are modeled by a lumped element π-model.

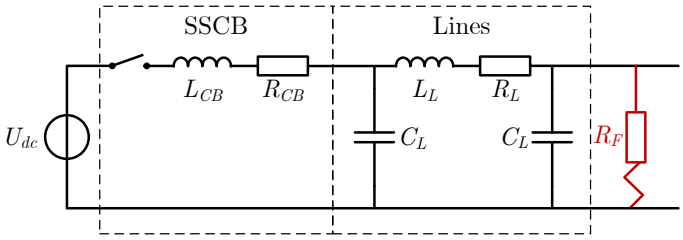

Figure 5.4: Equivalent circuit to calculate the worst-case short-circuit fault current in dc grids

Simulation results for the current during a low resistance fault (0.1 Ω) and a high resistance fault (10 Ω) are shown in Figure 5.5. The fault current is shown for different lengths of the distribution line between the SSCB and the fault, which have a typical resistance of 1 Ω/km, an inductance of 0.25 mH/km and a capacitance of 0.5 μF/km. Furthermore, during these simulations the grid voltage U_{dc} is 350 V, the on-resistance R_{CB} is 0.1 Ω, and the SSCB's inductance L_{CB} is 1 μH.

Since C_L is small, the fault current can be approximated by

$$I_F(t) = \frac{U_{dc}}{R_{CB} + R_L + R_F} \left(1 - e^{-\frac{R_{CB}+R_L+R_F}{L_{CB}+L_L} t}\right), \tag{5.1}$$

where R_F is the resistance of the fault.

Note that the steady-state fault current is only determined by the total resistance, which is the reason short-circuit currents are so high in dc grids. Moreover, the line length only has a significant influence on the steady-state current when the fault resistance is low. Furthermore, by differentiating (5.1) it becomes clear that the current rate of change is only determined by the sum of the inductances in the system.

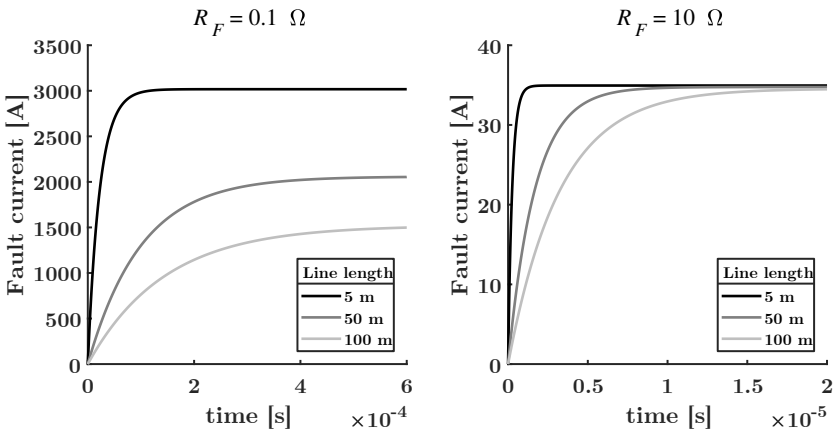

Figure 5.5: Simulation results for the fault current in the equivalent circuit of Figure 5.4 for different fault resistances and distribution line lengths

The thermal and electrical design of the SSCBs and other components in the grid are dependent on the duration and magnitude of the worst-case fault current that they need to be able to sustain. In the worst case, the short-circuit occurs close to the terminals of the SSCB, making the total inductance close to L_{CB}. Furthermore, SSCB's are designed to have as low on-state resistance as possible in order to improve the system's efficiency. Therefore, if the current before the fault was the nominal current I_{nom}, the worst-case fault current can be approximated by

$$I_{F,\max} = \frac{U_{dc} t_{\max}}{L_{CB}} + I_{\text{nom}}, \tag{5.2}$$

where $t_{\max}$ is the maximum time that the SSCB needs to detect the fault and open its switches.

From (5.2) it is clear that, in order to reduce the worst-case fault current, fast fault detection and interruption are essential. Furthermore, even though SSCBs can detect and clear faults within 1 μs, a current limiting inductance is often added to SSCBs in order to further limit the maximum fault current. For example, assuming a grid voltage of 350 V, an SSCB clearing time of 1 μs, a nominal current of 20 A, and a current limiting inductance of 1 μH, the maximum fault current is 370 A.

Since the worst-case fault current develops when the short-circuit occurs at the SSCB's terminals, this worst-case fault current is not dependent on the system's parameters or uncertainty in the system. Furthermore, pole-to-pole faults in (grounded) unipolar and bipolar grids exhibit similar behavior to the behavior described in this section, although the resistance and inductance of the return path has to be taken into account. However, because ground faults in these grids have an identical equivalent circuit and behavior, the maximum fault currents in these grids are the same.

5.3.2 Design and Experimental Validation of the SSCBs

The base design of the SSCBs that were developed to investigate non-unit protection schemes is shown in Figure 5.6. To interrupt the various short-circuit faults, two anti-series SiC (Cree C3M0065090D) switches are used for both the positive pole and the neutral. Furthermore, to prevent an avalanche breakdown of the switches and overvoltages in the grid, Metal Oxide Varistors (MOVs) are used to clamp the voltage. The design parameters of the SSCB are given in Table 5.1.

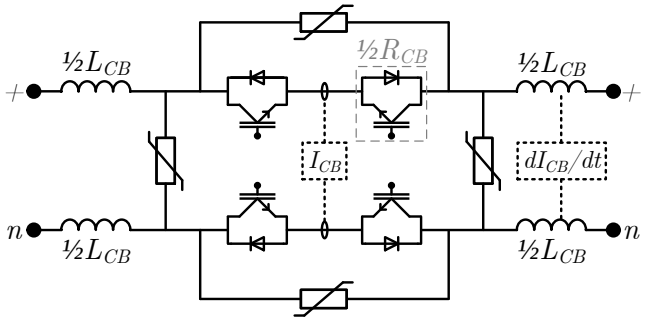

Figure 5.6: Base design of the solid-state circuit breakers that are used in this chapter

Parameter	Acronym	Value
Nominal voltage	U_{nom}	350 V
Nominal current	I_{nom}	10 A
On-state resistance per pole	R_{CB}	130 mΩ
Current limiting inductance	L_{CB}	1.0 μH
Maximum clearing time	t_{max}	1.0 μs

Table 5.1: Design parameters of the solid-state circuit breaker

The SSCB measures the current via a high bandwidth hall-sensor, and the current rate-of-change (di/dt) via the voltage across the current limiting inductor. Using analog comparators, logical gates, and a latch circuit, the switches are turned off when the current through the SSCB or the voltage across the inductor exceed their set thresholds. It will be shown that it is able to detect and open its switches within 1 μs after its thresholds are exceeded. A picture of the SSCB's hardware realization can be found in Appendix A in Figure A.4b.

To validate the operation of the developed SSCB, one side is connected to a voltage source of 350 V while a short-circuit is induced at the other side using a mechanical relay and a variable resistor, which is shown in Figure 5.7. For the experiments, the thresholds for the overcurrent and inductor voltage (di/dt) detection are set to 21 A and 20 V (20 MA/s) respectively.

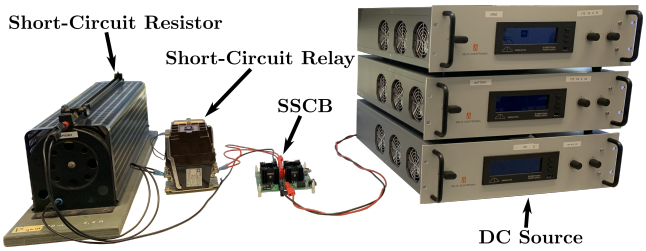

Figure 5.7: Experimental setup for the validation of the solid-state circuit breaker's operation

To show the correct operation of the overcurrent detection, the SSCB is short-circuited at its terminal with a relatively high fault resistance and low inductance (8 Ω and 0 μH respectively). The fault current I_F and the voltage over the current limiting inductor U_L for this experiment are shown in Figure 5.8. At the fault occurrence the di/dt is high, but because the analog detection circuits use small filter capacitors and the system's time constant is low (due to the large fault resistance), the voltage over the inductor does not exceed its 20 V threshold long enough to trip the di/dt detection circuit. However, when the fault current exceeds the 21 A threshold, overcurrent is detected by the analog control logics and the switches are opened within 1 μs.

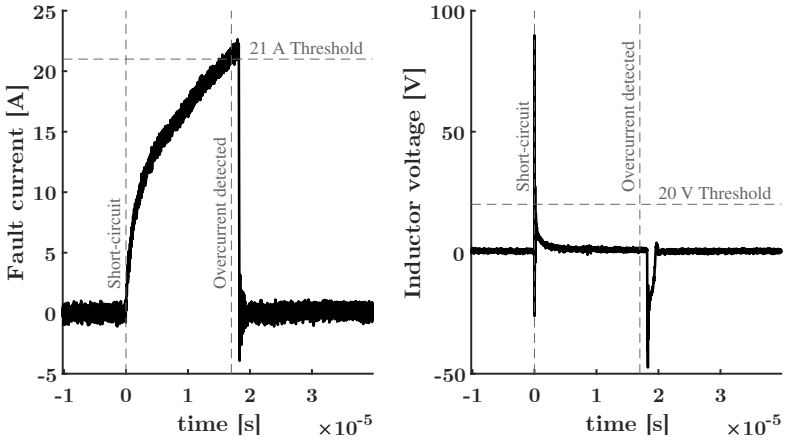

Figure 5.8: Experimental results when the SSCB is short-circuited with a high fault resistance resulting in the overcurrent detection being triggered when the current exceeds 21 A

To show the adequacy of the di/dt detection, the experiment is repeated with relatively low fault resistance (2 Ω). The results for this experiment are shown in Figure 5.9. Because the system's time constant is lower, the voltage over the inductor

remains above the threshold significantly longer. Therefore, the analog di/dt detection is triggered and the fault is cleared within 400 ns of its occurrence.

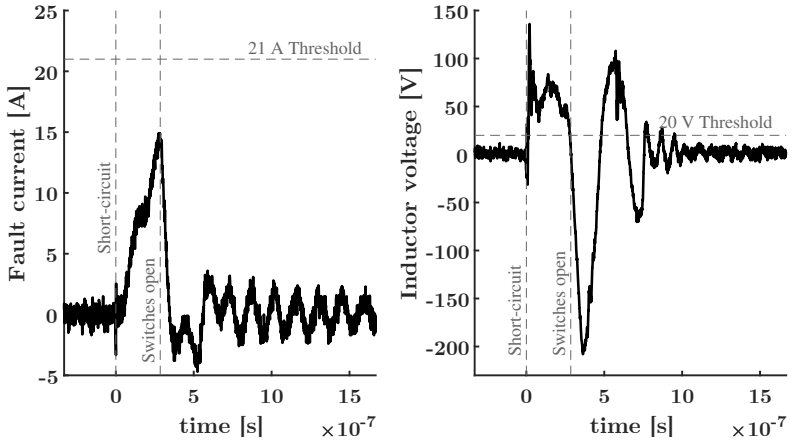

Figure 5.9: Experimental results when the SSCB is short-circuited with a low fault resistance resulting in the di/dt detection being triggered when the 20 V (20 MA/s) threshold is exceeded for a longer time

From these two experiments it can be concluded that both the overcurrent and di/dt detection circuits operate adequately, and the SSCB clears faults within 1 μs. In the remainder of this chapter three of these SSCBs will be used to experimentally validate the presented theoretical work.

5.3.3 Non-unit Protection Scheme Challenges

It was shown that faults can be cleared by measuring the current and current rate of change locally and tripping the breaker if preset thresholds are exceeded. Fast and robust fault interruption is possible with such an approach, since no communication infrastructure is utilized. However, it will be shown here that achieving selectivity is challenging when using these non-unit protection methods.

Low Impedance Faults in Low Inductive Sections

Although the SSCBs current limiting inductance ensures a maximum fault current magnitude, it does not always prevent the fault from propagating through the system and tripping multiple protection devices. To show this the experimental setup shown in Fig. 5.10 is used. In this setup, a constant voltage source of 350 V and two constant current loads of 5 A are connected to a low inductive dc bus via three SSCBs. This situation can occur, for example, in a dc household that is disconnected from the main grid, where the photovoltaic (PV) panels are providing the energy for loads in two other groups inside the house.

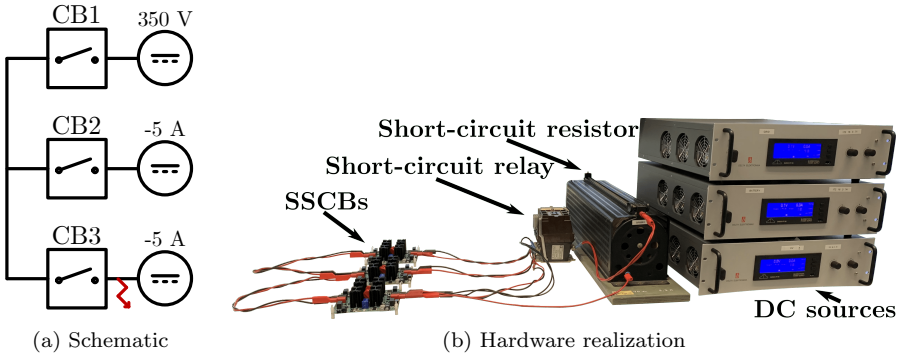

(a) Schematic (b) Hardware realization

Figure 5.10: Experimental setup consisting of a constant voltage source and two constant current loads connected through three SSCBs, and a short-circuit at the terminals of one of the SSCBs

To show that, in some cases, the fault propagates through the system and trips all the SSCBs before the SSCB in the faulted group can react, a short-circuit with a very low fault resistance (0.75 Ω) is induced at the load-side terminal of CB3. The experimental results for the voltage over the current limiting inductance of CB2 U_{L2} and the currents flowing in each circuit breaker are shown in Fig. 5.11. Observe that, even though the fault occurs at the load side of CB3, the voltage over the current limiting inductance and CB2 exceeds its threshold. Also note that the discharge of the load converter's capacitance contributes to the fault current.

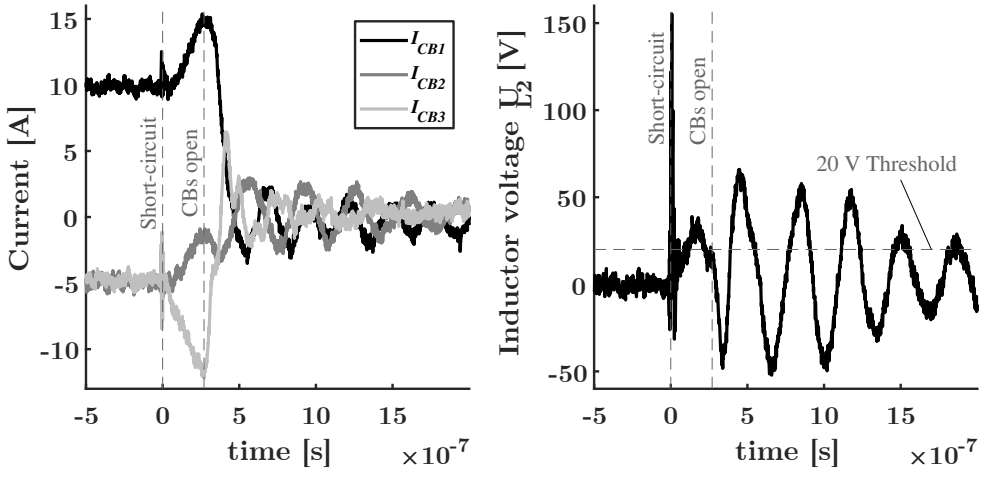

Figure 5.11: Experimental results for the system shown in Figure 5.10a when the fault resistance is 0.75 Ω

It is important to realize this is not a consequence of utilizing di/dt detection. If only overcurrent detection is used, the currents in CB1 and CB2 would exceed their limits by the time CB3 clears the fault, because of the high current rate of change. Therefore, a challenge for the selectivity of non-unit protection schemes is the fast propagation of low impedance faults through low inductive (sections of) grids. In radial grids, directional detection can be used to overcome this challenge, but for meshed grids this does not work.

Commutation of Inductive Currents

When an SSCB interrupts an inductive current the opening SSCB does not always dissipate the inductive energy, if the current has an alternative path. Consequently, for a transient period, the inductive current will flow through the remainder of the system, which can trip other SSCBs in the system. To show this the experimental setup shown in Fig. 5.12 is used.

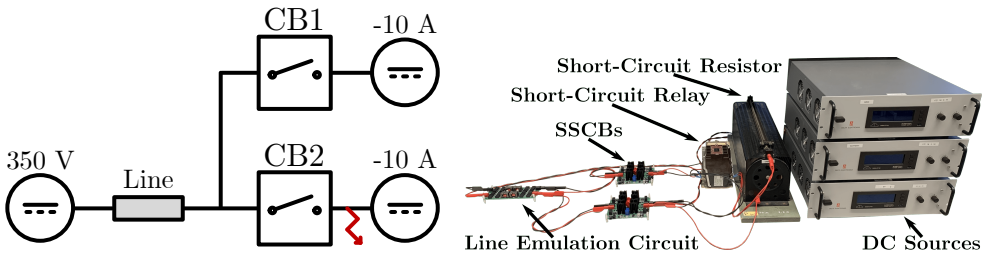

(a) Schematic (b) Hardware realization

Figure 5.12: Experimental setup consisting of a constant voltage source and two constant current loads connected through an inductive line and two SSCBs

For this experiment, a constant voltage source of 350 V is connected to two constant current loads, each consuming 10 A, via an inductive line and two SSCBs. This situation can occur, for example, when a dc household is connected to a main grid. The line in this experiment is emulated by an equivalent π-circuit with an inductance and resistance of 32 μH and 120 mΩ respectively for both poles, and a capacitance between them of 45 nF, which are typical values for a 100 m distribution.

To show that, in some cases, commutated inductive currents can trip SSCBs in non-faulted parts of the system, a short-circuit with a short-circuit resistance of 4.0 Ω is induced at the load side of CB2. The current in the line and the currents in the circuit breakers for this experiment are shown in Fig. 5.13.

Note that CB2 opens when the current exceeds its predetermined threshold. Subsequently, the inductive current in the line, which was first shared by CB1 and CB2, is commutated to CB1 almost immediately and its di/dt detection is tripped. However, if the di/dt measurement was not tripped, the overcurrent detection would have also been tripped since the current through CB1 also briefly exceeds 21 A. Afterwards, the inductive energy is dissipated in CB1's MOV's.

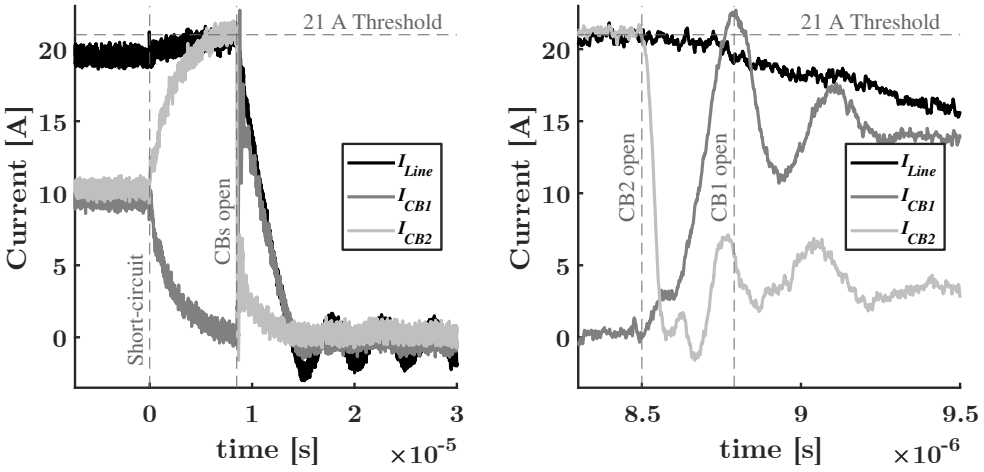

Figure 5.13: Experimental results for the system shown in Figure 5.12a when the fault resistance is 4.0 Ω

When SSCBs are operating near their rated current, the commutation of inductive currents would likely cause a cascade tripping circuit breakers in the system. Moreover, this challenge cannot be solved by directional detection, even in radial systems. Therefore, the commutation of inductive currents poses a challenge for the selectivity of non-unit protection schemes.

5.3.4 Proposed Plug-and-Play Protection Scheme

These challenges can be tackled by utilizing communication, but communication will likely slow down fault detection. Furthermore, (directional) thresholds could be designed to prevent unnecessary tripping, but doing so would require knowledge about the system's topology and parameters. Therefore, in order to achieve selective protection for plug-and-play low voltage dc grids, an alternative approach is proposed here.

Proposed SSCB Topology to Delay Fault Propagation

It is proposed to append the SSCB topology with an RC damper on each terminal, as is shown in Figure 5.14. The purpose of the dampers' capacitance is to temporarily provide a low impedance path for fault currents and commutated inductive currents, delaying their propagation. However, if just a capacitance was added, high frequency oscillations with low damping could occur between the damper capacitors through the current limiting inductance, since the on-state resistance of the switches is small. Therefore, resistances are added to the dampers in order to attenuate these oscillations.

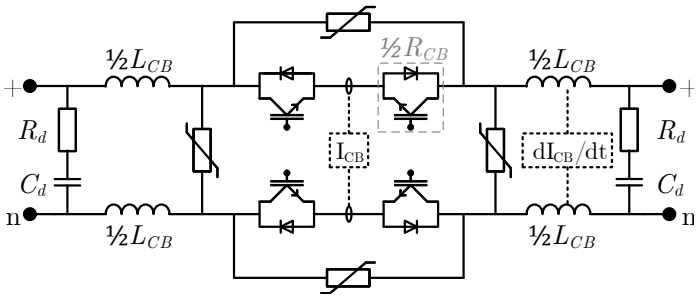

Figure 5.14: Proposed solid-state circuit breaker topology with added RC dampers

In the proposed topology, the RC dampers together with the current limiting inductance essentially form a low-pass LCR filter. Making a loop inside the SSCB, the sum of the voltages over the damper capacitors, damper resistors, on-state resistances and current limiting inductances must be zero. Therefore, the differential equation for the inductor current is given by

$$2L_{CB}\frac{\partial}{\partial t}I(t) + (2R_d + 2R_{CB})I(t) + \frac{2}{C_d}\int I(t)dt = 0. \tag{5.3}$$

Differentiating this equation, and dividing by $2L_{CB}$ yields

$$\frac{\partial^2}{\partial t^2}I(t) + \frac{R_d + R_{CB}}{L_{CB}}\frac{\partial}{\partial t}I(t) + \frac{1}{L_{CB}C_d}I(t) = 0. \tag{5.4}$$

Consequently, the transfer function of this system is given by

$$H(s) = \frac{I(s)}{I'(0)} = \frac{1}{s^2 + \frac{R_d+R_{CB}}{L_{CB}}s + \frac{1}{L_{CB}C_d}}. \tag{5.5}$$

The resonant frequency f_r and attenuation frequency α of this standard second-order system are

$$f_r = \frac{1}{2\pi\sqrt{L_{CB}C_d}}, \tag{5.6}$$

$$\alpha = \frac{R_d + R_{CB}}{4\pi L_{CB}}, \tag{5.7}$$

which will be used later in this section to provide design guidelines for the damper parameters.

Note that, the higher damper capacitor, the lower the resonant frequency of the SSCB's LCR circuit and the longer the SSCB will delay the propagation of fault currents. From a different perspective, a higher damper capacitance can provide the energy for the fault current for a longer time.

An additional benefit of the damper capacitance is that it delays and smoothes the commutation of an (inductive) current. This is illustrated by simulating the inductor current in the circuit from Figure 5.15. For the simulations the grid voltage U_{dc} is 350 V, the on-resistance R_{CB} is 0.1 Ω, the SSCB's inductance L_{CB} is 1 μH, and the damper resistance R_d is 2 Ω.

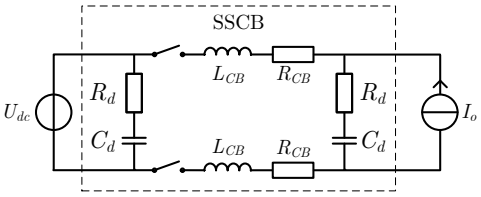

Figure 5.15: Circuit that is used to show the effect of the RC dampers on the commutation of an (inductive) current

The simulation results for the current in the SSCB's inductors, when the current I_o is stepped up from 0 to 10 A at $t = 0$, are given in Figure 5.16. It is shown that the damper capacitance absorbs the forced current, delaying the current from flowing inside the SSCB. It also illustrates that, at lower damper capacitances, current overshoot and underdamped high frequency oscillations can occur.

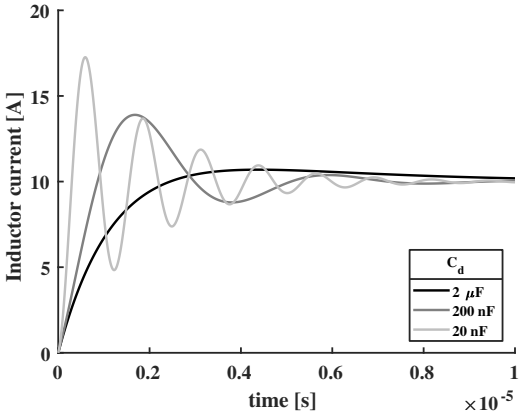

Figure 5.16: Simulation results for the inductor current in the circuit of Figure 5.15 for different damper capacitances

Proposed Time-Current Characteristic

In ac systems selective coordination between upstream and downstream circuit breakers is often achieved in radial systems by using time-current characteristics for the

protection devices. Time-current characteristics depict how long a protection device allows a current to flow before it interrupts it, and they are mainly determined by the thermal and magnetic characteristics of the circuit breakers. The upstream and downstream time-current characteristics are chosen in such a way that the downstream circuit breaker clears the fault first, and the upstream circuit breaker only clears the fault when the downstream circuit breaker fails.

It was shown that the commutation of inductive currents can cause the undesired tripping of SSCBs in non-faulted sections. Therefore, coordination among downstream circuit breakers is also required, not just between upstream and downstream SSCBs. Furthermore, since this chapter aims for a plug-and-play protection scheme, the coordination must also achieve selectivity in meshed low voltage dc grids.

To prevent unnecessary tripping due to commutated currents, the time-current current characteristic must take this current and its decay into account. In the worst-case, the commutated current is the nominal current and this current decays with the time constant of the line. If the SSCB is carrying the nominal current before commutation, the worst-case current after commutation is characterized by the LR time constant and is given by

$$I_{\text{total}} = I_{\text{nom}} \left(1 + e^{-\frac{R_L}{L_L} t}\right). \tag{5.8}$$

Therefore, in order to prevent the SSCB from tripping unnecessarily from commutated inductive currents, the proposed characteristic only interrupts immediately if the current exceeds twice the nominal current. Furthermore, between I_{nom} and $2I_{\text{nom}}$, the time-current characteristic is chosen as

$$t_{\text{clear}} = t_{\max} - \frac{L_L}{R_L} \ln(I - 1), \tag{5.9}$$

where $t_{\max}$ is the maximum time the SSCB takes to detect and clear an overcurrent, and I is the current in the SSCB in multiple of the nominal current.

Note that it is only necessary to know the slowest expected time constant of the lines in the system. Therefore, knowledge about the length of the lines in the system or their interconnection is not required. Moreover, a safety margin can be implemented in order to anticipate uncertainty in the system parameters. The proposed time-current characteristic for SSCBs is shown in Figure 5.17.

Because the time-current characteristic scales with nominal current, the proposed time-current characteristic inherently coordinates upstream and downstream SSCBs. To illustrate this, imagine the system of Figure 5.12a with an upstream SSCB that has a nominal current of 32 A and two downstream SSCBs that have a nominal current of 16 A. Now if all the SSCBs operate at their nominal current and a fault occurs downstream, the downstream SSCB will trip immediately when the current reaches 32 A. In this case the upstream current is 48 A, for which the upstream breaker will wait a significant time.

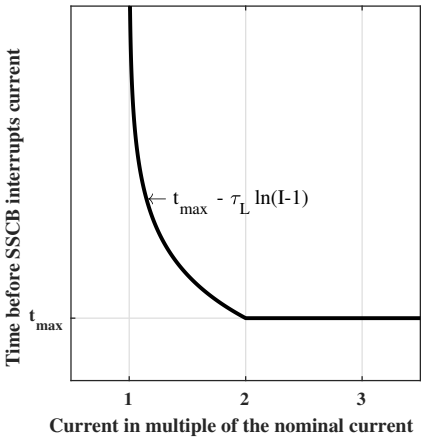

Figure 5.17: Proposed time-current characteristic for the SSCBs

Plug-and-Play Design Guidelines

In order to ensure selectivity, a solid-state circuit breaker topology and a time-current characteristic were proposed. Here it is described how these concepts can be incorporated in an SSCB, with a nominal current of I_{nom} and a nominal voltage of U_{nom}, in order to achieve system-wide plug-and-play protection selectivity.

The SSCB's di/dt detection is tripped if the voltage over the current limiting inductance is more than $U_{L,\text{max}}$. However, in the worst case the voltage is still U_{nom} for t_{max}. Therefore, assuming a sawtooth shaped pulse, the required current limiting inductance is determined by

$$L_{CB} = \frac{\sqrt{3} U_{\text{nom}} t_{\text{max}}}{I_{\text{pulse}}(t_{\text{max}})}, \tag{5.10}$$

where $I_{\text{pulse}}(t_{\text{max}})$ is the current carrying capability of the semiconductor switches for a t_{max} pulse, which usually is several times higher than then nominal current of the switches.

When the current is above two times the nominal current, the clearing time is given by t_{max}, while for currents between one and two times the nominal current (5.9) is used to determine the clearing time. Consequently, the maximum current when the overcurrent protection is tripped is given by

$$I_{\text{max}} = 2I_{\text{nom}} + \frac{U_{L,\text{max}} t_{max}}{L_{CB}}. \tag{5.11}$$

Although lowering the di/dt threshold $U_{L,\text{max}}$ decreases the maximum fault current, the detection will also become more sensitive to, for example, electromagnetic inter-

ference. The authors found a reasonable threshold voltage to be around

$$U_{L,\max} = \frac{2I_{\text{nom}}L_{CB}}{t_{max}}. \tag{5.12}$$

In general, changes in load current will not trigger the di/dt detection with this threshold, since the time constants of distribution lines and power electronic converters are several orders of magnitude higher than the time constant of the SSCB.

The topology that is used for the SSCB is shown in Figure 5.14, where the MOVs clamp the voltage to below the maximum rating of the switches. Alternatively, other circuits can be used to limit the voltage on the switches. Regardless, the rating of the clamping circuits determines the maximum inductive energy that the SSCBs can dissipate.

To size the damper components (5.6) and (5.7) are used. To ensure a smooth commutation of inductive current and prevent instant fault propagation, the resonant frequency of the SSCB is chosen to be an order of magnitude lower than the inverse of the maximum clearing time $t_{\max}$ (in this chapter a factor of 10 is chosen). The damper capacitor is then given by

$$C_{\text{d}} \gg \frac{t_{max}^2}{4\pi^2 L_{CB}}. \tag{5.13}$$

For a damped response, the damper resistance is sized such that the attenuation frequency is higher than the resonant frequency. Therefore,

$$R_d > 2\sqrt{\frac{L_{CB}}{C_d}}. \tag{5.14}$$

If possible, in order to clamp the voltage over the inductor to below the threshold voltage during commutation, the damper resistance should also be

$$R_d < \frac{U_{L,\max}}{I_{\text{nom}}}. \tag{5.15}$$

Utilizing these guidelines, the additional design parameters of the SSCB in this chapter are given in Table 5.1 and Table 5.2.

Parameter	Acronym	Value
Snubber resistance	R_d	2.0 [Ω]
Snubber capacitance	C_d	2.0 [μF]
Minimum clearing time	$t_{\max}$	1.0 [μs]
Overcurrent threshold	$I_{L,\max}$	20 [A]
di/dt threshold	$U_{L,\max}$	20 [V]

Table 5.2: Additional design parameters of the solid-state circuit breaker

5.4 Experimental Validation

The two experiments from Section 5.3.3 are repeated to show that the challenges with regard to fault propagation and inductive current commutation are solved. A third experiment is performed to show that these results are also valid for meshed systems.

To show that the plug-and-play SSCBs delay the propagation of the fault, the experiment shown in Fig. 5.10a is repeated. The experimental results for the currents in the SSCBs for this experiment are shown in Fig. 5.18. Observe that, contrary to the experiment in Fig. 5.11, only CB3 is tripped, while the currents in the other SSCBs are largely unaffected by the whole process. The current rises fast until the switches of CB3 are opened, after which CB1 and CB2 remain closed.

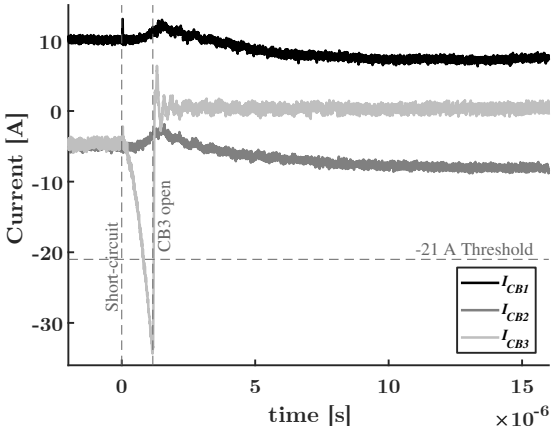

Figure 5.18: Experimental results for the system shown in Figure 5.10a when the fault resistance is 0.75 Ω and the plug-and-play SSCBs are used

To show that the plug-and-play SSCBs ensure smooth commutation and selectivity, the experiment shown in Fig. 5.12a is repeated. The experimental results for the SSCBs' currents for this experiment are shown in Fig. 5.19. Note that the commutation of the inductive current is smoothed out over roughly a 10 μs interval, which is an order of magnitude longer than in Fig. 5.13. Furthermore, although the inductive current is commutated to CB1, its thresholds are not exceeded and therefore its fault detection is not tripped.

It is clear that the plug-and-play protection scheme accounts for commutated currents, but does not prevent them. The addition of a significant capacitance at the interface of the SSCBs can reduce the commutated current by (temporarily) storing the inductive energy. The experimental results for the same experiment, but with an added 240 μF capacitance at the interface of the SSCBs, is shown in Fig. 5.20. The commutated current is reduced, but applying this solution in a plug-and-play fashion is impractical, since information about the system's capacitances and inductances is required. Therefore, this chapter adopted the proposed time-current characteristic.

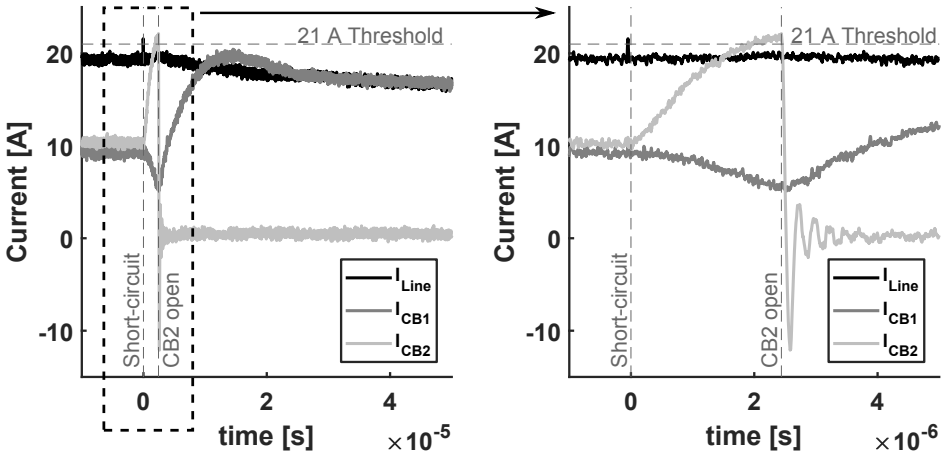

Figure 5.19: Experimental results for the system shown in Figure 5.12a when the fault resistance is 4.0 Ω and the plug-and-play SSCBs are used

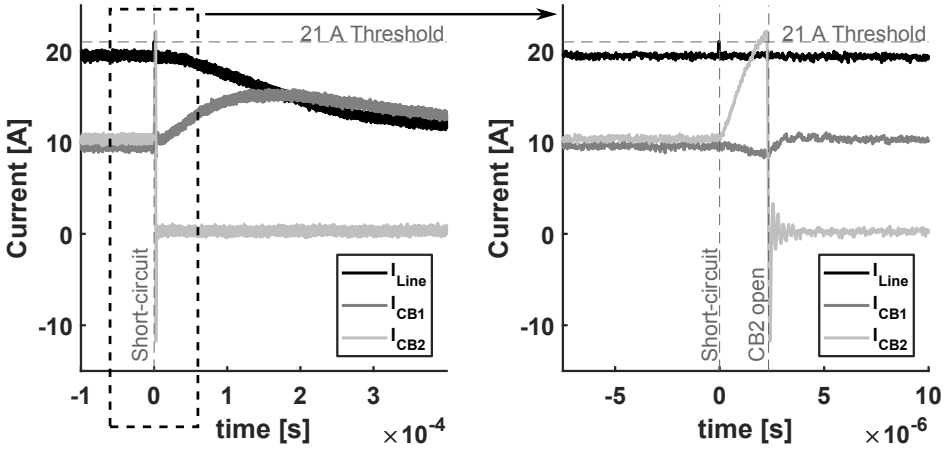

Figure 5.20: Experimental results for the system shown in Figure 5.12a when the fault resistance is 4.0 Ω and a capacitance of 240 μF is added at the interface of the plug-and-play SSCBs

To show that the decentralized plug-and-play protection scheme also works for meshed systems, the experiment shown in Fig. 5.21a is used. The setup consists of a constant voltage source of 350 V connected to two 5 A constant current loads in a ring configuration. The lines in this system are emulated by equivalent π-circuits with an inductance and resistance of 32 μH and 120 mΩ respectively. This situation can occur, for example, when dc households are interconnected.

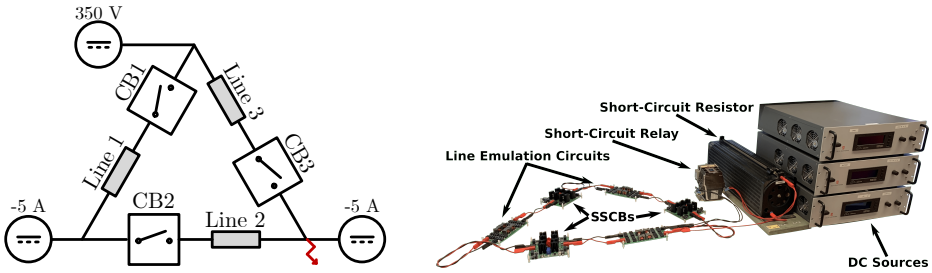

(a) Schematic (b) Hardware realization

Figure 5.21: Experimental setup consisting of a constant voltage source and two constant current loads connected through an inductive line and two SSCBs

The experimental results for the currents inside the SSCBs, when a short-circuit with a fault resistance of 2.5 Ω is induced at the load-side terminals of CB3, are given in Fig. 5.22. Observe that the di/dt detection of CB3 is triggered soon after the fault occurence since there is no line between the SSCB and the fault, while the overcurrent detection of CB2 is triggered after around 20 μs. Most importantly, CB1 is not triggered and the non-faulted section of the grid remains operational.

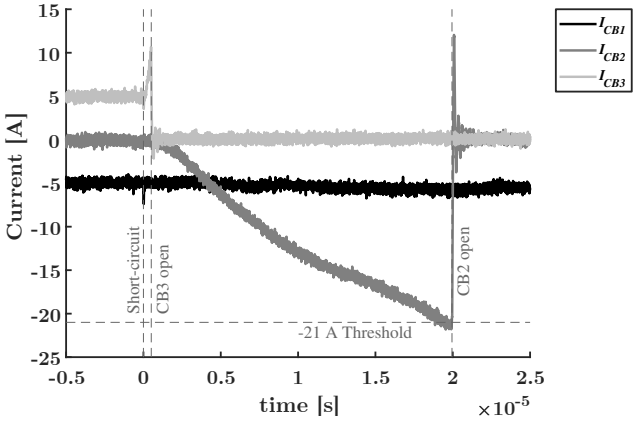

Figure 5.22: Experimental results for the system shown in Figure 5.21b when the fault resistance is 2.5 Ω

Overall, the experimental results show that the decentralized plug-and-play protection scheme is adequate for providing fast and selective fault interruption for radial and meshed low voltage dc grids. Furthermore, it is shown that it solves the challenges with respect to fault propagation and the commutation of inductive currents. For future research, the protection scheme can provide a solid foundation for the design of a low voltage dc protection system.

5.5 Conclusions

The lack of a zero-crossing makes interrupting inductive currents more challenging in dc grids than in conventional ac grids. Furthermore, fast fault interruption is often required for low voltage dc grids, in order to reduce the current stress on the components in the grid and prevent blackouts. Moreover, meshed topologies and bi-directional power flow complicate fault detection and selectivity.

It is essential to know the dangers and requirements for interacting with different parts of the grid. Therefore, a decentralized protection for low voltage dc grids was proposed in this chapter. The protection framework partitions the grid into zones and tiers according to their short-circuit potential and the provided level of protection, respectively. In general, the different zones are separated by galvanic isolation, which can be provided by a mechanical switch or a converter with isolation. Furthermore, the protection tier depends on the lowest tier of protection of the components connected to that section of the grid.

It was argued that current limiting inductances are essential in order to limit overcurrents during faults. Furthermore the design and hardware realization of a solid-state circuit breaker was presented, which trips when the current or current rate of change exceeds set thresholds. Experimental results showed that this circuit breaker is able to detect and clear different faults within 1 μs after its thresholds are exceeded.

Because of the fast fault interruption and meshed system structures, it is difficult to ensure protection selectivity in low voltage dc grids. It was experimentally shown that, in low inductive systems, the current (and current rate of change) in non-faulted circuit breakers can exceed its thresholds before the faulted circuit breakers can clear the fault. Furthermore, interrupted inductive currents (temporarily) commutate to healthy parts of the system, causing overcurrents. Consequently, undesired tripping can occur of circuit breakers in non-faulted parts of the system.

To ensure selectivity, literature presents several schemes that rely on communication, knowledge about the system's topology and parameters, or powering down the system. In this chapter a decentralized protection scheme was proposed that ensures security and selectivity, without any of these limitations. The protection scheme delays fault propagation by introducing a snubber circuit at both ends of the (solid-state) circuit breaker, which then forms a second order filter for the fault. Furthermore, commutated inductive overcurrents are ignored by designing the time-current characteristic with the lines' worst time constant. Additionally, design guidelines were provided for the different components in the solid-state circuit breaker. Several experiments were carried out that showed that the proposed protection scheme provides secure and selective fault interruption for radial and meshed low voltage dc grids.

The decentralized protection framework and protection scheme provide a foundation for the protection of low voltage dc grids. However, further research is required on an exhaustive protection approach that includes, for example, grounding, overvoltage protection, and residual current detection.

Chapter 6

Conclusions

The main objective of this thesis was to improve the modeling, stability, control and protection of dc distribution systems, since these topics are key technical challenges for the broad adoption of dc distribution systems. In general, the objectives of distribution systems remain the same, but for future (dc) distribution systems they must be achieved in a shorter time frame. In this chapter, the main conclusions for each research question and some recommendations for future research are given.

How can the modeling of dc distribution systems be improved?

Distribution grid models can be categorized into steady-state, dynamic and transient models. In this thesis two steady-state modeling methods were presented, which model non-linear converters as current sources or as a current source with an impedance in parallel and perform linear iterations to arrive at the power flow solution. For the tested systems, these methods were shown to be up to 93 % more computationally efficient than the established methods, while providing similar or better accuracy and convergence. Furthermore, a dynamic state-space model was proposed that models dc distribution systems according to their nodes, lines, conductors and incidence matrix. In contrast to existing methods it takes the mutual couplings between parallel conductors in the lines into account, allows for rapid analysis of different systems, and enables the algebraic analysis of stability. Additionally, it was proposed to decompose bipolar dc systems into three symmetrical components in stead of two, which facilitates the modeling of a metallic neutral and (ground) fault analysis. It was demonstrated that the method reduces the system model's degrees of freedom by up to a factor of three, and significantly simplifies fault analysis. Simulations and experimental results showed that these models are appropriate for modeling dc distribution systems.

How can the stability of dc systems be analyzed and ensured?

Ensuring the stability of distribution systems is becoming more challenging as the systems' inertia is decreasing and the amount of power electronic converters is increasing. The stability of dc systems can be analyzed by utilizing the minor loop gain, deriving

the eigenvalues, performing root a locus analysis, or by applying Lyapunov methods. However, no generalized methods for assessing stability or stability guidelines are given in literature. This thesis presented how the stability can be derived from the systems' state-space matrices, which, unlike other techniques, can be applied to any system and does not use an oversimplified representation of the systems. Using this method it was shown that increasing the capacitance of source converters can deteriorate stability, in contrast with increasing the capacitance of load converters. Furthermore, a Brayton-Moser representation of dc distribution systems was used to arrive at a suitable Lyapunov candidate function, and guidelines for global plug-and-play stability were derived. In order to prevent instability, the capacitance of constant power loads need to be appropriately sized and the voltage drops in the system need to be limited. Moreover, experimental results confirmed that these two requirements relate to the two main modes of instability in dc distribution systems: oscillatory instability and voltage instability.

How should the decentralized control of dc systems be organized?

Decentralized control is essential for dc systems, because of the decentralization and segmentation of the grid, but also in order to sustain operation when the communication infrastructure is unavailable. Existing control strategies did not guarantee system-wide stability unless the system was well defined or some form of communication was used. This thesis proposed a decentralized control strategy, which implements the plug-and-play stability guidelines without utilizing communication or knowledge about the system's topology. The voltages between the desired minimum and the maximum voltage were divided into demand response, emission, absorption and supply response regions, and the behavior of different converters was specified inside these regions. Moreover, to ensure precise control decisions, it was discussed that converters should ramp any changes over a significantly longer time than the system's time constants. Furthermore, it was experimentally shown that inadequate system and energy utilization can occur when converters have similar voltage thresholds at which they switch on or off. Therefore, the Grid Sense Multiple Access was proposed, which implements an exponential backoff routine to significantly improve energy utilization. Additionally, experiments showed that the decentralized control strategy ensures global stability and voltage propriety, and that the priority of converters that utilize the Grid Sense Multiple Access algorithm can be set according to their connection status and voltage thresholds by utilizing the algorithm's parameters.

How should the decentralized protection of dc systems be organized?

The lack of a zero-crossing, the required fast fault interruption and meshed topologies make the protection of dc grids significantly more challenging than conventional ac grids. In this thesis a decentralized protection framework was presented for low voltage dc grids, which partitions the grid into zones and tiers according to their short-circuit potential and the provided level of protection. Furthermore, it was experimentally shown that undesired tripping of circuit breakers in non-faulted parts

can occur, because of the propagation of fault currents before they can be cleared and the commutation of inductive currents after the fault has been cleared. Literature presents several schemes that utilize communication, information about the system's topology and parameters, or power down the system in order to ensure selectivity. This thesis achieved decentralized plug-and-play selectivity by introducing a snubber circuit at both ends of the circuit breaker, such that it forms a second order filter for the fault current, and by utilizing a time-current characteristic that is designed to avoid tripping on commutated currents. Moreover, design guidelines were provided for the components and time-current characteristic of a solid-state circuit breaker. Additionally, several experiments were carried out that showed that the proposed protection scheme provides secure and selective fault interruption for radial and meshed low voltage dc grids.

How can the research in this thesis be experimentally verified?

Various findings of this thesis were verified by utilizing an experimental dc microgrid setup. The main constituents of the setup are the developed converters, line emulation circuits and solid-state circuit breakers. For the emulation of, for example, loads and sources six power electronic converters were used that consist of three parallel half-bridges, such that they can be operated as bidirectional ac/dc or dc/dc converters. Furthermore, to interconnect the different components in the grid, π-equivalent circuits were used to emulate the behavior of 100 m distribution lines. Additionally, a solid-state circuit breaker was developed to test the protection scheme that was presented in this thesis. Experimental results showed that this circuit breaker is able to detect and clear different faults within 1 μs after its (current or current rate of change) thresholds are exceeded. The power in the experimental setup was supplied by SM 300-20 and SM 500-CP-90 power supplies, which are manufactured by Delta Elektronika. These components were used to compose a vast number of systems in order to do all the experiments in this thesis.

How can the built power electronic converters be modeled and tuned?

The converters in this thesis were modeled by idealized, average or switching models, depending on the required accuracy. It was experimentally shown that both the average and switching models are largely congruent with the behavior of real converters, while the idealized model only provides an accurate representation in longer time frames. Furthermore, to tune the converters' controllers, it was assumed that the power semiconductors behave as ideal switches, and that the converters control the voltage over an inductor. The inner and outer controllers of the converters in the experimental setup and simulations were tuned to achieve fast response while remaining stable. Consequently, the converters' inner current controllers were tuned by cancelling the pole from the converters' inductor and resistance, and maximizing the damping of the closed-loop system. On the other hand, the outer controllers were tuned by selecting the cross-over frequency of the closed-loop system, and maximizing the phase margin at this frequency.

Future Work

In this thesis improved methods were presented for the steady-state and dynamic analysis of dc distribution systems. The development of transient analysis methods are imperative for the verification of protection devices and schemes. Existing methods for dc power system transients are directly derived from ac network theory, therefore I suspect a significant reduction in computational time can be achieved if specialized dc methods are developed. However, due to time constraints and the scope of the thesis, these methods were not developed.

The plug-and-play stability guidelines and the stability experiments showed that achieving voltage propriety and sufficient damping is straightforward. However, the detailed analysis of the impedance and harmonic emissions of converters, and other grid components, proved to be another challenge. Therefore, it is my recommendation that detailed research is conducted in these topics. In general, it is likely that any undesired behavior within the control bandwidth of the converter can be solved via control, while outside of the control bandwidth passive compensation circuits need to be used.

This thesis deals with the decentralized control of dc distribution systems. Because much research was already published on these topics, higher level control that utilizes communication to achieve more complex objectives (e.g., the economic optimization or power flow control) was not inside the scope of this thesis. However, this does not mean that further research in this topic cannot benefit the broad adoption of dc distribution systems. For example, a distributed control scheme could be developed that integrates the decentralized control scheme presented in this thesis and aims to achieve more complex objectives. Such a system would be very reliable, while keeping the communication infrastructure minimal.

The presented decentralized protection framework and protection scheme can be used as a foundation for the protection of low voltage dc grids. However, further research is required on, for example, the optimal way of grounding dc systems, protection from lightning, and residual current detection. In the end, all these functions would be required to ensure the safety of the entities interacting with the grid. Capacitive grounding, residual current detection via a coupled inductor, and overvoltage protection via MOVs can become important topics for the protection of low voltage dc grids.

This thesis made several steps towards the technical feasibility of low voltage dc distribution grids. Nevertheless, some of the main non-technical challenges, such as overcoming the market inertia of ac grids and standardization, were not addressed in this thesis. Overall, I believe that the adoption of low voltage dc grids is a slow, but inevitable, incremental process.

Appendix A

Experimental Setup

In this chapter, the hardware used in the experimental dc distribution system is presented. The presented laboratory scale system is used throughout this thesis to verify and validate the research on the modeling, stability, control and protection of dc distribution systems.

A.1 Power Electronic Converters

The key constituents of the laboratory scale system are the six identical power electronic converters, which were designed, built and programmed for this project. A photo of the rack that contains these converters is shown in Figure A.1.

(a) Front of the rack (b) Rear of the rack

Figure A.1: Rack containing six power electronic converters which are used in the experimental dc distribution system

The topology of the power electronic converters and the hardware realization are shown in Figure A.2. The power electronic converters consist of three parallel half-bridges, which can be operated as an ac/dc controlled rectifier or a dc/dc interleaved boost converter, depending on how the microcontrollers are programmed.

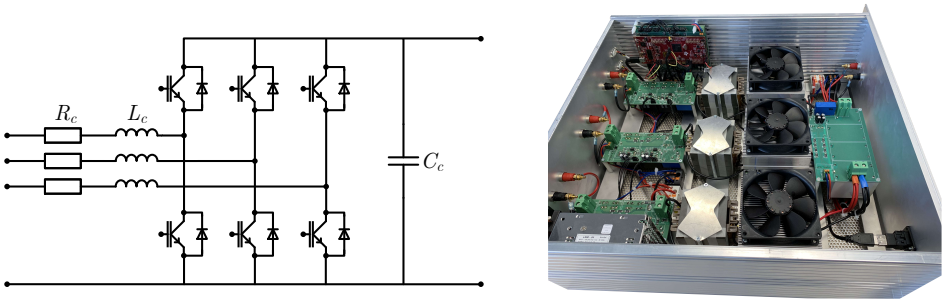

(a) Circuit topology

(b) Hardware realization

Figure A.2: Topology and hardware realization of the used power electronic converters

For the experiments, unless otherwise specified, the converters are operated as bidirectional interleaved dc/dc converters. In this case the PWM signals of the three half-bridges are phase shifted 120 degrees with respect to each other in order to reduce the current stress and consequently the voltage ripple in the output capacitance. Furthermore, these converters are controlled by a standard inner current controller, and an outer power, voltage or droop controller.

The microcontrollers of the converters can be programmed to adjust the behavior of the circuit. However, due to the hardware design, some of the (programmable) parameters have their limitations. The parameter maxima for the power electronic converters are given in Table A.1.

$P_{\max}$ [kW]	$U_{i,\max}$ [V]	$U_{o,\max}$ [V]	L_c [μH]	R_c [Ω]	C_c [μF]	$f_{s,\max}$ [kHz]
10	350	700	430	0.30	288	40

Table A.1: Parameter maxima for the power electronic converters which are used in the experimental dc distribution system

A.2 Distribution Lines

In this thesis (long) distribution lines are emulated by a π-equivalent circuit, which is shown in Figure A.3a. Moreover, the hardware realization of this π-equivalent line emulation is shown in Figure A.3b. This emulation circuit is used throughout this thesis to interconnect the various other components in the experimental dc distribution system.

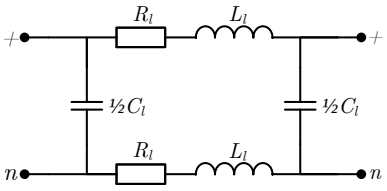

(a) π-equivalent emulation circuit

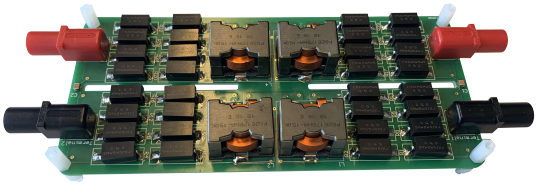

(b) Hardware realization

Figure A.3: Equivalent emulation circuit and hardware realization of the lines

Unless otherwise specified, the parameters of the distribution line emulation circuits that are mostly used for the experiments are given by Table A.2.

Emulated length [m]	L_l [μH]	R_l [mΩ]	C_l [nF]
100	32	120	45

Table A.2: Parameters for the line emulation circuits, which are used in the experimental dc distribution system

A.3 Solid-state Circuit Breaker

For the experiments regarding the protection of dc distribution systems, a solid-state circuit breaker (SSCB) was developed. The electrical circuit of the SSCB and its hardware realization are given in Figure A.4.

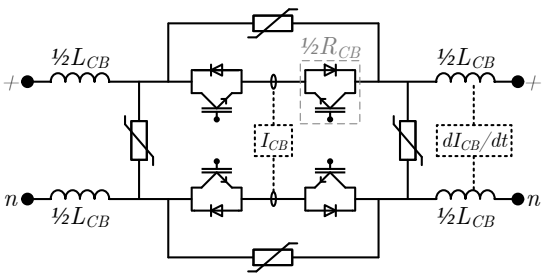

(a) Circuit topology

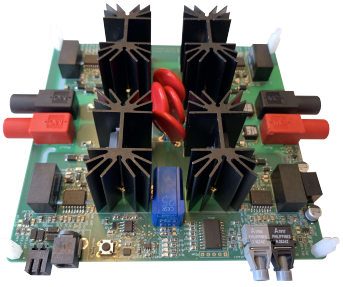

(b) Hardware realization

Figure A.4: Solid-state circuit breaker circuit schematic and hardware realization

To detect short-circuits, the SSCB measures the current via a high bandwidth hall-effect current sensor and the current rate-of-change via a differential voltage measurement over the added current limiting inductance, L_b. Analog circuits are used to identify fault conditions by comparing these measured values to user defined

reference thresholds and thus an open action of the solid-state switches is performed if the set thresholds are exceeded. A latching function is used to keep the switches opened until the user acknowledges that the fault is cleared. The key parameters of the developed SSCB are given in Table A.3.

U_{nom} [V]	I_{nom} [A]	R_{CB} [mΩ]	L_{CB} [μH]	C_b [μF]	t_{min} [μs]
350	10	130	1.0	1.2	1.0

Table A.3: Parameters of the SSCBs in the experimental setup

A.4 Laboratory Power Supplies

Unless otherwise specified, throughout this thesis the input side of the power electric converters are connected to either a SM 300-20 or a SM 500-CP-90 power supply, which are manufactured by Delta Elektronika. The SM 300-20 is a unidirectional power supply rated for 300 V and 20 A. Furthermore, the SM 500-CP-90 is a bidirectional power supply rated for 500 V and 90 A in two quadrants, and can therefore be used a source as well as an electronic load. Pictures of these power supplies are shown in Figure A.5 and Figure A.6 for illustrative purposes.

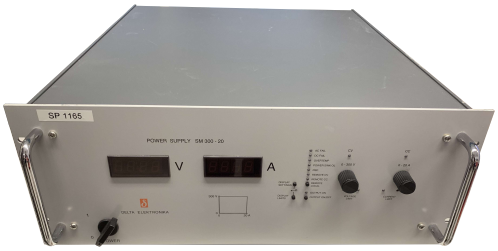

Figure A.5: SM 300-20 unidirectional power supply from Delta Elektronika

Figure A.6: SM 500-CP-90 bidirectional power supply from Delta Elektronika

Appendix B

Converter Controller Design and Models

In this chapter it is shown how the controllers for the inner current, outer voltage and power of the converters can be tuned. Furthermore, different converter models are presented, validated and benchmarked.

B.1 Converter Controller Design

Simplified diagrams of ac/dc, boost and buck converters are shown in Figure B.1. Many other converter topologies exist, however some general observations can be made. The power electronic converters contain some energy storage elements, such as inductors and capacitors, and discrete elements, such as power electronic switches. Therein, the semiconductor block can assume a half-bridge or a chopper configuration.

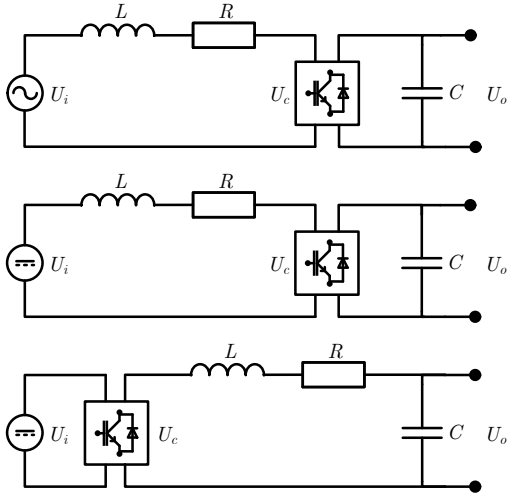

Figure B.1: Simplified diagrams of ac/dc, boost and buck converters

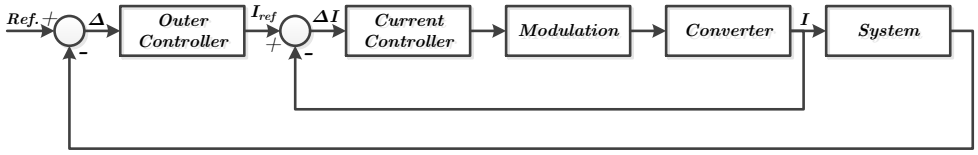

Figure B.2: Block diagram of a power electronic converter including its control

A generalized block diagram of the power electronic converters and their control is shown in Figure B.2. In the converters shown in Figure B.1 the discrete switches regulate the voltage on one side of the inductor, while the voltage on the other side is pre-determined. Therefore, if the inductor is on the input side of the converter, the average inductor current of these converters can be approximated by the differential equation

$$\dot{I}_L = \frac{1}{L}\left(U_i - U_c - I_L R\right), \tag{B.1}$$

where U_i is the primary side voltage and U_c is the voltage controlled by the discrete switches. Therefore, the transfer functions for the input current is given by

$$H_{\mathrm{c,in}}(s) = \frac{1}{R + Ls} \tag{B.2}$$

The dynamic behavior of the converters is not only determined by the converter's transfer function, but also the behavior of its modulation and control. Assuming digital control is used in the implementation, the converter follows the voltage reference (U_c) with an average delay of half a switching cycle. Therefore, the transfer function of the modulation is assumed to be

$$H_{\mathrm{mod}}(s) = \frac{1}{1 + \frac{1}{2f_s}s}, \tag{B.3}$$

where f_s is the switching frequency.

For both the inner and outer controllers, proportional and integral compensation (PI) is used which has the transfer function

$$H_{\mathrm{PI}}(s) = K_p + \frac{K_i}{s}, \tag{B.4}$$

where K_p is called the proportional gain and K_i is called the integral gain.

If it is assumed that the system's dynamics are slow, the system's behavior is mostly defined by the output capacitance of the converter. Therefore, the transfer function of the system can be approximated by

$$H_{\mathrm{system}}(s) = \frac{U_i}{U_o C s}, \tag{B.5}$$

where U_o is the output voltage of the converter.

B.1.1 Inner Current Controller

The inner current loop is tuned for speed and simplicity by utilizing its open- and closed-loop transfer functions. The open-loop transfer function for the input current, including the current controller, is given by

$$\begin{aligned} H_{\mathrm{I,ol}}(s) &= \left(K_p + \frac{K_i}{s}\right)\left(\frac{1}{1+\frac{1}{2f_s}s}\right)\left(\frac{1}{R+Ls}\right) \\ &= K_p\left(\frac{1+\frac{K_p}{K_i}s}{\frac{K_p}{K_i}s}\right)\left(\frac{1}{1+\frac{1}{2f_s}s}\right)\frac{1}{R}\left(\frac{1}{1+\frac{L}{R}s}\right). \end{aligned} \tag{B.6}$$

The slowest pole, the pole from the converter's transfer function, can be canceled by choosing $\frac{K_p}{K_i} = \frac{L}{R}$. Consequently, the open-loop transfer function becomes

$$H_{\mathrm{I,ol}}(s) = \frac{K_i}{R}\left(\frac{1}{s+\frac{1}{2f_s}s^2}\right). \tag{B.7}$$

Subsequently, the closed-loop transfer function is derived to be

$$H_{\mathrm{I,cl}}(s) = \frac{\frac{2K_i f_s}{R}}{\frac{2K_i f_s}{R} + 2f_s s + s^2}. \tag{B.8}$$

This closed loop transfer function represents a second order system with a natural angular frequency and damping factor of

$$\omega_n = \sqrt{\frac{2K_i f_s}{R}}, \tag{B.9}$$

$$\zeta = \sqrt{\frac{Rf_s}{2K_i}}. \tag{B.10}$$

This closed-loop system is designed to have a damping factor of 1 by choosing $K_i = \frac{Rf_s}{2}$ and consequently $K_p = \frac{Lf_s}{2}$. Moreover, a general rule of thumb is that the bandwidth of each controller should be at least an order of magnitude lower than the system it is controlling, and this is indeed the case as the cut-off frequency of the resulting system is around $\frac{f_s}{10}$.

As a result of choosing $K_i = \frac{Rf_s}{2}$ and $K_p = \frac{Lf_s}{2}$ for the inner current controller, the closed loop transfer function is given by

$$H_{\mathrm{I,cl}}(s) = \frac{1}{1+\frac{2}{f_s}s+\frac{1}{f_s^2}s^2}. \tag{B.11}$$

To simplify the design of the outer controllers it is assumed that

$$H_{\mathrm{I,cl}}(s) \approx \frac{1}{1+\frac{2}{f_s}s}, \tag{B.12}$$

which is a reasonable approximation if the outer controllers are much slower than the inner current controller [156, 157].

B.1.2 Outer Voltage Controller

When the system can be approximated by the behavior of the converter's output capacitance, the open-loop transfer function for the output voltage is given by

$$\begin{aligned} H_{\mathrm{U,ol}}(s) &= \left(K_p + \frac{K_i}{s}\right)\left(\frac{1}{1+\frac{2}{f_s}s}\right)\left(\frac{K}{Cs}\right) \\ &= \left(\frac{K_i K}{Cs^2}\right)\left(\frac{1+\frac{K_p}{K_i}s}{1+\frac{2}{f_s}s}\right), \end{aligned} \tag{B.13}$$

where the third term is the transfer function for the output capacitance and K is the current gain of the system given by $\frac{U_i}{U_o}$.

In this case the remaining pole cannot be canceled as this would lead to an unstable system with two poles at the origin. Therefore, the outer voltage controller is tuned to have maximum phase margin at a designated gain crossover frequency. If the gain crossover angular frequency, ω_{cg}, is defined as

$$|H_{\mathrm{U,ol}}(j\omega_{cg})| = 1, \tag{B.14}$$

then the phase margin is defined as

$$\phi_M = 180^\circ + \measuredangle H_{\mathrm{U,ol}}(j\omega_{cg}). \tag{B.15}$$

Substituting (B.13) into (B.15) yields

$$\begin{aligned} \phi_M &= 180^\circ + \measuredangle\left(\frac{K_i K}{-C\omega_{cg}^2}\right) + \measuredangle\left(1 + j\frac{K_p}{K_i}\omega_{cg}\right) - \measuredangle\left(1 + j\frac{2}{f_s}\omega_{cg}\right) \\ &= \measuredangle\left(1 + j\frac{K_p}{K_i}\omega_{cg}\right) - \measuredangle\left(1 + j\frac{2}{f_s}\omega_{cg}\right) \\ &= \arctan\left(\frac{K_p}{K_i}\omega_{cg}\right) - \arctan\left(\frac{2}{f_s}\omega_{cg}\right). \end{aligned} \tag{B.16}$$

The derivative of this function for the phase margin is

$$\frac{\partial \phi_M}{\partial \omega_{cg}} = \frac{\frac{K_p}{K_i}}{1+\left(\frac{K_p}{K_i}\omega_{cg}\right)} - \frac{\frac{2}{f_s}}{1+\left(\frac{2}{f_s}\omega_{cg}\right)^2}. \tag{B.17}$$

From the derivative the phase margin is found to be maximum when the gain crossover angular frequency is

$$\omega_{cg} = \frac{1}{\sqrt{\frac{2K_p}{K_i f_s}}}. \tag{B.18}$$

The modulus of the open-loop transfer function at this gain crossover angular frequency is given by

$$\begin{aligned} |H_{\mathrm{U,ol}}(j\omega_{cg})| &= \left| \left(-\frac{K_i K}{C\omega_{cg}^2} \right) \left(\frac{1 + j\frac{K_p}{K_i}\omega_{cg}}{1 + j\frac{2}{f_s}\omega_{cg}} \right) \right| \\ &= \frac{K_i K}{C\omega_{cg}^2} \sqrt{\frac{1 + \left(\frac{K_p}{K_i}\omega_{cg}\right)^2}{1 + \left(\frac{2}{f_s}\omega_{cg}\right)^2}}. \end{aligned} \tag{B.19}$$

Substituting (B.18) into (B.19) yields

$$\begin{aligned} |H_{\mathrm{U,ol}}(j\omega_{cg})| &= \frac{K_i K}{C\omega_{cg}} \sqrt{\frac{2K_p}{K_i f_s}} \sqrt{\frac{K_p f_s}{2K_i}} \\ &= \frac{K_p K}{C\omega_{cg}}. \end{aligned} \tag{B.20}$$

At the gain crossover frequency the modulus of the open-loop transfer function should be equal to one and therefore the control parameters are derived to be

$$K_p = \frac{C\omega_{cg}}{K}, \tag{B.21}$$

$$K_i = \frac{2C\omega_{cg}^3}{f_s K}, \tag{B.22}$$

where the gain crossover angular frequency, ω_{cg}, can be chosen freely.

When the gain crossover frequency is chosen as $\frac{f_s}{100}$ (an order of magnitude lower than the cut-off frequency of the inner current controller), the proportional and integral gain of the outer voltage controller become

$$K_p = \frac{2\pi C f_s}{100K}, \tag{B.23}$$

$$K_i = \frac{16\pi^3 C f_s^2}{100^3 K}. \tag{B.24}$$

B.1.3 Outer Power Controller

For the outer power controller it is assumed that the losses can be neglected (and therefore the output and input power are equal). The open-loop transfer function for the output power is then given by

$$\begin{aligned} H_{\mathrm{P,ol}} &= \left(K_p + \frac{K_i}{s} \right) \left(\frac{1}{1 + \frac{2}{f_s}s} \right) U_i \\ &= \frac{K_i U_i}{s} \left(\frac{1 + \frac{K_p}{K_i}s}{1 + \frac{2}{f_s}s} \right). \end{aligned} \tag{B.25}$$

In an analogous fashion to the outer voltage controller the proportional and integral gains of the outer power controller can then be derived. Consequently, they are given by

$$K_p = \frac{1}{U_i}, \tag{B.26}$$

$$K_i = \frac{2\omega_{cg}^2 K_p}{f_s} = \frac{8\pi^2 f_s}{100^2 U_i}. \tag{B.27}$$

B.2 Converter Models

Throughout this thesis three different kind of models are used to mimic the behavior of the power electronic converters in dc distribution systems. Firstly, a switching model is used where the power electronic switches are assumed to behave as ideal on/off switches. Secondly, a model where the behavior of the switches is averaged in a pulse period assuming that this pulse period is negligible when compared to the fundamental frequency of the system. Lastly, an idealized model is used, where the converters are assumed to act instantaneously to changes in the system and their set-points. Examples of these models, for the converters presented in Appendix A, are shown in Figure B.3.

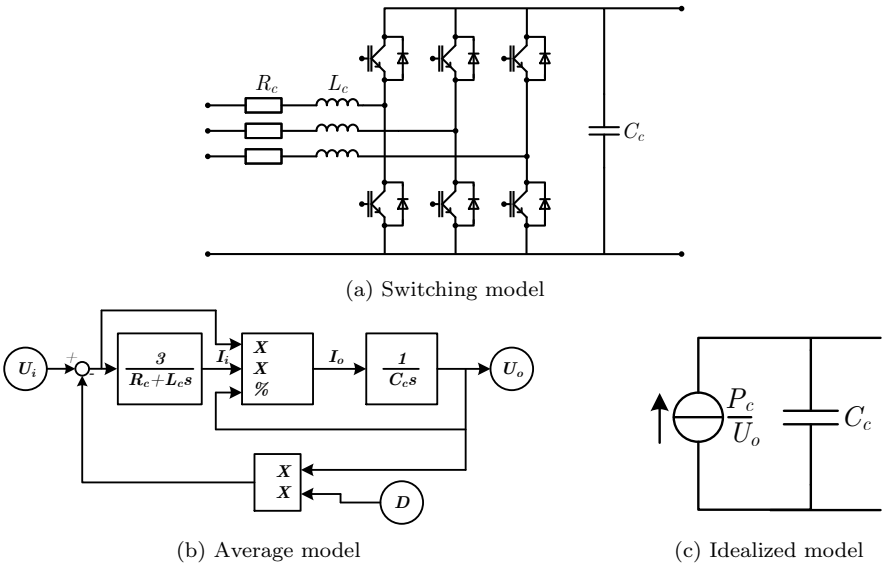

(a) Switching model

(b) Average model

(c) Idealized model

Figure B.3: Different types of circuit models of the power electronic converters in the experimental laboratory setup presented in Appendix A

To verify the validity of the different models an experiment is conducted with one of the converters of the laboratory setup. The input side of the converter is

connected to a dc source and the output is connected to a resistor. The schematic of this experiment is shown in Figure B.4.

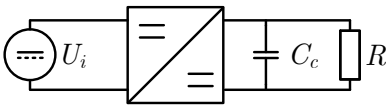

(a) Equivalent circuit

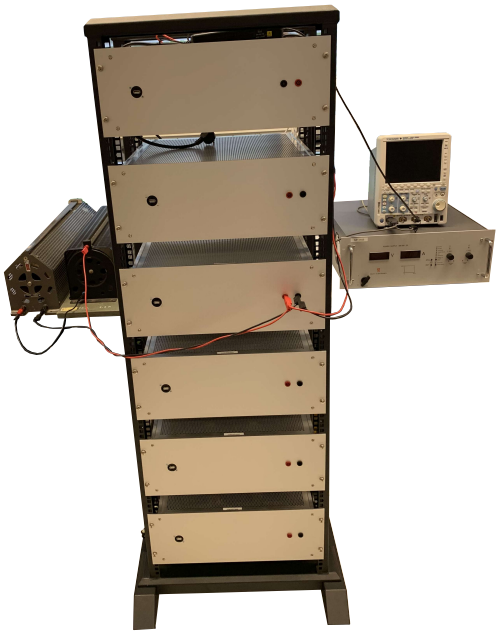

(b) Picture of the experiment

Figure B.4: Experiment for the verification of the power electronic converter models

For the experiment the converter is programmed with a droop controller where the reference for the average current flowing in each leg's inductor is given by

$$I_i = \frac{U_d - U_o}{Z_d}, \tag{B.28}$$

where U_d is the reference voltage and Z_d is the impedance of the droop controller.

For the experiment the input voltage U_i is set to 175 V, the switching frequency to 10 kHz, the droop impedance Z_0 is set to 3 Ω, the inherent output capacitance of the converter is 288 μF, and the load resistance R is 115 Ω. At the start of the experiment the reference voltage U_d of the droop controller is set to 350 V, while at around $t = 1.0$ ms the reference voltage is changed to 370 V.

The experimental results and the simulation results from the various models are shown in Figure B.5. It is seen that the switching model closely follows the experimental results. Furthermore, the average model is still relatively accurate but does not capture the dynamic behavior during a switching cycle. Moreover, the idealized model is less accurate since it neglects the dynamic behavior of the controllers. However, it has a control bandwidth in which it is reasonably accurate.

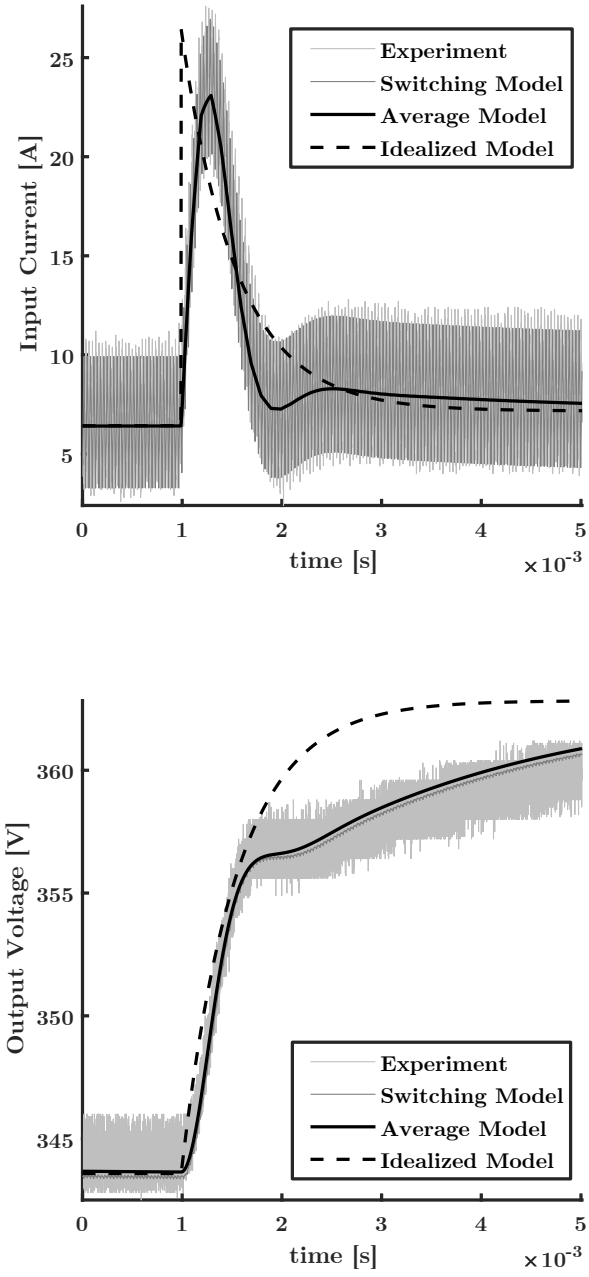

Figure B.5: Input current and output voltage when the reference voltage of the droop converter is stepped up from 350 V to 370 V

References

[1] A. Ipakchi and F. Albuyeh, "Grid of the future," *IEEE Power and Energy Magazine*, vol. 7, no. 2, March 2009.

[2] "Smart grid: reinventing the electric power system," IEEE Power and Energy Magazine for Electric Power Professionals, IEEE Power and Energy Society, 2012.

[3] J. W. Coltman, "The transformer [historical overview]," *IEEE Industry Applications Magazine*, vol. 8, no. 1, Jan 2002.

[4] T. McNichol, *AC/DC: The savage tale of the first standards war.* John Wiley & Sons, 2011.

[5] D. M. Larruskain, I. Zamora, O. Abarrategui, and Z. Aginako, "Conversion of ac distribution lines into dc lines to upgrade transmission capacity," *Electric Power Systems Research*, vol. 81, no. 7, 2011.

[6] L. Mackay, T. G. Hailu, G. C. Mouli, L. Ramirez-Elizondo, J. A. Ferreira, and P. Bauer, "From dc nano- and microgrids towards the universal dc distribution system - a plea to think further into the future," in *2015 IEEE Power Energy Society General Meeting*, July 2015.

[7] N. Flourentzou, V. G. Agelidis, and G. D. Demetriades, "Vsc-based hvdc power transmission systems: An overview," *IEEE Transactions on Power Electronics*, vol. 24, no. 3, March 2009.

[8] A. T. Ghareeb, A. A. Mohamed, and O. A. Mohammed, "Dc microgrids and distribution systems: An overview," in *2013 IEEE Power Energy Society General Meeting*, July 2013.

[9] A. Pratt, P. Kumar, and T. V. Aldridge, "Evaluation of 400v dc distribution in telco and data centers to improve energy efficiency," in *INTELEC 07 - 29th International Telecommunications Energy Conference*, Sep. 2007.

[10] D. J. Becker and B. J. Sonnenberg, "Dc microgrids in buildings and data centers," in *2011 IEEE 33rd International Telecommunications Energy Conference (INTELEC)*, Oct 2011.

[11] V. Vossos, K. Garbesi, and H. Shen, "Energy savings from direct-dc in u.s. residential buildings," *Energy and Buildings*, vol. 68, 2014.

[12] B. T. Patterson, "Dc, come home: Dc microgrids and the birth of the "enernet"," *IEEE Power and Energy Magazine*, vol. 10, no. 6, Nov 2012.

[13] E. Rodriguez-Diaz, M. Savaghebi, J. C. Vasquez, and J. M. Guerrero, "An overview of low voltage dc distribution systems for residential applications," in *2015 IEEE 5th International Conference on Consumer Electronics - Berlin (ICCE-Berlin)*, Sep. 2015.

[14] B. Wunder, L. Ott, M. Szpek, U. Boeke, and R. Weiss, "Energy efficient dc-grids for commercial buildings," in *2014 IEEE 36th International Telecommunications Energy Conference (INTELEC)*, Sep. 2014.

[15] B. A. Thomas, I. L. Azevedo, and G. Morgan, "Edison revisited: Should we use dc circuits for lighting in commercial buildings?" *Energy Policy*, vol. 45, 2012.

[16] M. Hulsebosch, P. Willigenburg, J. Woudstra, and B. Groenewald, "Direct current in public lighting for improvement in led performance and costs," in *2014 International Conference on the Eleventh industrial and Commercial Use of Energy*, Aug 2014.

[17] M. A. D. Costa, G. H. Costa, A. S. dos Santos, L. Schuch, and J. R. Pinheiro, "A high efficiency autonomous street lighting system based on solar energy and leds," in *2009 Brazilian Power Electronics Conference*, Sep. 2009.

[18] E. Planas, J. Andreu, J. I. Garate, I. M. de Alegria, and E. Ibarra, "Ac and dc technology in microgrids: A review," *Renewable and Sustainable Energy Reviews*, vol. 43, 2015.

[19] J. Driesen and K. Visscher, "Virtual synchronous generators," in *2008 IEEE Power and Energy Society General Meeting - Conversion and Delivery of Electrical Energy in the 21st Century*, July 2008.

[20] N. Bottrell, M. Prodanovic, and T. C. Green, "Dynamic stability of a microgrid with an active load," *IEEE Transactions on Power Electronics*, vol. 28, no. 11, Nov 2013.

[21] J. Kim, S. Cho, and H. Shin, "Advanced power distribution system configuration for smart grid," *IEEE Transactions on Smart Grid*, vol. 4, no. 1, March 2013.

[22] G. Pepermans, J. Driesen, D. Haeseldonckx, R. Belmans, and W. D'haeseleer, "Distributed generation: definition, benefits and issues," *Energy Policy*, vol. 33, no. 6, 2005.

[23] L. Mackay, T. Hailu, L. Ramirez-Elizondo, and P. Bauer, "Towards a dc distribution system - opportunities and challenges," in *2015 IEEE First International Conference on DC Microgrids (ICDCM)*, June 2015.

[24] N. Hatziargyriou, H. Asano, R. Iravani, and C. Marnay, "Microgrids," *IEEE Power and Energy Magazine*, vol. 5, no. 4, July 2007.

[25] R. Pegado, Z. Naupari, Y. Molina, and C. Castillo, "Radial distribution network reconfiguration for power losses reduction based on improved selective bpso," *Electric Power Systems Research*, vol. 169, 01 2019.

[26] J. M. Guerrero, M. Chandorkar, T. Lee, and P. C. Loh, "Advanced control architectures for intelligent microgrids - part i: Decentralized and hierarchical control," *IEEE Transactions on Industrial Electronics*, vol. 60, no. 4, April 2013.

[27] A. H. Etemadi, E. J. Davison, and R. Iravani, "A decentralized robust control strategy for multi-der microgrids - part i: Fundamental concepts," *IEEE Transactions on Power Delivery*, vol. 27, no. 4, Oct 2012.

[28] G. D. Gregory, "Applying low-voltage circuit breakers in direct current systems," *IEEE Transactions on Industry Applications*, vol. 31, no. 4, July 1995.

[29] T. Dragicevic, X. Lu, J. C. Vasquez, and J. M. Guerrero, "Dc microgrids - part i: A review of control strategies and stabilization techniques," *IEEE Transactions on Power Electronics*, vol. 31, no. 7, July 2016.

[30] B. J. Brearley and R. R. Prabu, "A review on issues and approaches for microgrid protection," *Renewable and Sustainable Energy Reviews*, vol. 67, 2017.

[31] T. Hailu, L. Mackay, M. Gajic, and J. A. Ferreira, "Protection coordination of voltage weak dc distribution grid: Concepts," in *2016 IEEE 2nd Annual Southern Power Electronics Conference (SPEC)*, Dec 2016.

[32] Z. J. Shen, "Ultrafast solid-state circuit breakers: Protecting converter-based ac and dc microgrids against short circuit faults [technology leaders]," *IEEE Electrification Magazine*, vol. 4, no. 2, pp. 72–70, June 2016.

[33] M. Laughton and D. Warne, *Electrical Engineer's Reference Book*. Elsevier Science, 2002.

[34] C. R. Paul, *Analysis of Multiconductor Transmission Lines*, 2nd ed. Wiley-IEEE Press, 2007.

[35] J. J. Justo, F. Mwasilu, J. Lee, and J.-W. Jung, "Ac-microgrids versus dc-microgrids with distributed energy resources: A review," *Renewable and Sustainable Energy Reviews*, vol. 24, 2013.

[36] O. D. Montoya, L. Grisales-Norena, D. Gonzalez-Montoya, C. Ramos-Paja, and A. Garces, "Linear power flow formulation for low-voltage dc power grids," *Electric Power Systems Research*, vol. 163, 2018.

[37] A. Gomez-Exposito, A. J. Conejo, and C. Canizares, *Electric energy systems: analysis and operation*. CRC press, 2018.

[38] R. Teixeira Pinto, "Multi-terminal dc networks: System integration, dynamics and control," 2014.

[39] C. Jayarathna, P. Binduhewa, J. Ekanayake, and J. Wu, "Load flow analysis of low voltage dc networks with photovoltaic," in *2014 9th International Conference on Industrial and Information Systems (ICIIS)*, Dec 2014.

[40] M. Pirnia, C. A. Canizares, and K. Bhattacharya, "Revisiting the power flow problem based on a mixed complementarity formulation approach," *IET Generation, Transmission Distribution*, vol. 7, no. 11, November 2013.

[41] J. A. Momoh, R. Adapa, and M. E. El-Hawary, "A review of selected optimal power flow literature to 1993. i. nonlinear and quadratic programming approaches," *IEEE Transactions on Power Systems*, vol. 14, no. 1, Feb 1999.

[42] A. B. Fernandes, W. L. A. Neves, E. G. Costa, and M. N. Cavalcanti, "Transmission line shunt conductance from measurements," *IEEE Transactions on Power Delivery*, vol. 19, no. 2, April 2004.

[43] R. D. C. Monteiro and I. Adler, "Interior path following primal-dual algorithms. part ii: Convex quadratic programming," *Mathematical Programming*, vol. 44, no. 1, May 1989.

[44] F. Delbos and J. C. Gilbert, "Global linear convergence of an augmented lagrangian algorithm to solve convex quadratic optimization problems," *Journal of Convex Analysis*, vol. 12, 01 2005.

[45] C. van de Panne and A. Whinston, "The simplex and the dual method for quadratic programming," *Journal of the Operational Research Society*, vol. 15, no. 4, Dec 1964.

[46] O. Afolabi, W. Ali, P. Cofie, J. Fuller, P. Obiomon, and E. Kolawole, "Analysis of the load flow problem in power system planning studies," *Energy and Power Engineering*, vol. 07, 01 2015.

[47] M. L. Crow, *Computational methods for electric power systems*. Crc Press, 2009.

[48] P. Schavemaker and L. Van der Sluis, *Electrical power system essentials*. John Wiley & Sons, 2017.

[49] W. Wang and M. Barnes, "Power flow algorithms for multi-terminal vsc-hvdc with droop control," *IEEE Transactions on Power Systems*, vol. 29, no. 4, July 2014.

[50] J. B. Ekanayake, N. Jenkins, K. Liyanage, J. Wu, and A. Yokoyama, *Smart grid: technology and applications*. John Wiley & Sons, 2012.

[51] A. Mahmoudi and S. H. Hosseinian, "Direct solution of distribution system load flow using forward/backward sweep," in *2011 19th Iranian Conference on Electrical Engineering*, May 2011.

[52] U. Eminoglu and M. H. Hocaoglu, "Distribution systems forward/ backward sweep-based power flow algorithms: A review and comparison study," *Electric Power Components and Systems*, vol. 37, no. 1, 2008.

[53] (2019, Jan.) IEEE PES Distribution Systems Analysis Subcommittee Radial Test Feeders. [Online]. Available: http://sites.ieee.org/pes-testfeeders/resources/

[54] Y. B. Khoo, C.-H. Wang, P. Paevere, and A. Higgins, "Statistical modeling of electric vehicle electricity consumption in the victorian ev trial, australia," *Transportation Research Part D: Transport and Environment*, vol. 32, pp. 263 – 277, 2014.

[55] N. Sadeghianpourhamami, N. Refa, M. Strobbe, and C. Develder, "Quantitive analysis of electric vehicle flexibility : a data-driven approach," *International Journal of Electrical Power & Energy Systems*, vol. 95, pp. 451–462, 2018.

[56] A. P. N. Tahim, D. J. Pagano, E. Lenz, and V. Stramosk, "Modeling and stability analysis of islanded dc microgrids under droop control," *IEEE Transactions on Power Electronics*, vol. 30, no. 8, Aug 2015.

[57] T. Hailu, L. Mackay, L. Ramirez-Elizondo, J. Gu, and J. A. Ferreira, "Voltage weak dc microgrid," in *2015 IEEE First International Conference on DC Microgrids (ICDCM)*, June 2015.

[58] Q. Shafiee, T. Dragicevic, J. C. Vasquez, and J. M. Guerrero, "Modeling, stability analysis and active stabilization of multiple dc-microgrid clusters," in *2014 IEEE International Energy Conference (ENERGYCON)*, May 2014.

[59] S. Anand and B. G. Fernandes, "Reduced-order model and stability analysis of low-voltage dc microgrid," *IEEE Transactions on Industrial Electronics*, vol. 60, no. 11, Nov 2013.

[60] M. T. Dat, G. Van den Broeck, and J. Driesen, "Modeling the dynamics of a dc distribution grid integrated of renewable energy sources," in *IECON 2014 - 40th Annual Conference of the IEEE Industrial Electronics Society*, Oct 2014.

[61] M. K. Zadeh, R. Gavagsaz-Ghoachani, J. Martin, S. Pierfederici, B. Nahid-Mobarakeh, and M. Molinas, "Discrete-time modelling, stability analysis, and active stabilization of dc distribution systems with constant power loads," in *2015 IEEE Applied Power Electronics Conference and Exposition (APEC)*, March 2015.

[62] P. B. Silvio Rodrigues, Rodrigo Teixeira Pinto, *Dynamic Modeling and Control of VSC-based Multi-terminal DC Networks*, 1st ed. Lambert Academic Publishing, 2012.

[63] J. Han, Y.-S. Oh, G.-H. Gwon, D.-U. Kim, C.-H. Noh, T.-H. Jung, S.-J. Lee, and C.-H. Kim, "Modeling and analysis of a low-voltage dc distribution system," *Resources*, vol. 4, 09 2015.

[64] H. Kakigano, Y. Miura, and T. Ise, "Low-voltage bipolar-type dc microgrid for super high quality distribution," *IEEE Transactions on Power Electronics*, vol. 25, no. 12, Dec 2010.

[65] L. van der Sluis, *Transient Analysis of Three-Phase Power Systems.* John Wiley & Sons, Ltd, 2002.

[66] Y. Gu, Y. Chi, Y. Li, W. Sun, W. Li, and X. He, "Dc symmetrical component method for analysis and control of bipolar lvdc grid," in *2015 IEEE Applied Power Electronics Conference and Exposition (APEC)*, 2015.

[67] Y. Gu, W. Li, and X. He, "Analysis and control of bipolar lvdc grid with dc symmetrical component method," *IEEE Transactions on Power Systems*, vol. 31, no. 1, 2016.

[68] C. L. Fortescue, "Method of symmetrical co-ordinates applied to the solution of polyphase networks," *Transactions of the American Institute of Electrical Engineers*, vol. XXXVII, no. 2, July 1918.

[69] T. Dhaene and D. de Zutter, "Selection of lumped element models for coupled lossy transmission lines," *IEEE Transactions on Computer-Aided Design of Integrated Circuits and Systems*, vol. 11, no. 7, Jul 1992.

[70] R. M. D. B. B. Gustavsen, G. Irwin and K. Kent, "Transmission line models for the simulation of interaction phenomena between parallel ac and dc overhead lines," *International Conference on Power System Transients*, vol. 11, no. 7, Jul 1992.

[71] J. Yang, J. O'Reilly, and J. E. Fletcher, "An overview of dc cable modelling for fault analysis of vsc-hvdc transmission systems," in *Universities Power Engineering Conference (AUPEC), 2010 20th Australasian*, Dec 2010.

[72] A. Emadi, A. Khaligh, C. H. Rivetta, and G. A. Williamson, "Constant power loads and negative impedance instability in automotive systems: definition, modeling, stability, and control of power electronic converters and motor drives," *IEEE Transactions on Vehicular Technology*, vol. 55, no. 4, July 2006.

[73] R. Ahmadi and M. Ferdowsi, "Improving the performance of a line regulating converter in a converter-dominated dc microgrid system," *IEEE Transactions on Smart Grid*, vol. 5, no. 5, Sep. 2014.

[74] A. Riccobono and E. Santi, "Comprehensive review of stability criteria for dc power distribution systems," *IEEE Transactions on Industry Applications*, vol. 50, no. 5, Sep. 2014.

[75] Xiaopeng Wang, Ruoping Yao, and Fangquan Rao, "Three-step impedance criterion for small-signal stability analysis in two-stage dc distributed power systems," *IEEE Power Electronics Letters*, vol. 1, no. 3, Sep. 2003.

[76] G. Sulligoi, D. Bosich, G. Giadrossi, L. Zhu, M. Cupelli, and A. Monti, "Multiconverter medium voltage dc power systems on ships: Constant-power loads instability solution using linearization via state feedback control," *IEEE Transactions on Smart Grid*, vol. 5, no. 5, Sep. 2014.

[77] S. Sanchez and M. Molinas, "Degree of influence of system states transition on the stability of a dc microgrid," *IEEE Transactions on Smart Grid*, vol. 5, no. 5, Sep. 2014.

[78] X. Lu, K. Sun, L. Huang, J. M. Guerrero, J. C. Vasquez, and Y. Xing, "Virtual impedance based stability improvement for dc microgrids with constant power loads," in *2014 IEEE Energy Conversion Congress and Exposition (ECCE)*, Sep. 2014.

[79] D. I. Makrygiorgou and A. T. Alexandridis, "Stability analysis of dc distribution systems with droop-based charge sharing on energy storage devices," *Energies*, vol. 10, Mar. 2017.

[80] D. I. Makrygiorgou and A. T. Alexandridis, "Modeling and stability of autonomous dc microgrids with converter-controlled energy storage systems," in *2017 IEEE Second International Conference on DC Microgrids (ICDCM)*, June 2017.

[81] D. Bosich, M. Gibescu, and G. Sulligoi, "Large-signal stability analysis of two power converters solutions for dc shipboard microgrid," in *2017 IEEE Second International Conference on DC Microgrids (ICDCM)*, June 2017.

[82] J. A. Belk, W. Inam, D. J. Perreault, and K. Turitsyn, "Stability and control of ad hoc dc microgrids," in *2016 IEEE 55th Conference on Decision and Control (CDC)*, Dec 2016.

[83] A. Kwasinski and C. N. Onwuchekwa, "Dynamic behavior and stabilization of dc microgrids with instantaneous constant-power loads," *IEEE Transactions on Power Electronics*, vol. 26, no. 3, March 2011.

[84] M. A. Abdelwahed and E. F. El-Saadany, "Droop gains selection methodology for offshore multi-terminal hvdc networks," in *2016 IEEE Electrical Power and Energy Conference (EPEC)*, Oct 2016.

[85] P. Shamsi and B. Fahimi, "Stability assessment of a dc distribution network in a hybrid micro-grid application," *IEEE Transactions on Smart Grid*, vol. 5, no. 5, Sep. 2014.

[86] M. Tabari and A. Yazdani, "A mathematical model for stability analysis of a dc distribution system for power system integration of plug-in electric vehicles," *IEEE Transactions on Vehicular Technology*, vol. 64, no. 5, May 2015.

[87] Z. Jin, L. Meng, and J. M. Guerrero, "Comparative admittance-based analysis for different droop control approaches in dc microgrids," in *2017 IEEE Second International Conference on DC Microgrids (ICDCM)*, June 2017.

[88] L. Zadeh and C. Desoer, *Linear system theory: the state space approach*, ser. McGraw-Hill series in system science. McGraw-Hill, 1963.

[89] L. Mirsky, *An Introduction to Linear Algebra*, ser. Dover Books on Mathematics. Dover Publications, 2012.

[90] R. Seroul, *Programming for Mathematicians*, ser. Universitext, Springer-Verlag. Springer Berlin Heidelberg, 2000.

[91] S. Barnett and D. Šiljak, "Routh's algorithm: a centennial survey," *SIAM Review*, vol. 19, no. 3, 1977.

[92] F. Gao, S. Bozhko, A. Costabeber, C. Patel, P. Wheeler, C. I. Hill, and G. Asher, "Comparative stability analysis of droop control approaches in voltage-source-converter-based dc microgrids," *IEEE Transactions on Power Electronics*, vol. 32, no. 3, March 2017.

[93] A. Korompili and A. Monti, "Analysis of the dynamics of dc voltage droop controller of dc-dc converters in multi-terminal dc grids," in *2017 IEEE Second International Conference on DC Microgrids (ICDCM)*, June 2017.

[94] B. T. Irving and M. M. Jovanovic, "Analysis, design, and performance evaluation of droop current-sharing method," in *APEC 2000. Fifteenth Annual IEEE Applied Power Electronics Conference and Exposition (Cat. No.00CH37058)*, Feb 2000.

[95] P. Karlsson and J. Svensson, "Dc bus voltage control for a distributed power system," *IEEE Transactions on Power Electronics*, vol. 18, no. 6, Nov 2003.

[96] M. Lee, D. Chen, K. Huang, C. Liu, and B. Tai, "Modeling and design for a novel adaptive voltage positioning (avp) scheme for multiphase vrms," *IEEE Transactions on Power Electronics*, vol. 23, no. 4, July 2008.

[97] A. Maknouninejad, Z. Qu, F. L. Lewis, and A. Davoudi, "Optimal, nonlinear, and distributed designs of droop controls for dc microgrids," *IEEE Transactions on Smart Grid*, vol. 5, no. 5, Sep. 2014.

[98] F. Chen, R. Burgos, D. Boroyevich, and W. Zhang, "A nonlinear droop method to improve voltage regulation and load sharing in dc systems," in *2015 IEEE First International Conference on DC Microgrids (ICDCM)*, June 2015.

[99] P. Prabhakaran, Y. Goyal, and V. Agarwal, "Novel nonlinear droop control techniques to overcome the load sharing and voltage regulation issues in dc microgrid," *IEEE Transactions on Power Electronics*, vol. 33, no. 5, May 2018.

[100] Zhihong ye, D. Boroyevich, Kun Xing, and F. C. Lee, "Design of parallel sources in dc distributed power systems by using gain-scheduling technique," in *30th Annual IEEE Power Electronics Specialists Conference. Record. (Cat. No.99CH36321)*, July 1999.

[101] H. Kakigano, A. Nishino, and T. Ise, "Distribution voltage control for dc microgrid with fuzzy control and gain-scheduling control," in *8th International Conference on Power Electronics - ECCE Asia*, May 2011.

[102] T. V. Vu, D. Perkins, F. Diaz, D. Gonsoulin, C. S. Edrington, and T. El-Mezyani, "Robust adaptive droop control for dc microgrids," *Electric Power Systems Research*, vol. 146, 2017.

[103] Y. Gu, X. Xiang, W. Li, and X. He, "Mode-adaptive decentralized control for renewable dc microgrid with enhanced reliability and flexibility," *IEEE Transactions on Power Electronics*, vol. 29, no. 9, Sep. 2014.

[104] A. Khorsandi, M. Ashourloo, and H. Mokhtari, "A decentralized control method for a low-voltage dc microgrid," *IEEE Transactions on Energy Conversion*, vol. 29, no. 4, Dec 2014.

[105] H. Li, C. Liu, G. Li, and R. Iravani, "An enhanced dc voltage droop-control for the vsc–hvdc grid," *IEEE Transactions on Power Systems*, vol. 32, no. 2, March 2017.

[106] C. Dierckxsens, K. Srivastava, M. Reza, S. Cole, J. Beerten, and R. Belmans, "A distributed dc voltage control method for vsc mtdc systems," *Electric Power Systems Research*, vol. 82, no. 1, 2012.

[107] S. Bolognani and S. Zampieri, "On the existence and linear approximation of the power flow solution in power distribution networks," *IEEE Transactions on Power Systems*, vol. 31, no. 1, Jan 2016.

[108] R. Brayton and J. Moser, "Some results on the stability of nonlinear networks containing negative resistances," *IEEE Transactions on Circuit Theory*, vol. 11, no. 1, March 1964.

[109] D. Jeltsema and J. M. A. Scherpen, "Multidomain modeling of nonlinear networks and systems," *IEEE Control Systems Magazine*, vol. 29, no. 4, Aug 2009.

[110] L. Meng, Q. Shafiee, G. F. Trecate, H. Karimi, D. Fulwani, X. Lu, and J. M. Guerrero, "Review on control of dc microgrids and multiple microgrid clusters," *IEEE Journal of Emerging and Selected Topics in Power Electronics*, vol. 5, no. 3, Sep. 2017.

[111] J. C. Vasquez, J. M. Guerrero, J. Miret, M. Castilla, and L. Garcia de Vicuna, "Hierarchical control of intelligent microgrids," *IEEE Industrial Electronics Magazine*, vol. 4, no. 4, Dec 2010.

[112] L. Che, M. Shahidehpour, A. Alabdulwahab, and Y. Al-Turki, "Hierarchical coordination of a community microgrid with ac and dc microgrids," *IEEE Transactions on Smart Grid*, vol. 6, no. 6, Nov 2015.

[113] T. Morstyn, B. Hredzak, and V. G. Agelidis, "Control strategies for microgrids with distributed energy storage systems: An overview," *IEEE Transactions on Smart Grid*, vol. 9, no. 4, July 2018.

[114] K. E. Antoniadou-Plytaria, I. N. Kouveliotis-Lysikatos, P. S. Georgilakis, and N. D. Hatziargyriou, "Distributed and decentralized voltage control of smart distribution networks: Models, methods, and future research," *IEEE Transactions on Smart Grid*, vol. 8, no. 6, Nov 2017.

[115] X. Wang, Y. W. Li, F. Blaabjerg, and P. C. Loh, "Virtual-impedance-based control for voltage-source and current-source converters," *IEEE Transactions on Power Electronics*, vol. 30, no. 12, Dec 2015.

[116] H. Mahmood, D. Michaelson, and J. Jiang, "Reactive power sharing in islanded microgrids using adaptive voltage droop control," *IEEE Transactions on Smart Grid*, vol. 6, no. 6, Nov 2015.

[117] M. Tucci, S. Riverso, J. C. Vasquez, J. M. Guerrero, and G. Ferrari-Trecate, "A decentralized scalable approach to voltage control of dc islanded microgrids," *IEEE Transactions on Control Systems Technology*, vol. 24, no. 6, Nov 2016.

[118] F. Cingoz, A. Elrayyah, and Y. Sozer, "Plug-and-play nonlinear droop construction scheme to optimize islanded microgrid operations," *IEEE Transactions on Power Electronics*, vol. 32, no. 4, pp. 2743–2756, April 2017.

[119] D. Chen, L. Xu, and L. Yao, "Dc voltage variation based autonomous control of dc microgrids," *IEEE Transactions on Power Delivery*, vol. 28, no. 2, April 2013.

[120] Y. Gu, W. Li, and X. He, "Frequency-coordinating virtual impedance for autonomous power management of dc microgrid," *IEEE Transactions on Power Electronics*, vol. 30, no. 4, April 2015.

[121] R. A. Mastromauro, M. Liserre, and A. Dell'Aquila, "Control issues in single-stage photovoltaic systems: Mppt, current and voltage control," *IEEE Transactions on Industrial Informatics*, vol. 8, no. 2, May 2012.

[122] D. Salomonsson and A. Sannino, "Load modelling for steady-state and transient analysis of low-voltage dc systems," *IET Electric Power Applications*, vol. 1, no. 5, Sep. 2007.

[123] A. G. Tsikalakis and N. D. Hatziargyriou, "Centralized control for optimizing microgrids operation," *IEEE Transactions on Energy Conversion*, vol. 23, no. 1, March 2008.

[124] "Ieee standards for local area networks: Carrier sense multiple access with collision detection (csma/cd) access method and physical layer specifications," 1985.

[125] B.-J. Kwak, N.-O. Song, and L. E. Miller, "Performance analysis of exponential backoff," *IEEE/ACM Trans. Netw.*, vol. 13, no. 2, pp. 343–355, Apr. 2005.

[126] Z. J. Haas and Jing Deng, "On optimizing the backoff interval for random access schemes," *IEEE Transactions on Communications*, vol. 51, no. 12, pp. 2081–2090, Dec 2003.

[127] L. Mackay, N. H. van der Blij, L. Ramirez-Elizondo, and P. Bauer, "Toward the universal dc distribution system," *Electric Power Components and Systems*, vol. 45, no. 10, 2017.

[128] T. Guillod, F. Krismer, and J. W. Kolar, "Protection of mv converters in the grid: The case of mv/lv solid-state transformers," *IEEE Journal of Emerging and Selected Topics in Power Electronics*, vol. 5, no. 1, March 2017.

[129] D. Fulchiron, "Protection of mv/lv substation transformers," *Cahier technique*, no. 192, 1998.

[130] P. Purgat, L. Mackay, Z. Qin, and P. Bauer, "On the protection of the power flow control converter in meshed low voltage dc networks," in *2018 IEEE Energy Conversion Congress and Exposition (ECCE)*, Sep. 2018.

[131] L. Qi, A. Antoniazzi, and L. Raciti, "DC distribution fault analysis, protection solutions, and example implementations," *IEEE Transactions on Industry Applications*, vol. 54, no. 4, pp. 3179–3186, July 2018.

[132] J. P. Brozek, "Dc overcurrent protection-where we stand," *IEEE Transactions on Industry Applications*, vol. 29, no. 5, Sep. 1993.

[133] L. B. ABB SACE, A division of ABB S.p.A., "Abb circuit-breakers for direct current applications," 2017.

[134] R. Lazzari and L. Piegari, "Design and implementation of lvdc hybrid circuit breaker," *IEEE Transactions on Power Electronics*, vol. 34, no. 8, Aug 2019.

[135] Y. Sato, Y. Tanaka, A. Fukui, M. Yamasaki, and H. Ohashi, "SiC-SIT circuit breakers with controllable interruption voltage for 400-V dc distribution systems," *IEEE Transactions on Power Electronics*, vol. 29, no. 5, pp. 2597–2605, May 2014.

[136] Z. Miao, G. Sabui, A. Chen, Y. Li, Z. J. Shen, J. Wang, Z. Shuai, A. Luo, X. Yin, and M. Jiang, "A self-powered ultra-fast dc solid state circuit breaker using a normally-on SiC JFET," in *IEEE Applied Power Electronics Conference and Exposition (APEC)*, March 2015, pp. 767–773.

[137] N. Bayati, A. Hajizadeh, and M. Soltani, "Protection in dc microgrids: a comparative review," *IET Smart Grid*, vol. 1, no. 3, 2018.

[138] S. Mirsaeidi, D. Said, M. Mustafa, M. Habibuddin, and M. Miveh, "A comprehensive overview of different protection schemes in micro-grids," *International Journal of Emerging Electric Power Systems (IJEEPS)*, vol. 14, 07 2013.

[139] D. Salomonsson, L. Soder, and A. Sannino, "Protection of low-voltage dc microgrids," *IEEE Transactions on Power Delivery*, vol. 24, no. 3, July 2009.

[140] A. Meghwani, S. C. Srivastava, and S. Chakrabarti, "A non-unit protection scheme for dc microgrid based on local measurements," *IEEE Transactions on Power Delivery*, vol. 32, no. 1, Feb 2017.

[141] J. Sneath and A. D. Rajapakse, "Fault detection and interruption in an earthed hvdc grid using rocov and hybrid dc breakers," *IEEE Transactions on Power Delivery*, vol. 31, no. 3, June 2016.

[142] J. Yang, J. E. Fletcher, and J. O'Reilly, "Short-circuit and ground fault analyses and location in vsc-based dc network cables," *IEEE Transactions on Industrial Electronics*, vol. 59, no. 10, Oct 2012.

[143] R. Mohanty and A. K. Pradhan, "A superimposed current based unit protection scheme for dc microgrid," *IEEE Transactions on Smart Grid*, vol. 9, no. 4, July 2018.

[144] R. Bertho, V. A. Lacerda, R. M. Monaro, J. C. M. Vieira, and D. V. Coury, "Selective nonunit protection technique for multiterminal VSC-HVdc grids," *IEEE Transactions on Power Delivery*, vol. 33, no. 5, pp. 2106–2114, Oct 2018.

[145] S. Som and S. R. Samantaray, "Efficient protection scheme for low-voltage dc micro-grid," *IET Generation, Transmission Distribution*, vol. 12, no. 13, 2018.

[146] X. Feng, L. Qi, and J. Pan, "A novel fault location method and algorithm for dc distribution protection," *IEEE Transactions on Industry Applications*, vol. 53, no. 3, pp. 1834–1840, May 2017.

[147] L. Tang and B. Ooi, "Locating and isolating dc faults in multi-terminal dc systems," *IEEE Transactions on Power Delivery*, vol. 22, no. 3, July 2007.

[148] A. A. S. Emhemed and G. M. Burt, "An advanced protection scheme for enabling an lvdc last mile distribution network," *IEEE Transactions on Smart Grid*, vol. 5, no. 5, Sep. 2014.

[149] S. D. A. Fletcher, P. J. Norman, K. Fong, S. J. Galloway, and G. M. Burt, "High-speed differential protection for smart dc distribution systems," *IEEE Transactions on Smart Grid*, vol. 5, no. 5, Sep. 2014.

[150] M. Farhadi and O. A. Mohammed, "Event-based protection scheme for a multiterminal hybrid dc power system," *IEEE Transactions on Smart Grid*, vol. 6, no. 4, July 2015.

[151] ——, "A new protection scheme for multi-bus dc power systems using an event classification approach," *IEEE Transactions on Industry Applications*, vol. 52, no. 4, pp. 2834–2842, July 2016.

[152] A. A. S. Emhemed, K. Fong, S. Fletcher, and G. M. Burt, "Validation of fast and selective protection scheme for an LVdc distribution network," *IEEE Transactions on Power Delivery*, vol. 32, no. 3, pp. 1432–1440, June 2017.

[153] M. Monadi, C. Gavriluta, A. Luna, J. I. Candela, and P. Rodriguez, "Centralized protection strategy for medium voltage dc microgrids," *IEEE Transactions on Power Delivery*, vol. 32, no. 1, pp. 430–440, Feb 2017.

[154] J. Park and J. Candelaria, "Fault detection and isolation in low-voltage dc-bus microgrid system," *IEEE Transactions on Power Delivery*, vol. 28, no. 2, pp. 779–787, April 2013.

[155] L. Wang, "The fault causes of overhead lines in distribution network," *MATEC Web of Conferences*, vol. 61, 01 2016.

[156] C. Bajracharya, "Control of vsc-hvdc for wind power," Master's thesis, Institutt for elkraftteknikk, 2008.

[157] T. Kalitjuka, "Control of voltage source converters for power system applications," Master's thesis, Institutt for elkraftteknikk, 2011.

List of Publications

Journal Publications

- N. H. van der Blij, L. M. Ramirez-Elizondo, M. T. J. Spaan and P. Bauer, "A State-Space Approach to Modelling DC Distribution Systems", IEEE Transactions on Power Systems, vol. 33, no. 1, Jan. 2018.
- N. H. van der Blij, L. M. Ramirez-Elizondo, M. T. J. Spaan and P. Bauer, "Symmetrical Component Decomposition of DC Distribution Systems", IEEE Transactions on Power Systems, vol. 33, no. 3, May 2018.
- N. H. van der Blij, L. M. Ramirez-Elizondo, M. T. J. Spaan and P. Bauer, "Stability of DC Distribution Systems: An Algebraic Derivation", Energies, vol. 10, Jul. 2017.
- N. H. van der Blij, L. M. Ramirez-Elizondo, M. T. J. Spaan and P. Bauer, "Stability and Decentralized Control of Plug-and-Play DC Distribution Grids", IEEE Access, vol. 6, 2018.
- N. H. van der Blij, L. M. Ramirez-Elizondo, M. T. J. Spaan and P. Bauer, "Grid Sense Multiple Access: A Decentralized Control Algorithm for DC Grids", International Journal of Electrical Power & Energy Systems, 2020.
- N. H. van der Blij, P. Purgat, T. B. Soeiro, L. M. Ramirez-Elizondo, M. T. J. Spaan and P. Bauer, "Decentralized Plug-and-Play Protection Scheme for Low Voltage DC Grids", Energies, vol. 13, Jun. 2020.

Co-authored Journal Publications

- L. Mackay, N. H. van der Blij, L. M. Ramirez-Elizondo and P. Bauer, "Toward the Universal DC Distribution System", Electric Power Components and Systems, vol. 45, no. 10, 2017.

- E. Walraven, N. H. van der Blij and M. T. J. Spaan, "Planning under Uncertainty for Congestion Management in Smart Grids", Autonomous Agents and Multi-Agent Systems (STATUS: SUBMITTED)
- P. Purgat, N. H. van der Blij, Z. Qin and P. Bauer, "Partially Rated Power Flow Control Converter Modeling for Low Voltage DC Grids", IEEE Journal of Emerging and Selected Topics in Power Electronics, 2019.
- B. Mashhoodi, A. van Timmeren, N. H. van der Blij, "The two and half minute walk: Fast charging of electric vehicles and the economic value of walkability", Environment and Planning B: Urban Analytics and City Science, Nov. 2019.

Conference Publications

- N. H. van der Blij, L. M. Ramirez-Elizondo, M. T. J. Spaan and P. Bauer, "Design guidelines for stable DC distribution systems", IEEE Second International Conference on DC Microgrids (ICDCM), 2017.
- N. H. van der Blij, L. M. Ramirez-Elizondo, M. T. J. Spaan, W. Li and P. Bauer, "State-Space Modeling of DC Distribution Systems: Experimental Validation", 10th International Conference on Power Electronics and ECCE Asia (ICPE - ECCE Asia), 2019.
- N. H. van der Blij, L. M. Ramirez-Elizondo, M. T. J. Spaan, W. Li and P. Bauer, "Stability of DC Distribution Systems: Analytical and Experimental Results", IEEE Third International Conference on DC Microgrids (ICDCM), 2019.
- D. Chaifouroosh, N. H. van der Blij, L. M. Ramirez-Elizondo and P. Bauer, "Steady-State Power Flow Analysis of DC Distribution Systems", IEEE Third International Conference on DC Microgrids (ICDCM), 2019.
- N. H. van der Blij, D. Chaifouroosh, T. B. Soeiro, L. M. Ramirez-Elizondo, M. T. J. Spaan, Claudio A. Cañizares and P. Bauer, "Novel Power Flow Methods for DC Grids", 29th International Symposium on Industrial Electronics (ISIE), 2020.
- N. H. van der Blij, P. Purgat, T. B. Soeiro, L. M. Ramirez-Elizondo, M. T. J. Spaan and P. Bauer, "Protection Framework for Low Voltage DC Grids", 19th Power Electronics and Motion Control Conference (PEMC), 2020.
- N. H. van der Blij, T. B. Soeiro, L. M. Ramirez-Elizondo, M. T. J. Spaan and P. Bauer, "Design, Modeling and Validation of an Experimental DC Microgrid Setup", 46th Annual Conference of the IEEE Industrial Electronics Society (IECON), 2020.

Acknowledgements

The journey leading up to this PhD thesis has been long, but not lonely nor unpleasant. Here, I will take the opportunity to thank some of the people that I have crossed paths with, without them this thesis would not have been possible.

First of all, I would like to than my promotor, Professor Pavol Bauer, for giving me the opportunity to pursue a PhD in the DCE&S group. Throughout my PhD project, he has given me a lot of freedom and many opportunities to develop my research project and myself. Thanks to him I was able to experience a lot of new things, and push the boundaries of my research even further.

I would also like to thank my other promotor, Matthijs Spaan, and my supervisors, Laura Ramirez-Elizondo and Thiago Batista-Soeiro, for supporting me and providing me with feedback throughout my PhD project. Thanks to you, I was able to learn a lot and develop myself as a researcher.

Next, I want to thank the supervisors at Zhejiang University, Professor Wuhua Li, and Waterloo University, Professor Claudio Cañizares. Both supervisors have welcomed me with open arms and I never felt like I was alone, although I was far from home. Both research exchanges were valuable experiences to me.

I also want to thank the lab managers, Bart Roodenburg, Joris Koeners and Harry Olsthorn specifically, for the support in the lab. Together we were able to build some really nice experimental setups, and get great experimental results.

A special thanks to the researchers that I have collaborated with throughout my PhD project, Pavel Purgat, Laurens Mackay, Erwin Walraven and Bardia Mashhoodi. I'm recommending any PhD student to collaborate with people with different expertises than yourself, which is educational in many ways.

Colleagues and friends, past and present, from the DCE&S group; Thank you for keeping me sane and laughing throughout my PhD journey, I will never forget the time we spent together during lunch, on the football field and in Locus. To name a few: Pavel "The power electronics expert" Purgat, Laurens "The baron" Mackay, Udai "Regular gym-goer" Shipurkar, Soumya "Suicide squad" Bandyopadhyay, and Mladen "Russian spy" Gagic.

Last, but not least, I am particularly grateful for my friends, my mother and my sister, who have always been supportive throughout this journey.

Biography

Nils Hans van der Blij was born in Leiden, the Netherlands, in 1990. He received his BSc. degree in Electrical Engineering and MSc. degree in Electrical Power Engineering in 2011 and 2013, respectively, from the Delft University of Technology, The Netherlands. From 2013 to 2016, he participated in several research projects in the field of electromagnetics and wind turbine design. From May 2016, he pursued a PhD degree with the DC Energy conversion & Storage (DCE&S) group, at the Delft University of Technology, on the topic of "DC Distribution Systems". His main research interests are in the fields of renewable energy generation, electromagnetics, energy conversion and dc systems.